DEVELOPMENT AND ASSESSMENT OF PHYSICALLY BASED NUMERICAL SEDIMENT TRANSPORT MODELS FOR SHALLOW OVERLAND FLOW

By

Thomas Seever

A thesis submitted in partial fulfillment

of the requirements for the degree of

MASTER OF SCIENCE

in

Geosciences

Middle Tennessee State University

December 2023

Thesis Committee:

Henrique Momm, Chair

Racha El Kadiri

Jeremy Abers

ACKNOWLEDGEMENTS

I would like to express my thanks to Dr. Momm, my committee chair and thesis advisor, for his continued support and encouragement. I want to thank Dr. El Kadiri and Dr. Abers as well for their support and encouragement as my committee members. Lastly, I would like to extend my thanks to my friends and family who have supported me throughout my work.

ABSTRACT

Sediment transport models for shallow water flow are important to the prediction of erosion and to support decision-makers in the development of conservation plans for agricultural and natural environments. This study proposes and evaluates two models based on empirical and numerical equations to quantify topographic change with shallow water flows. The first model is constructed with rill erosion and landscape evolution equations. The second model uses finite element methodologies to evaluate a sediment transport equation with different erosions and deposition. The hydrology of both models is generated using an uncoupled overland flow model. The models are validated against observed topography of shallow water flow with observed data of sediment discharge and runoff rate. The hydrology matches the runoff rate over the timescale used. The simulated sediment discharge matches well with observed sediment discharge for erosion equations with no deposition implemented. Preliminary results with deposition look promising but require further development. The simulated geomorphology cannot be concluded to confidently match observed geomorphology for the equations used. The two models are compared to results in literature. Further development of the models is required to improve the accuracy and capabilities of the model.

TABLE OF CONTENTS

LIST OF FIGURES

LIST OF TABLES

LIST OF SYMBOLS AND ABBREVIATIONS

$\alpha, \beta, \delta, \gamma$ ..... Best fit parameter in Equation 7

α_{st} ..... A calibration coefficient in Equation 36

A, B ..... Fitting parameters in Equation 13

b, p ..... Exponents for calibration in Equation 37

β_1, β_2 ..... Slope angles parallel and perpendicular to the direction of flow respectively

C ..... A calibration coefficient in Equation 22

C_{si} ..... A calibration coefficient in Equation 34

C_t ..... A coefficient for the timestep size used in Equation 5 and Equation 19

C_0 ..... Combined coefficient for calibration in Equation 36

D ..... Deposition (kg m^{-2} s^{-1})

d ..... Sediment diameter (m)

E ..... Erosion (kg m^{-2} s^{-1})

E_I ..... Soil detachment by rainfall impact (kg m^{-2} s^{-1})

ϵ ..... Effective water depth (m)

e_Q, e_S ..... Exponents for flow discharge and slope in Equation 11

g ..... Gravity (m s^{-2})

γ ..... A calibration coefficient in Equation 22

h .....Surface water depth (m)

h_c ..... Minimum concentrated flow depth (m)

h_f ..... Water flow depth at the links (m)

h_{max} ..... Maximum water depth in the simulation (m)

h_s .....Maximum sheet flow depth (m)

h_0 ..... Break point depth (m)

I .....Incision rate (m)

I_R ..... Rainfall intensity (m s^{-1})

i .....Summation subscript representing links at a node

K_{sp} ..... A calibration coefficient in Equation 11

k ..... A calibration coefficient in Equation 10

k_s .....Roughness height of the bed surface (m)

κ .....Curvature of topography (m^{-1})

L_{comb} .....Combined adaptation length for erosion and deposition (m)

L_D .....Adaptation length for deposition (m)

L_S .....Slope length (m)

Λ, Λ_P ..... Binary parameters in Equation 22

M_X ..... Mixing function value of a variable X

N ..... An arbitrary integer

n ..... Manning's n

n_c ..... Manning's n for concentrated flow

n_s ..... Manning's n for sheet flow

$\hat{n}$ ..... Unit normal vector at a grid cell boundary

ν ..... Kinematic viscosity of water ($m^2\ s^{-1}$)

Ψ ..... Sediment concentration ($kg\ m^{-3}$)

ϕ ..... Angle of repose

Q ..... Flow discharge ($m^3\ s^{-1}$)

Q_P ..... Flow discharge perpendicular to a link ($m^3\ s^{-1}$)

q ..... Unit flow discharge ($m^2\ s^{-1}$)

q_{att} ..... Attenuated unit flow discharge ($m^2\ s^{-1}$)

q_s ..... Unit sediment load ($kg\ m^{-1}\ s^{-1}$)

ρ_b ..... Soil bulk density ($kg\ m^{-3}$)

ρ_s ..... Sediment density ($kg\ m^{-3}$)

ρ_w ..... Water density (kg m^{-3})

S ..... Slope gradient

s ..... Sediment transport rate (kg m^{-1} s^{-1})

s_I ..... Sheet and splash erosion (kg m^{-2} s^{-1})

s_x, s_y ..... Sediment transport rate in the x and y directions

T ..... Entrainment threshold (m)

T_c ..... Transport capacity (kg m^{-1} s^{-1})

t ..... Time (s)

τ ..... Bed shear stress (Pa)

τ_x, τ_y ..... Bed shear stress in x and y directions (Pa)

Δt ..... Time step size (s)

θ ..... Shields parameter

θ_c ..... Critical Shields parameter

Θ_1, Θ_2 ..... Correction terms for the critical Shields parameter

U ..... Uplift rate (m)

V_b ..... Bed flow velocity (m s^{-1})

V ..... Runoff velocity (m s^{-1})

V_x, V_y ..... Runoff velocity in the x and y direction (m s^{-1})

$V_\star$ ..... Shear velocity at the bed (m s^{-1})

ω ..... Stream power

X ..... Arbitrary, generic variable

Δx ..... Spatial resolution of the grid (m)

y ..... Surface water elevation (m)

z ..... Topographic elevation (m)

z_o ..... Flow parameter for smoothness of flow

CHAPTER I

INTRODUCTION

Overview of water-driven soil erosion models

Water-driven soil erosion models are essential for the analysis and prediction of landscape changes in agriculture and land development. They allow decision makers to determine what land is at risk of erosion and develop targeted mitigation plans. Models such as RUSLE (Renard et al., 1991) have been developed to assist in such decision making, and they have been successful in long-term predictions of sediment yields considering different management alternatives. However, models like RUSLE and RUSLE2 (Renard et al., 2001; USDA-Agricultural Research Service, 2013) were developed based on empirical relationships and were designed to represent the landscape as a one-dimensional profile. They do not have the tools to represent the topographic changes due to erosion. Furthermore, these models do not disaggregate between the different flow regimes governing the erosion process. This is a hindrance when working to understand the effects of different flow regimes on soil erosion since different types of conservation practices may be more effective for some flow regimes than others. A comprehensive soil erosion model is needed to model shallow water flow as well as sediment detachment and transport in concentrated and sheet flow to address the stated issues. The soil erosion model also needs to identify the independent and combined contributions of erosion processes associated with raindrop splash, laminar flow (sheet), rill, and gully erosion.

When considering the development of any new model, it is necessary to evaluate existing models. There are four common categories of models used for soil erosion: empirical models, conceptual models, physically based models, and hybrid models (Hajigholizadeh et al., 2018). Empirical models are based on observation rather than working scientific theory. Conceptual models are like empirical models with the exception that they are fit to conceptual frameworks to answer general questions. Physically based models operate based on scientific theory. Lastly, hybrid models are models that are some combination of the other three models, often being physically based or conceptual at their core while being empirical in the calibration.

An example of an empirical model is a detachment-limited model for drainage basin evolution (Howard, 1994). The detachment-limited model uses the topographic slope and the water's flow discharge to estimate the erosion rate of landform surfaces. It returns results that appear like general landforms generated by long term water flow. Landscape evolution models are rarely validated, so their exact accuracy is unknown (Tucker & Hancock, 2010). They are primarily designed to estimate long-term evolution of landscapes at regional scales; therefore, they may not be an optimal choice for modeling field-scale erosional features.

RillGrow is an illustration of a conceptual model for rill development in soil mantled landscapes. It is designed to function based on a cellular automata algorithm, and it operates using the concept of stream power to estimate erosion (D. Favis-Mortlock, 1998; D. T. Favis-Mortlock et al., 2000). It has been demonstrated to generate good rill topography, but it has a high computational overhead because it operates on individual

raindrops. Additionally, accounting for individual raindrops makes it difficult to relate to real time steps. However, it is simple to implement in a raster grid structure for model development since the equation is based on stream power.

No existing soil erosion model is fully physically based since many underlying parameters that need to be empirically determined, but models can be mostly physically based with minimal empirical calculations implemented. One example of a model that is considered physically based is the Dynamic Watershed Simulation Model (DWSM) (Borah et al., 1999). It simulates flood waves, soil erosion, and entrainment and transport of sediments; the model also tracks chemicals in agricultural and rural watersheds. This model requires many inputs such as topographic data, channel data, reservoir data, and precipitation data. These inputs are then used to calculate hydrology, sediment and chemical transport, and infiltration. The model is effective in predicting soil erosion behavior, but this approach is not useful for smaller scale applications such as flumes since it is designed for larger regions of at least the size of agricultural fields (Hajigholizadeh et al., 2018). Furthermore, physically based models are usually designed for longer timescales, and landscape evolution models of all types are hard to validate for long timescales (Tucker & Hancock, 2010). However, physically based models such as these have proven their success and are often maintained by laboratories, universities, and federal agencies.

The CCHE2D tool (Jia & S.Y. Wang, 2001) is an example of a hybrid model, and it is built on a raster grid with a staggered grid on the vertices to allow for exact flux calculations. It calculates sediment transport and hydrology using physically based

equations. It also calculates many of the underlying parameters with empirical equations, and it is designed for the desired spatial scale. A hybrid model such as CCHE2D has a robust structure and set of equations that makes it very accurate when calculating sediment transport and hydrology, but the empirical nature of many of the equations in CCHE2D make it difficult to calibrate. Different soils and topographies may require different empirical equations and calibrations, making CCHE2D require unique calibrations for different landscapes. The advantage is that it can accurately simulate hydrology and sediment transport for any similar landscape once calibrated for the sediment sizes and spatial scales.

Objectives and scope

The main objectives of this study are to understand and evaluate the existing soil-mantled erosion models and to propose enhancements to support the disaggregation of erosion processes in time and space. To accomplish these objectives, the following steps were performed:

- Evaluate the applicability of Landlab's Overland Flow component (Adams et al., 2017) as a potential hydrodynamic model.
- Develop a hybrid erosion model by integrating a hydrodynamic component with the combined empirical erosion formulation proposed in RillGrow and in the integrated rill and landscape evolution model (D. Favis-Mortlock, 1998; D. T. Favis-Mortlock et al., 2000; Howard, 1994).
- Develop an erosion model by integrating hydrodynamic component with sediment detachment and transport component based on finite difference methods – representing the proposed erosion model (Jia & S.Y. Wang, 2001, Lai, 2020).
- Quantify the accuracy of sediment load at the outlet and spatial-temporal geomorphological changes by comparing estimates from the proposed models with observed values.
- Investigate strengths and limitations of each model in simulating the various disaggregated erosion mechanisms and determine how the erosion mechanisms compare to previous studies (Momm et al., 2018).

After discussing each of these objectives and how well they were accomplished, the conclusions of the study and possibilities for future model research are stated.

CHAPTER II

REFERENCE DATASET

Observed dataset used in model development and evaluation

Data obtained from the USDA-ARS National Sedimentation Laboratory is used as a reference dataset for this study. The dataset used was obtained from a soil-mantled flume that is 1.8m wide, 9.3m long, and 0.3m deep (Momm et al., 2018). The flume has a drain at the bottom where the overland flow and sediments can drain. Rainfall was simulated using 14 nozzles over the flume, and after 360 minutes of 30 mm/hr rainfall, a rainfall rate of 105 mm/hr rainfall was applied until 1095 minutes had passed in total (elapsed time). The sediment used in the flume has a bulk soil density of 1450 kg/m^3 with a composition of 3% sand, 73% silt, and 24% clay. Topographic raster grids of the flume that were generated at different time steps using close-range digital photogrammetric methods (Figure 1). The sediment discharge of the flume was also recorded at set intervals at the outlet (Figure 2).

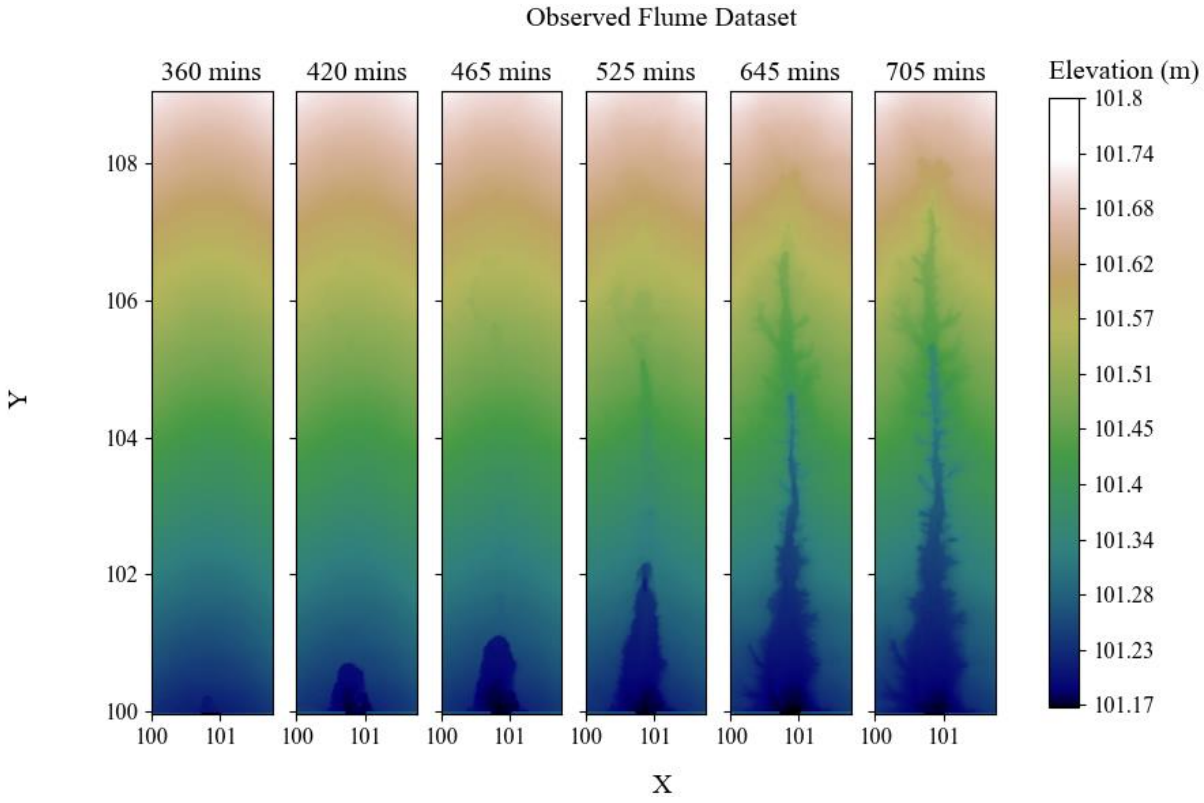

Figure 1

Bed surface topography of the observed flume topography as a function of time (Momm et al., 2018)

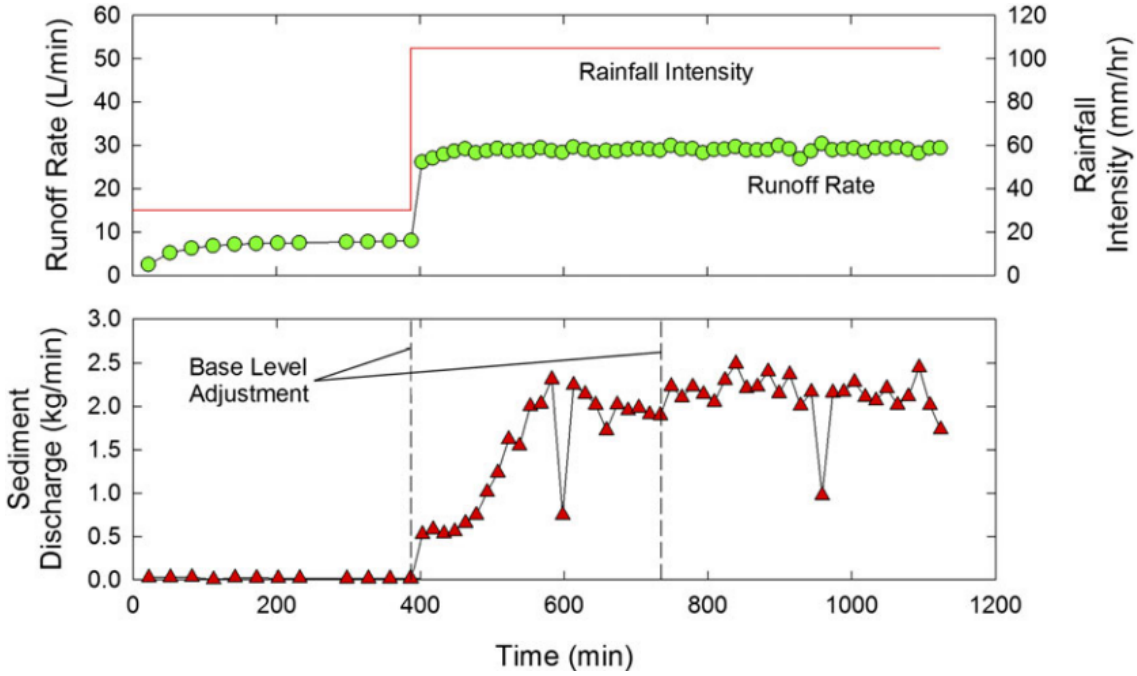

Figure 2

Time variation of runoff rate and sediment discharge rate as measured at the flume outlet, as well as rainfall intensity, as a function of time (Momm et al., 2018)

CHAPTER III

HYDROLOGICAL MODEL

Description of hydrological model

The models presented in the introduction all have different hydrological calculations to drive the sediment transport and erosion. The basics of hydrological simulation are well understood, and many models for calculating 2D and 3D water flows are present in literature. For simplicity and to encourage fast model deployment, water flow is simulated using the formulation proposed by de Almeida (2012) and implemented in the Python (Rossum & Drake, 2009) module Landlab (Adams et al., 2017). Landlab is a Python package for numerical modeling of Earth surface dynamics, and hydrology can be simulated using the OverlandFlow module (de Almeida et al., 2012). OverlandFlow functions using 2D shallow water equations on a raster grid containing the topographic elevation, and it uses an offset grid established on the edge centers for flux calculations. This can be used to obtain the flow discharge and water depth on the surface such that the erosion of surfaces can be calculated.

Landlab uses a structure of nodes and links to calculate the hydrology, and this structure is important to understand when using it as the basis to calculate overland flow (Figure 3) (Barnhart et al., 2020; Hobley et al., 2017; Hutton et al., 2020). The methodology of having two grids – which is a grid of nodes and a grid of links in this case – is called the finite element method, and it allows for the exact calculation of fluxes between nodes instead of requiring approximations on a single grid of nodes (Jia & S.Y. Wang, 2001). This study refers to the links and the nodes in equations by stating that a

value on the link is X_L given a generic variable X while the head and the tail of the link are referred to as X_H and X_T respectively. Conversely, a node will be referred to as X_{node} and the links at the edges will be referred to as X_{up}, X_{down}, X_{left}, and X_{right}.

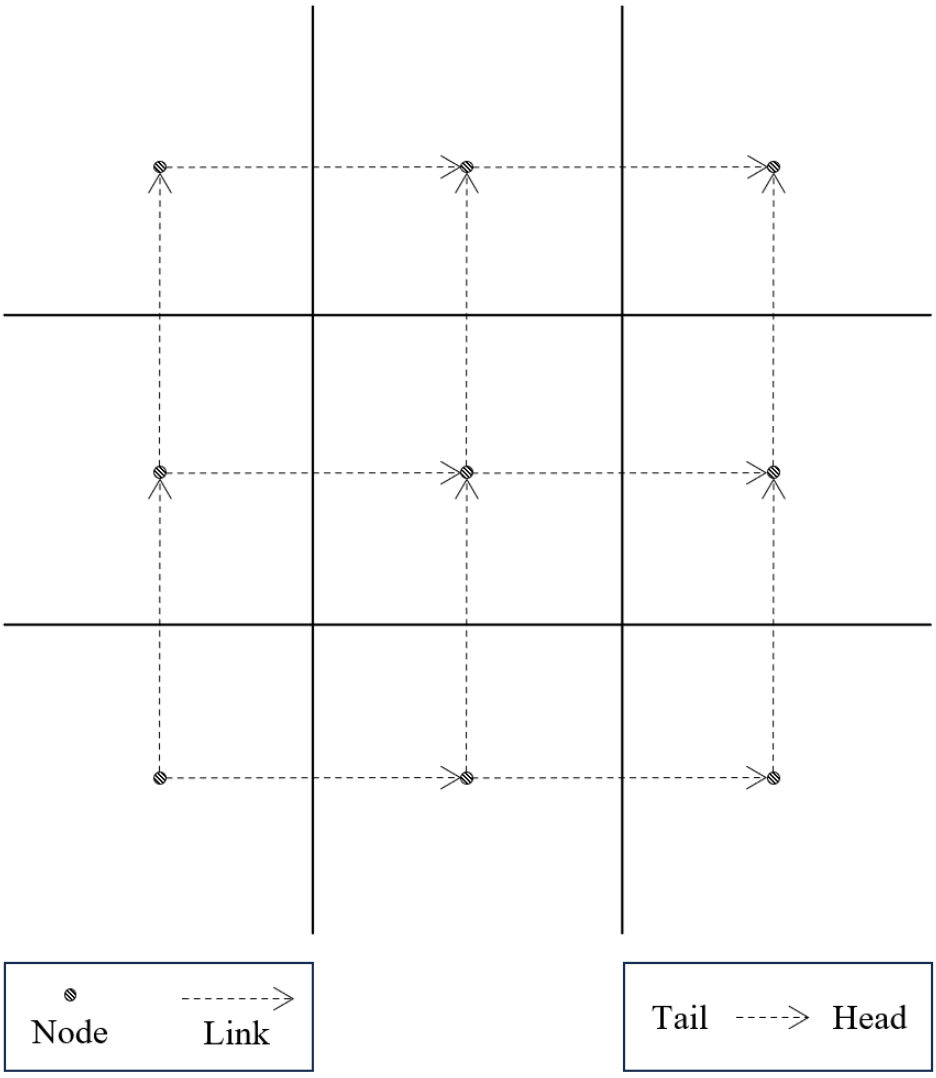

Figure 3

Diagram of the raster grid setup in Landlab's RasterModelGrid (Barnhart et al., 2020; Hobley et al., 2017; Hutton et al., 2020)

Note: The head and tail of the links is explicitly shown in the bottom right.

Time stepping in computer simulations is also a matter of paramount importance when considering programs that simulate real time. There are multiple methods that can

be used when performing time stepping that vary from simple, linear steps using the Euler method to fourth order Runge-Kutte methods (de Almeida et al., 2012; Li & Duffy, 2011; Jia & S.Y. Wang, 2001). This study uses a simple Euler time stepping scheme in models, but the important matter to take away is that there is always some time stepping scheme in the equations. Variables at a given time $t = N$ are referred to in this study as X^N.

OverlandFlow uses the grid-based structure depicted in Figure 3 by storing elevation features such as topographic elevation and water depth on the nodes while storing transport related features such as discharge on the links (Adams et al., 2017). The water depth h at each node is set to $h = 10^{-7}$ meters to prevent issues with zero division and computational underflows. In de Almeida (2012), the discharge of the next time step calculated using a version of Equation 1 below which uses an upwind scheme.

$$Q_L^{N+1} = \frac{Q_L^N - g h_f \frac{\Delta t}{\Delta x}(y_H - y_T)}{1 + \frac{g n^2 |Q_L^n| \Delta t}{h_f^{\frac{7}{3}}}} \quad (1)$$

In Equation 1, Q is the flow discharge, g is gravity, Δt is the time step size, Δx is the spatial resolution of the grid, y is the surface water elevation, h_f is the water flow depth, and n is Manning's n. The water flow depth in Equation 1 refers to the maximum surface water elevation minus the maximum topographic elevation as is shown in Equation 2, where z is the topographic elevation.

$$h_f = \max(y_H, y_T) - \max(z_H, z_T) \quad (2)$$

In Landlab's OverlandFlow, the Manning's n is set to a constant by default. This is not necessarily accurate since this parameter is expected to vary in concentrated flow and sheetflow. An empirical equation estimating the Manning's n for the flow is used in this study to correct for this issue (Jia et al., 2023).

$$n = \left(1 - \frac{\max(\min(h, h_c), h_s) - h_s}{h_c - h_s}\right)(n_s - n_c) + n_c \quad (3)$$

In Equation 3, h_c is the minimum concentrated flow depth, h_s is the maximum sheet flow depth, n_c is the Manning's n for concentrated flow, and n_s is the Manning's n for sheet flow. Using the values given in Jia et al. (2023), the following values are used in Equation 3: $n_c = 0.1$, $n_s = 0.03$, $h_c = 0.01m$, and $h_s = 0.001m$.

The surface water depth is updated based on the flow discharge using Equation 1. This is done using a 2D version of Equation 4 below, which is represented in 1D for simplicity as was done in de Almeida (2012).

$$y_{node}^{N+1} = y_{node}^{N} + \frac{\Delta t}{\Delta x}\left(Q_{right}^{N+1} - Q_{left}^{N+1}\right) \quad (4)$$

After the surface water depth is updated using Equation 4, the other parameters used in the equations are updated and the process is repeated.

When designing hydrological models, it is important for modern models to be able to autonomously determine the best timestep size. A dynamic timestep calculator

that determines the timestep size is included in OverlandFlow, and it is shown in Equation 5.

$$\Delta t = \frac{C_t \Delta x}{\sqrt{g h_{max}}} \tag{5}$$

In Equation 5, h_{max} is the maximum water depth within the simulation and C_t is a constant. By default, $C_t = 0.7$ but it can be adjusted with user input.

Brief evaluation of hydrological model

The methods implemented in Landlab's OverlandFlow module are difficult to test and verify since there are no images representing the surface water depth of the flume. However, the observed surface water runoff at the outlet is shown in Figure 2, and a simple test can be performed using 105 mm/hr rainfall to evaluate the match between simulated and measured. Performing such a simulation over the course of 5 minutes returns runoff rates near 30 L/min (Figure 4). Comparing the results of Figure 4 with Figure 2 demonstrates the agreement between simulated and observed values.

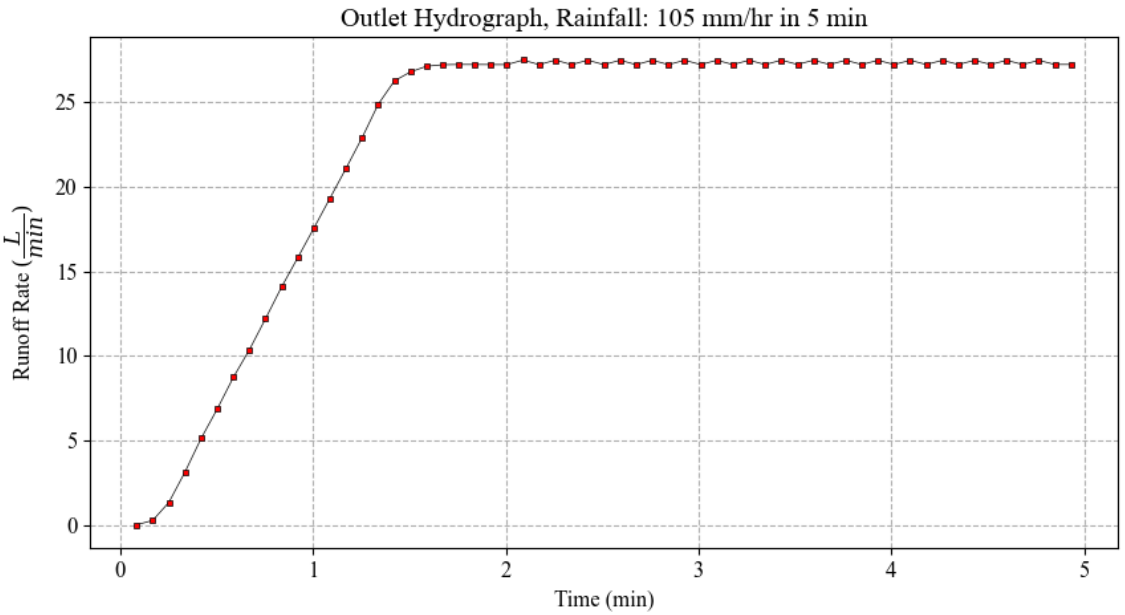

Figure 4

Surface water runoff over the topography shown in Figure 1 over the course of five minutes

Note: The hydrograph's points were recorded in 5 second intervals.

CHAPTER IV

EROSION MODELS

Overview of models

Many equations are presented in this study, so Table 1 is presented to break down the organizational structure of the model. In Table 1, the models are simple broken down into two models labeled Model 1 and Model 2. Each model has a subset of equations tested in it, and they have the same hydrodynamics model. However, Model 1 uses a simple equation where topographic elevation is adjusted using an empirical equation. Model 2 uses a numerical sediment transport model to adjust sediment concentration and topographic elevation in the simulation using sets of empirical erosion and deposition terms.

Table 1

Models presented in this study

Model Name	***Equation Name***	
Model 1	1.1.	Rillgrow erosion
	1.2.	Detachment limited erosion
	1.3.	Integrated Rillgrow and Detachment limited erosion
Model 2	2.1.	Shields erosion
	2.2.	Curvature erosion
	2.3.	Shields erosion with deposition
	2.4.	Curvature erosion with deposition
	2.5.	Integrated transport capacity erosion and deposition

The models that are designed to operate on a dynamic timescale determined by the spatial resolution of the input data. The empirical equations used are designed for specific timescales and spatial resolutions, but they can easily be replaced with other equations for different spatial scales and timescales. This study uses a spatial scale such that the timescale of the dataset is over the course of a few hours. This adjustability of the dynamic timestep is useful when compared to other models such as RUSLE2 and RillGrow which operate over the course of decades or a few minutes.

Evaluation and customization of existing erosion models (Model 1)

Development

Rill erosion (Model 1.1)

RillGrow is used as a basis for the development of the rill erosion equations. However, there are two versions of RillGrow that needed to be understood to model the erosion: RillGrow 1 and RillGrow 2. RillGrow 1 is a cellular automata model that drops raindrops on a topographic grid and calculates raindrop flow and rill erosion per raindrop using simple erosion equations (Favis-Mortlock, 1998). This operates by calculating the slope between the current cell and the lowest surrounding cell before calculating the stream power ω and unit sediment load q_s shown in Equation 6 and Equation 7 below.

$$\omega = \rho_w g S q \tag{6}$$

$$\log(\mathrm{q_s}) = \frac{\alpha + \beta e^{\gamma + \delta \log(\omega)}}{1 + e^{\gamma + \delta \log(\omega)}} \tag{7}$$

In Equation 6, ρ_w is the density of water, S is the slope gradient, and q is the unit flow discharge. In Equation 7, α, β, γ, and δ are best fit parameters (Nearing et al., 1997). After calculating the unit sediment load, RillGrow 1 calculates the soil depth change $\frac{dz}{dt}$ of the topography due to erosion using Equation 8.

$$\frac{dz}{dt} = \frac{q_s L_S}{\rho_b V \Delta \mathrm{x}} \tag{8}$$

In Equation 8, L_S is the slope length, ρ_b is the soil bulk density, and V is the runoff velocity. The next time is solved from $\frac{dz}{dt}$ using the Euler method $\frac{dz}{dt} = \frac{z^N - z^{N-1}}{\Delta t}$.

It is worth noting that the runoff velocity V is calculated empirically in RillGrow. In this study it is derived from the hydrodynamic calculations in Landlab's overland flow module. It can be calculated using Equation 9 below on the links, ensuring that the water flow depth used is from the previous time since a small flow depth at the current time can cause erroneous discharge calculations.

$$V_L^n = \frac{Q_L^n}{h_f^{n-1}} \tag{9}$$

RillGrow 2 is the successor to RillGrow 1 with improvements to the formulations and computational efficiency. A primary difference between RillGrow 1 and RillGrow 2 is that RillGrow 2 operates in a real-time domain by dropping raindrops in packets that process synchronously. This makes the results more realistic and more easily translatable to real-world applications. Another major difference is that RillGrow 2 implements the depth attenuation to the unit sediment load shown in Equation 10.

$$q_{att} = \mathrm{q_s} e^{[kh(\epsilon - h)]} \tag{10}$$

In Equation 10, q_{att} is the attenuated unit sediment load, k is a constant and ϵ is the effective water depth. The constant k and the effective water depth ϵ are not provided so they must be determined through calibration. Since RillGrow 1 and RillGrow 2 are modeled using cellular automata, Equations 6 through 10 are implemented with the Landlab hydrology to erode the surface.

Landscape evolution (Model 1.2)

The DetachmentLtdErosion class in Landlab is used in this study to describe landscape evolution (Barnhart et al., 2020; Hobley et al., 2017; Hutton et al., 2020; Howard, 1994). The class operates in the same manner as the rill erosion where erosion is calculated at every time step using simple empirical formulas. Equations 11 and 12 below describe the equations used in the landscape evolution formulation.

$$I = \max\left[(K_{sp} Q^{e_Q} S^{e_S} - T), 0\right] \tag{11}$$

$$\frac{dz}{dt} = (U - I) \tag{12}$$

In Equation 11, I is the incision rate, K_{sp} is the stream power constant, T is the entrainment threshold, and e_Q and e_S are the exponents for the flow discharge and slope. In Equation 12, U is the uplift rate, and $\frac{dz}{dt}$ is solved with the Euler method. These two equations are used together to update the system of landform evolution equations.

Integrated rill and landscape evolution (Model 1.3)

A formulation for combining the equations of RillGrow and DetachmentLtdErosion is proposed since RillGrow is intended to model rill erosion and DetachmentLtdErosion is intended to model drainage basin evolution (Favis-Mortlock, 1998; Howard, 1994). Equation 13 shows the mathematics used to combine the equations with the generic variable X, the mixing function value M, and the fitting parameters A and B.

$$M_X = \frac{\arctan\left(-A \cdot (X - B)\right)}{\pi} + 0.5 \tag{13}$$

Figure 5 shows some graphical examples of the mixing function after calibration, with a value of 1 meaning only rill erosion and a value of 0 meaning only the landform erosion. The water depth and slope are used to determine which erosion is dominant since they have a strong correlation with the flow regime, and they are combined using Equation 14.

$$M_{S,h} = M_S M_h \tag{14}$$

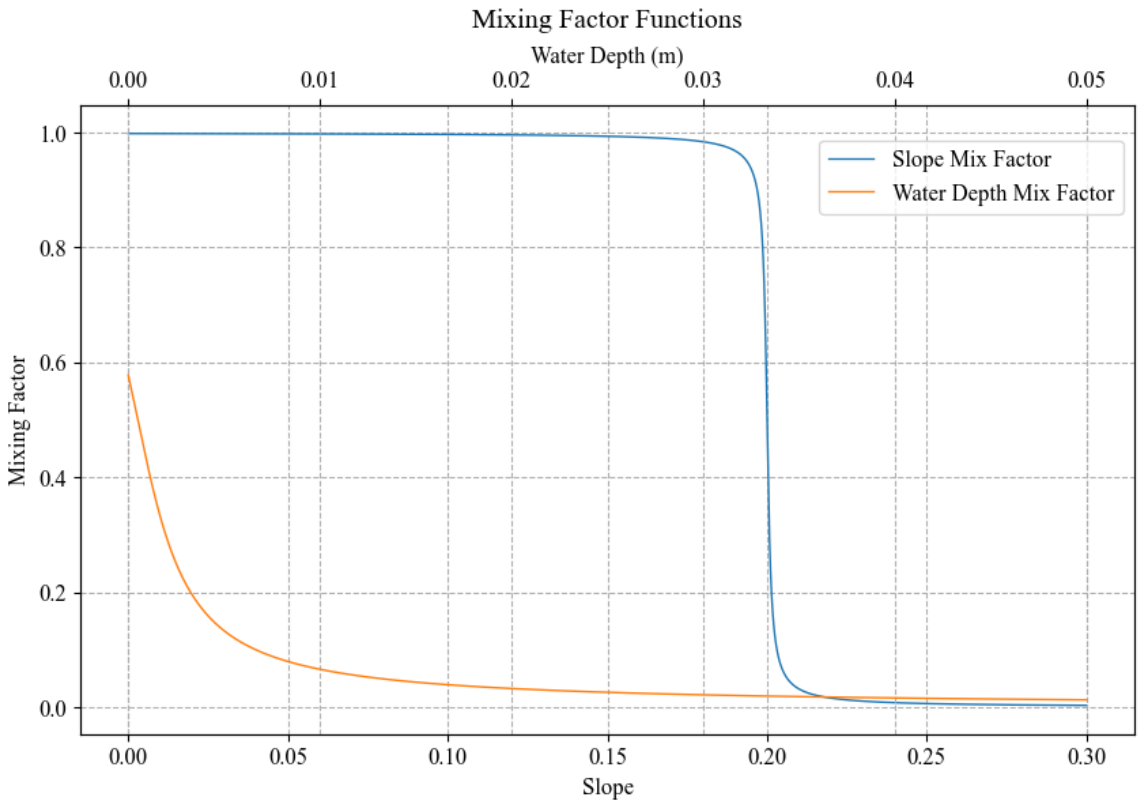

Figure 5

Mixing functions of slope and height using Equation 13

Note: In this image, $(A, B) = (500, 0.0005)$ for the water depth mixing factor, and $(A, B) = (1000, 0.2)$ for the slope mixing factor.

When using Equation 13, values for A and B need to be established as in Figure 5. For the water depth mix factor, B is set to 0.0005m since the rill erosion is expected to quickly fall off as water depth increases and leads to gully erosion and landscape evolution. The value of A is set to 500 after adjusting the function such that the landscape evolution is nearly negligible at near-zero water depths and rill erosion is nearly negligible after 0.02m of water depth. For the slope mix factor, a steep tradeoff is

imposed at a 20% slope with $(A, B) = (1000, 0.2)$. This is because the validity of Equation 7 is unknown for slopes above 20% (Nearing et al., 1997). and because water flow is expected to cause downcutting at steeper slopes and quickly form gullies.

Calibration

These formulations are manually calibrated by comparing the simulated sediment discharge against the observed sediment discharge in Figure 2 and visually comparing the geomorphology. The calibration is kept simplistic in this manner since the simulations have large runtimes and the behavior of each equation is not necessarily the same, making it challenging to automate the process in an efficient manner. The rill erosion is calibrated first by varying k and ϵ in Equation 10. The landscape evolution is then calibrated next by adjusting the value of K_{sp}, leaving $e_Q = 0.5$, $e_S = 1$, and $U = 0$ according to the default values provided (Barnhart et al., 2020; Hobley et al., 2017; Hutton et al., 2020; Howard, 1994). This is done to simplify the calibrations since no uplift rate is assumed and there is not much motivation to try and recalibrate the exponential constants; furthermore, the high computational time of the simulation makes it slow to recalibrate multivariable systems within a reasonable time frame. After the rill erosion and landscape evolution are calibrated, the calibrated results are integrated using Equations 13 and 14.

Evaluation

The rill erosion, landscape evolution, and integrated rill and landscape evolution all have their sediment discharge and geomorphology compared to the observed results after calibration. For the sediment discharge, the R^2 will be calculated to numerically

assess the accuracy of the results. The geomorphology of the simulations require a more thorough analysis due to its complicated nature. First, select cross-sections of the simulated results are compared to those from the observed surfaces to assess the accuracy of each formulation. Next, the soil loss between the current surface and the prior time's surface is calculated, and the NSE is calculated for the simulated to numerically assess of the accuracy of the geomorphology. Lastly, the average cross section of the simulation's rows and columns are compiled and the R^2 is calculated to assess how well the model matched the average vertical and horizontal profile.

Proposed erosion model (Model 2)

Mathematical formulation

The proposed methodology is based on the finite element methodology presented by other studies (Jia & S.Y. Wang, 2001; Lai, 2020). The formulation for the finite element methods are modified to operate with the Landlab grid structure (Figure 3) because the grid was developed with functions supporting operations on it, streamlining the mapping of OverlandFlow parameters between nodes and links. Since limited documentation is available describing the sediment transport equations, a novel set of equations and mappings is proposed.

Sediment transport and elevation change

The differential equations for sediment transport and elevation change are well documented in literature (Jia & S.Y. Wang, 2001; Lai, 2020), and they are defined in Equation 15 and Equation 16 respectively.

$$\frac{1}{V_b}\frac{\partial s}{\partial t} + \nabla \cdot \vec{s} = -(E + D) + s_I \tag{15}$$

$$\rho_b \frac{\partial z}{\partial t} = E + D - s_I \tag{16}$$

In Equation 15 and Equation 16, s is the sediment transport rate, $\vec{s}$ is a vector composed of the x and y components of the sediment transport rate s_x and s_y, E is the erosion, D is the deposition, s_I is the sheet and splash effects, and V_b is the bed flow velocity. One feature to note about Equation 15 is that $\nabla \cdot \vec{s}$ represents the flux of the sediment transport rate at any given location, and the flux requires finite element methodologies to be correctly solved.

Using finite element methodology presented in studies (de Almeida et al., 2012; Lai, 2020) with the Euler method, Equation 12 and Equation 13 can be rewritten into Equation 17 and Equation 18.

$$\frac{1}{V_b}\frac{(s^{N+1} - s^N)}{\Delta t} + \frac{1}{\Delta x}[\sum_{i=1}^{4} \vec{s}_i \cdot \hat{n}_i] = -(E + D) + s_I \tag{17}$$

$$\rho_b \frac{(z^{N+1} - z^N)}{\Delta t} = E + D - s_I \tag{18}$$

In Equation 17 $\hat{n}$ represents the unit normal vector at a grid cell boundary and the subscript i represents a link at the grid cell. Equation 17 and Equation 18 can be solved for s^{N+1} and z^{N+1} to update the time of the simulation. Due to the structure of Landlab's raster grid, $\hat{n}$ is always either entirely vertical or entirely horizontal, making the normal

vector's mathematics very simple. At boundaries, the sediment transport rate at the links should be 0, so no special boundary corrections are required.

The timesteps for this model are computed differently than the OverlandFlow timestep model used in Equation 5. This is because the sediment transport speed is dependent on the velocity, and it is important that the timestep is taken based on maximum flow speed in the simulation. Due to this concern, a separate timestep equation is used to calculate the timestep size for the sediment transport model, and it overwrites the timestep OverlandFlow uses in Equation 5. The timestep equation used for the sediment transport model is shown in Equation 19 (Simpson & Castelltort, 2006).

$$\Delta t = \frac{C_t \Delta x}{|V|_{max}} \tag{19}$$

In Equation 19, $|V|_{max}$ represents the maximum speed in the simulation. For this timestep, $C_t = 0.5$ so that the timestep size only allows the flow at the fastest point to move half the width of a grid cell.

Sediment transport rate and upwind scheme

Due to the flux term in Equation 15, there needs to be a set of equations to calculate the sediment transport rate in the x and y directions to calculate the flux. This can be done by using Equation 20.

$$(s_x, s_y) = \Psi h * (V_x, V_y) \tag{20}$$

In Equation 20, Ψ is the sediment concentration in the water. The sediment concentration is tracked by instantiating the variable with zero at all locations, and then updating the

sediment concentration to the current time using the updated sediment transport rate. The sediment concentration must be mapped from the nodes onto the links to calculate the flux since the sediment transport rate and the sediment concentration are stored on the nodes; this is done by using an upwind scheme.

An upwind scheme is implemented in sediment transport modeling to prevent the sediment concentration of downstream nodes from affecting the upstream nodes. In this model, a simple upwind scheme is used where the sediment concentration of a link is equivalent to the sediment concentration of the upstream node. This sediment concentration is then used to calculate the sediment transport rate at the link. The sediment transport rate is then used to calculate the fluxes at the adjacent nodes.

Bed velocity

In this model, the bed velocity is assumed to be the same as the runoff velocity since they should be similar for shallow water flow. The velocity is calculated using Equation 9. The velocity on the links is then mapped onto the nodes for Equation 17 by first calculating the velocities in the x and y directions on the node. This is done by taking the weighted average of the velocities on the links in the horizontal and vertical directions based on the discharge magnitude. The magnitude of the velocity at the node is then calculated from the x and y velocities to obtain the runoff velocity used on the nodes.

Erosion

Two erosion equations are tested in this study. The first equation (Model 2.1) shown in Equation 21 operates on the nodes of the grid, and it is a modification to a basic form of a bed shear stress equation commonly found in literature (Rinaldi et al., 2008).

$$E = -\max[\mathrm{K}(\theta - \theta_c), 0] \quad (21)$$

In Equation 21, K is a calibration constant, θ is the Shields parameter, and θ_c is the critical Shields parameter. The Shields parameter in this equation is meant to represent the forces on the bed, and erosion can only occur when the forces on the bed exceed the critical force required to displace sediments represented with the critical Shields parameter. This equation is also commonly represented using the bed shear stress and the critical bed shear stress, and it is easy to translate Equation 21 into such a form.

Equation 21 is a simple calculation, but there is one problem with calculating the erosion resulting from it on the nodes: the critical shields parameter is calculated on the links, while the shields parameter is calculated on the nodes. A correction for this can be performed by subdividing each grid cell into four parts with x and y components from the nearest vertical and horizontal link and calculating the shields parameter at each of the cell corners. Equation 18 is then calculated and averaged on each subdivided grid cell using the critical shields parameters at the two nearest links. Lastly, the shields parameter calculated at each of the grid cells is averaged onto the node to get a more accurate representation of erosion. The motivation for this calculation is to prevent the inaccurate overestimation or underestimation at the node due to errors introduced when trying to map critical shields parameters from the links to the nodes.

The second erosion equation (Model 2.2) used is one that is developed based on observations of gully development, and the proposed equation operates on the links instead of the nodes. It is shown in Equation 22.

$$E = -\mathrm{C}[|SQ| * \Lambda + |SQ_P| * \Lambda_P] \tag{22A}$$

$$\Lambda = \begin{cases} 1 \; if \; |\kappa SQ| - \gamma > 0 \\ 0 \; otherwise \end{cases} \tag{22B}$$

$$\Lambda_{\mathrm{P}} = \begin{cases} 1 \; if \; |\kappa SQ_P| - \gamma > 0 \\ 0 \; otherwise \end{cases} \tag{22C}$$

In Equation 22, C and γ are calibration constants, κ is the curvature of the topography, Λ and Λ_P are binary parameters, and Q_P is the flow discharge perpendicular to a link. Q_P is calculated by mapping discharges in the x and y direction onto the node, and then calculating the average discharge in the perpendicular direction to the link at the head and tail of the link.

The motivation for the development of Equation 22 is to try and target locations where headcut erosion occurs since headcut tend to evolve the fastest in regions with high topographic slope, high topographic curvature, and high flow discharge. Perpendicular flow discharge is implemented in a preliminary attempt to account for lateral erosion. The binary parameters in Equation 22B and Equation 22C are implemented to enable stronger control over the strength of the erosion with the parameter C.

A major issue with erosion formulations such as this is how holes tend to develop where they are not desirable. The presented erosion equations are all subject to the same conditions that they only erode when the elevation of the current node is greater than at least one of the surrounding nodes. This is a fairly easy way to account for the erosion that is true most of the time. However, greater accuracy could be achieved with a more elegant solution in some flow cases.

Bed shear stress and Shields parameter

Equation 21 requires a formulation to calculate the Shields parameter, which is reliant upon the bed shear stress. This is a difficult step since the bed shear stress is fully empirical, and different equations succeed in different flow scenarios (Biron et al., 2004). After analyzing the different forms of equations and testing candidates against expected values (Yang, 2010), it is determined that the bed shear stress calculations based on the logarithmic law were best in this flow scenario. This is because it makes no assumptions about the hydraulic radius and it does not rely on turbulent velocity data. The downsides to this method are that it is computationally inefficient since it requires an implicit solution, and it assumes a logarithmic vertical velocity profile. This assumption is accurate in open channels and smooth flow surfaces, but it may not be accurate for rill or headcut erosions.

The equations described for calculating the bed shear stress were implemented by Jia & S.Y. Wang (2001). First, the bed shear stress equations for the x and y direction are described in Equation 23.

$$\left(\tau_{b,x}, \tau_{b,y}\right) = \frac{\rho_w f_c V}{8}\left(V_x, V_y\right) \tag{23}$$

In Equation 23, V_x and V_y are the runoff velocity in the x and y direction and f_c is the Darby-Weisbach coefficient. This coefficient has no explicit solution when using the logarithmic law for the velocity profile, so it is solved implicitly with Equations 24 through 26 (Jia & S.Y. Wang, 2001).

$$f_c = \begin{cases} \dfrac{8}{\sqrt{3 + 2.5ln\left(\frac{V_\star h}{\nu}\right)}}, & \dfrac{V_\star k_s}{\nu} \leq 5 \\ \dfrac{8}{\sqrt{6 + 2.5\ln\left(\frac{h}{k_s}\right)}}, & \dfrac{V_\star k_s}{\nu} \geq 70 \\ \dfrac{8}{\sqrt{6 + 2.5\ln\left(\frac{h}{k_s + 3.3\frac{\nu}{V_*}}\right)}}, & 5 < \dfrac{V_\star k_s}{\nu} < 70 \end{cases} \tag{24}$$

$$\frac{V}{V_*} = \frac{1}{h}\left[\frac{z_o}{h} - 1 + \ln\left(\frac{h}{z_o}\right)\right] \tag{25}$$

$$z_o = \begin{cases} 0.11\dfrac{\nu}{V_*}, & \dfrac{V_\star k_s}{\nu} \leq 5 \\ 0.0333k_s, & \dfrac{V_\star k_s}{\nu} \geq 70 \\ 0.11\dfrac{\nu}{V_*} + 0.0333k_s, & 5 < \dfrac{V_\star k_s}{\nu} < 70 \end{cases} \tag{26}$$

In Equations 24 through 26 above, $V_\star$ is the shear velocity at the bed, k_s is the bed roughness height, ν is the kinematic viscosity of water, and z_o is a flow parameter used to determine if the flow is smooth, rough, or transitional. The bed roughness height is assumed to be the same as the sediment diameter in this case since the bed roughness height should be constant in sheet flow (Zuo et al., 2022); however, the exact equation to calculate bed roughness height in sheet flow is not easily available in literature. The Darby-Weisbach coefficient is implicitly solved using the bisection method on Equations 24 through 26 with a precision of 0.01.

Once the bed shear stress has been calculated, the Shields parameter is simple to find using Equation 27 (Lai, 2020).

$$\theta = \frac{\tau_b}{\rho_w g \left(\frac{\rho_s}{\rho_w} - 1\right) d} \tag{27}$$

In Equation 27, ρ_s is the sediment density and d is the sediment diameter. This equation works since this model only considers a singular sediment diameter; more complicated sediment profiles require more complicated methods of converting between the Shields parameter and the bed shear stress.

Lastly, the critical Shields parameter needs to be calculated to be used with Equation 27 and Equation 21. The critical Shields parameter is calculated using Equation 28 and Equation 29 in this model (Jia & S.Y. Wang, 2001).

$$\theta_c = \begin{cases} 0.24 D_*^{-1}, & 1 < D_* \leq 4 \\ 0.14 D_*^{-0.64}, & 4 < D_* \leq 10 \\ 0.04 D_*^{-0.1}, & 10 < D_* \leq 20 \\ 0.013 D_*^{0.29}, & 20 < D_* \leq 150 \\ 0.055, & D_* > 150 \end{cases} \tag{28}$$

$$D_* = d \left(\left(\frac{\rho_s}{\rho_w} - 1 \right) \frac{g}{\nu^2} \right)^{\frac{1}{3}} \tag{29}$$

In Equation 28 and Equation 29, $D_\star$ is a dimensionless parameter that is used to determine the soil detachment conditions in an area. The critical shields parameter is correct for surfaces with 0% slope. However, the critical Shields parameter needs to be corrected for sloped surfaces, and that is done using Equation 30.

$$\theta_c = \Theta_1 \Theta_2 \theta_{c,f} \tag{30A}$$

$$\Theta_1 = \begin{cases} \dfrac{\sin(\phi - \beta_1)}{\sin(\phi)}, & Downslope\ flow \\ \dfrac{\sin(\phi + \beta_1)}{\sin(\phi)}, & Upslope\ flow \end{cases} \tag{30B}$$

$$\Theta_2 = \cos(\beta_2)\left[1 - \left(\frac{\tan^2 \beta_2}{\tan^2 \phi}\right)\right]^{0.5} \tag{30C}$$

In Equation 30, Θ_1 and Θ_2 are correction coefficients, ϕ is the angle of repose of the soil, β_1 is the slope in the direction of flow, and β_2 is the slope perpendicular to the direction of flow.

Deposition

The deposition term used is based on the transport capacity and adaptation length of the flow, and it is given by Equation 31 (Jia et al., 2023).

$$D = \frac{s - T_c}{L_D} \tag{31}$$

In Equation 31, T_c is the transport capacity and L_D is the adaptation length for deposition. This form of the deposition equation is motivated by the concept that any sediment in the water over the transport capacity should deposit out of the water and back on the bed within a certain distance. The primary difficulties associated with this form of the deposition equation are that the transport capacity is difficult to verify for the flow conditions used and the adaptation length is not a well-known parameter.

Integrated Erosion and Deposition

In Jia et al. (2023) the erosion and deposition are integrated into a single equation (Model 2.5) in the form of Equation 31, except with some modifications as is shown in Equation 32.

$$E + D = \frac{s - T_c}{L_{comb}} \tag{32}$$

In Equation 32, L_{comb} is the combined adaptation length for erosion and deposition.

Transport capacity and adaptation length

The transport capacity is heavily influenced by the sediment diameter, the flow depth, and the flow discharge of the hydrology, making it difficult to find specific equations that work well for models. After thoroughly examining different equations' valid ranges and testing the results they return against existing data, Equation 33 is decided to represent transport capacity for this study (Li et al., 2023; Wang et al., 2015; G. Zhang et al., 2009; K. Zhang et al., 2021).

$$T_c = 0.054\tau_b^{1.982} \tag{33}$$

The adaptation length is similarly studied, but unlike the transport capacity, there are very few simple equations to determine the adaptation length and there is no data to verify the parameter against. As such, a simple equation for the adaptation length is implemented after being modified for deposition, and it is given in Equation 34 (Lai, 2020).

$$L_D = C_{si}\theta d \tag{34}$$

In Equation 34, the C_{si} is a model constant which is set to $C_{si} = 4000$ based on the Lai (2020). The adaptation length for erosion and deposition is defined in a similar way as Equation 34 in Equation 35.

$$\begin{cases} L_D & if\ s > T_c \\ C_{si}(\theta - \theta_c)d & if\ s < T_c \end{cases} \tag{35}$$

Sheet and splash

The sheet and splash equation used is given in Equation 36 (Jia et al., 2023), and it is constructed as a combination of raindrop impact and sheet flow with a correction for downslope sediment transport.

$$s_I = C_0 E_I \left[\frac{V_b}{\max(h, h_s)} + \alpha_{st}\left(1 - e^{-2.2\tan(J_b)}\right) \right] \tag{36}$$

$$E_I = \min\left(1, \frac{h_0}{h}\right)^b I_R^p \tag{37}$$

In Equation 36, C_0 is a combined coefficient for calibration, E_I is soil detachment by rainfall impact, α_{st} is a calibration coefficient for adjusting downslope sheet flow strength. In Equation 37, h_0 is the break point depth, I_R is the rainfall intensity, and b and p are exponents for calibration. Based on the values provided in the source of the equations, the following variables are set: $b = 1.5$, $p = 2$, and $h_0 = 0.001m$.

Calibration

Only erosion

There are multiple terms that need to be calibrated in Equation 15, so the initial calibration of the model is performed by setting the erosion and deposition terms to zero,

setting elevations equal to or below the outlet elevation to be non-erodible, and calibrating the sheet and splash erosion. The calibration is done by comparing the percentage of sediment discharge at the first timestep with the mass eroded percentage in Figure 9 in Momm et al. (2018) for raindrop and sheetflow erosions combined. This step of calibration allows the analysis of the sheet and splash erosion term's success without influence from other forms of erosion or deposition, and it simplifies the calibration of the rosionn term. After calibrating the sheet and splash erosion, the shear stress erosion in Equation 21 and the curvature-based erosion in Equation 22 are calibrated while leaving the sheet and splash constant. This is done by manually adjusting the K and the C and γ until the sediment discharge of the simulations roughly match the observed sediment discharge in Figure 2.

Erosion and Deposition

After the erosion is calibrated using the methods described, the deposition is enabled, and results are compared. Little calibration is expected in this stage since the erosion with deposition should be close to the calibration without deposition.

Evaluation

The evaluation of Model 2 is the same as the evaluation of Model 1.

CHAPTER IV

DISCUSSION AND RESULTS

Sediment load over time

Rill (Model 1.1)

Initially RillGrow 1 equations were used and tested to simulate the observed flume topography. The nature of these equations led to unrealistic results by generating parallel channels one raster grid cell wide. Alternatively, RillGrow 2 equations were implemented with changes to the depth attenuation leading to more realistic results. Upon implementing RillGrow 2, calibration became a necessity due to the variables in Equation 10. The constant k is varied freely since no starting value is provided (Favis-Mortlock, 1998), while the effective water depth ϵ is varied between 0cm and 10cm since the water depth is expected to be within that range. Upon performing the calibration, the results shown in Figure 6 are generated with $k = 5$ and $\epsilon = 0.1$ for the sediment load.

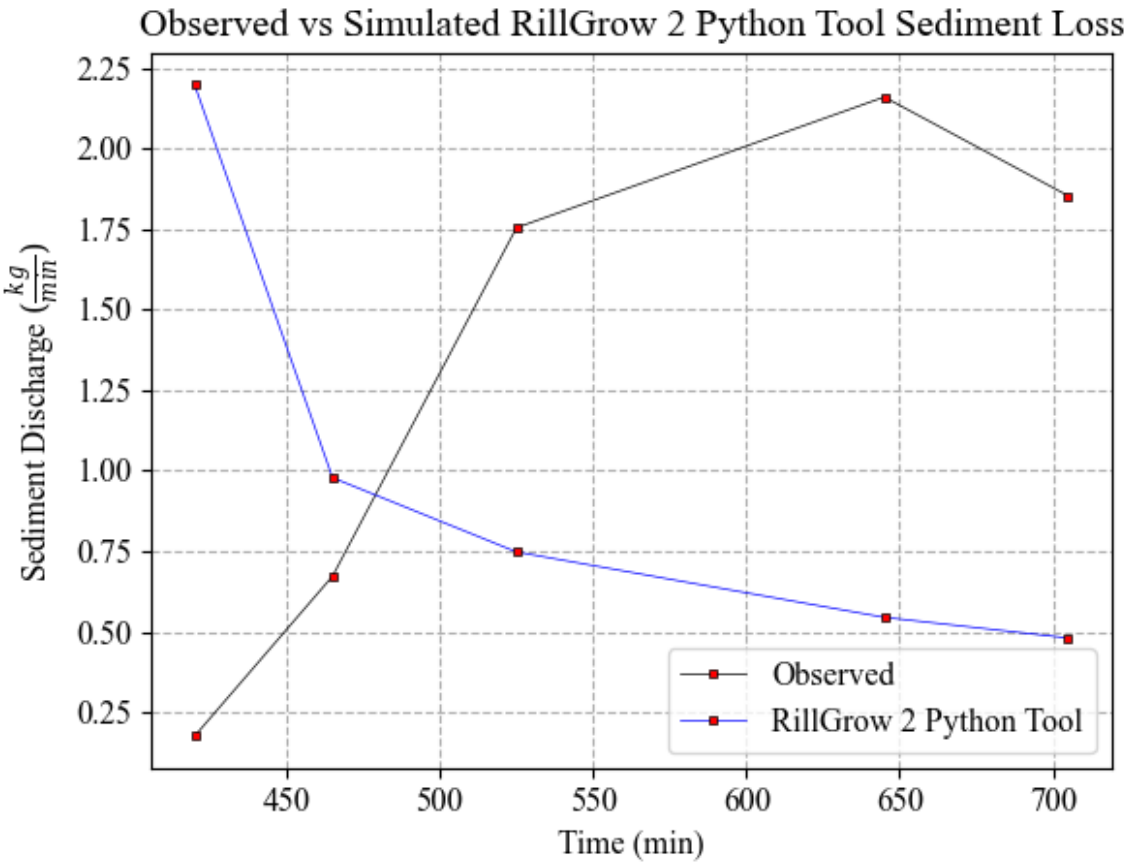

Figure 6

Sediment loss obtained with the formulation proposed in the RillGrow 2 erosion formulation

Note: Calibrated values of $k = 5$ and $\epsilon = 0.1$ compared with the observed sediment discharge.

The RillGrow erosion does not match the observed sediment discharge. It rather appears that the simulated erosion from RillGrow decreases over time while the observed data increases. This makes sense since the erosion is depth attenuated, which means that any erosion that would occur in concentrated flows, like gullies, is not well modeled with

this equation specifically formulated for rills. This is not an issue since the rill erosion is not expected to match the sediment discharge without other equations to model gully, sheet, and splash erosion.

Landscape evolution (Model 1.2)

Integrating the hydrodynamic model with equations from the landscape evolution improved the results. The parameter K_{sp} is manually calibrated to a value of $5x10^{-3}$ to obtain the results shown in Figure 7. The sediment discharge of the landscape evolution matches very well to the observed data, especially when compared to RillGrow's sediment discharge.

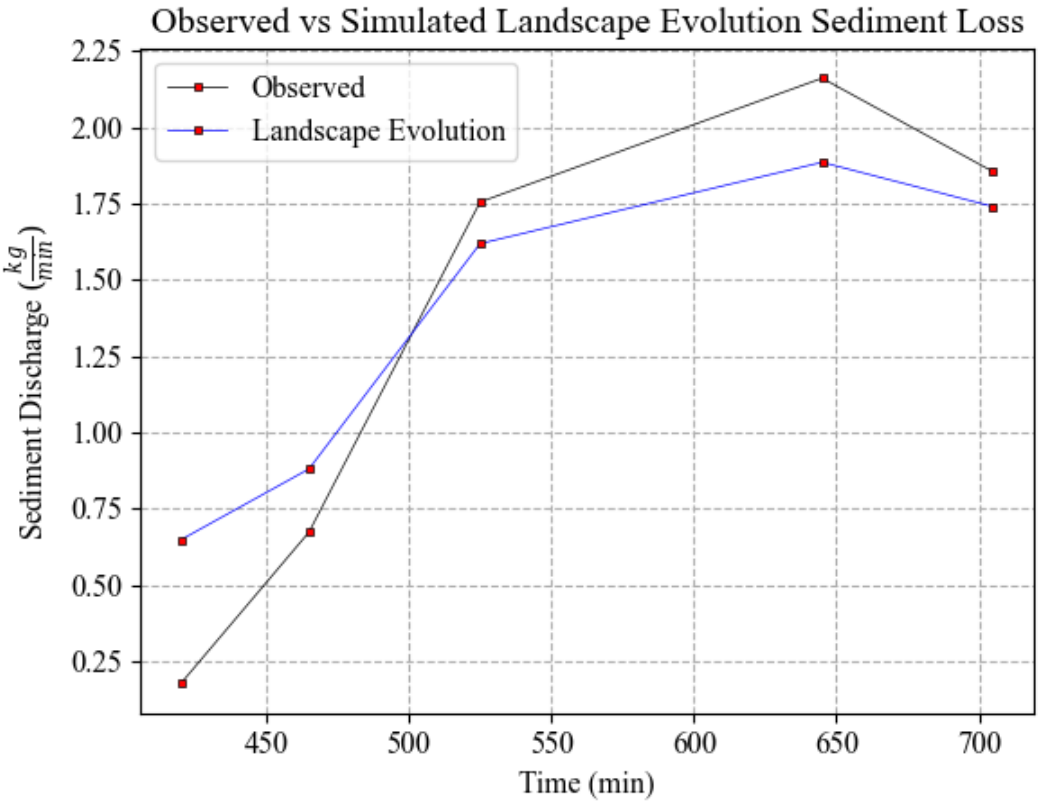

Figure 7

Sediment loss obtained with the landscape evolution formulation

Note: Calibrated values of $(K_{sp}, e_Q, e_S) = (5 \times 10^{-3}, 0.5, 1)$ compared with the observed sediment discharge.

It may be possible to improve the fit of the data by adjusting the exponents around the values used and testing for changes in the overall trend. However, this type of fit would be computationally expensive as it would increase the number of fitting parameters that are calibrated.

Integrated rill and landscape evolution erosion (Model 1.3)

After a minor recalibration where K_{sp} changed from $5x10^{-3}$ to $1x10^{-2}$, Figure 8 is generated. Figure 8 depicts a worse match than the sediment discharge of the landscape evolution formulation is on its own. This is likely due to water either flowing in main channels that have reached a bed minimum or flowing over shallow water areas where rill erosion causes little discharge. However, the shape shown in Figure 7 is maintained, indicating that it should be possible to mix the rill and landscape evolution formulations in such a way that better sediment discharge is obtained.

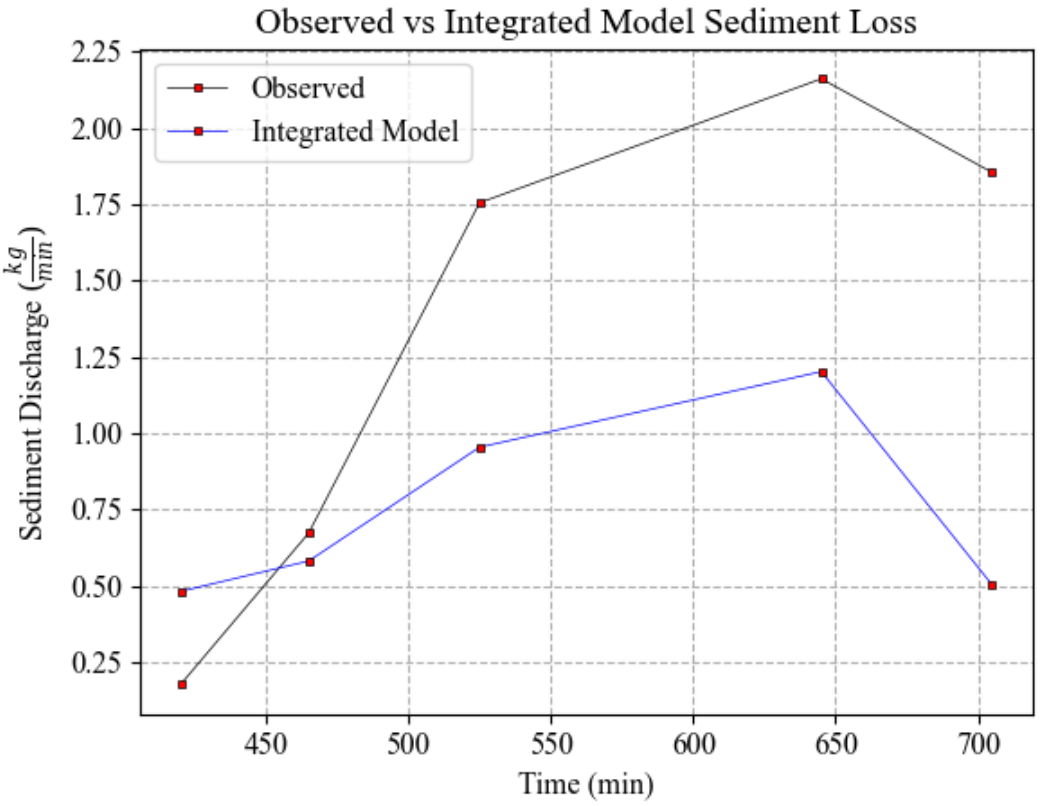

Figure 8

Sediment loss obtained with the integrated rill and landscape evolution

Note: K_{sp} recalibrated to $1x10^{-2}$ compared with the observed sediment discharge.

Proposed erosion model

Erosion (Models 2.1 and 2.2)

The plot of the sheet and splash calibration is first presented (Figure 9), obtaining the best results with a value of $C_0 = 40000$ while $\alpha_{st} = 1$ is imposed on the equation. Looking at Figure 9 and qualitatively comparing it with the percentage of mass lost by raindrop or sheetflow erosion in Figure 9 in Momm et al. (2018), it can be determined that Equation 36 and Equation 37 are not accurately representing the raindrop and

sheetflow erosion. This is because the observed mass loss percentage of raindrop and sheetflow erosion is approximately 50% for all timesteps.

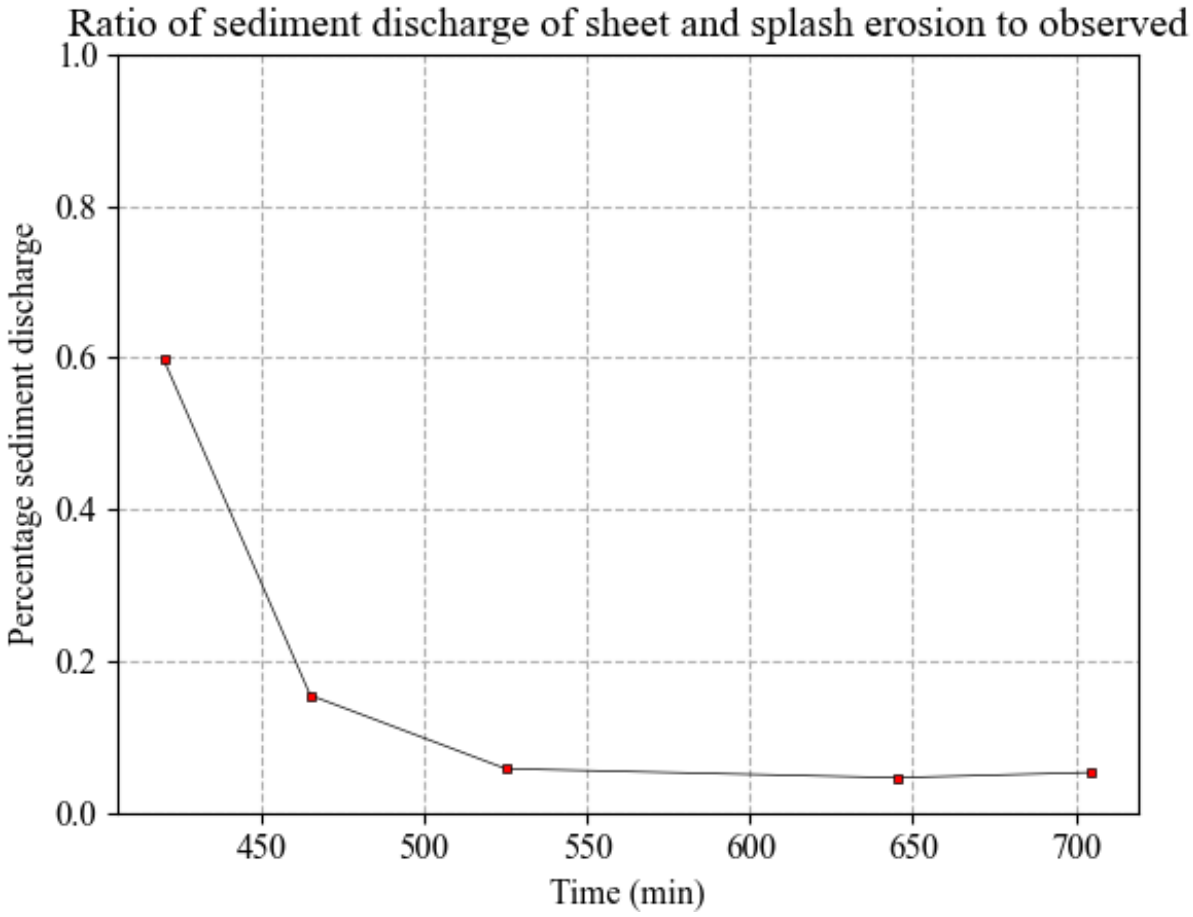

Figure 9

Ratio of sediment discharge simulated with only sheet and splash erosion to observed sediment discharge

Note: The sheet and splash coefficients are $(C_0, \alpha_{st}) = (40000,1)$.

Figure 9 demonstrates a quick decrease in the percentage of mass lost by raindrop and sheetflow erosion after the first timestep even when the first timestep is properly

calibrated. This is likely because the sheetflow erosion is dependent on the raindrop erosion in Equation 36. In the observed mass loss percentage, sheetflow erosion increases while raindrop erosion decreases, but in Equation 36, that is not possible since the sheetflow transport capacity and downslope adjustment are multiplied by the raindrop erosion. This means that a lower raindrop erosion leads to a lower sheetflow erosion, and as such it is not possible to match the identified sheet and splash erosion with Equation 36.

After calibrating the sheet and splash, Equation 21 is calibrated with a value of $K = 2.5$. The resulting plot of sediment discharge in Figure 10 demonstrates good results.

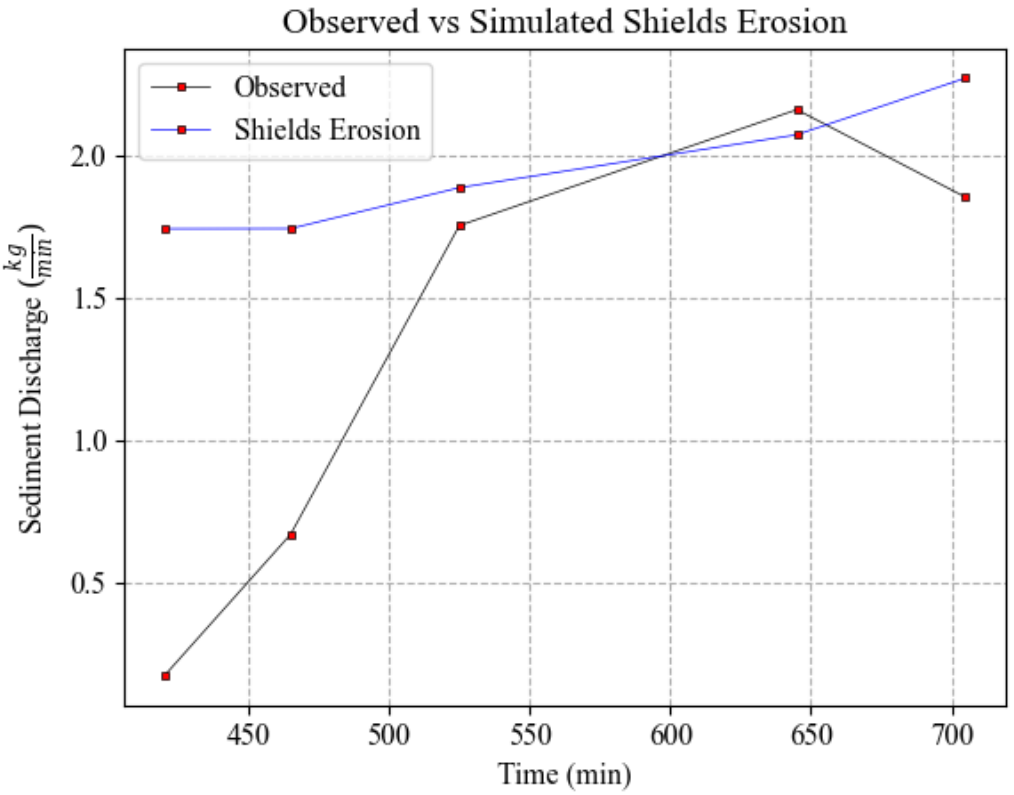

Figure 10

Comparison of sediment discharge between the observed data in Figure 2 and the simulated using model 2.1

Figure 10 shows that the erosion in Equation 21 is better than some results obtained by Model 1, but it is still lacking proper estimation of sediment discharge over time. This issue can be due to a combination of the inaccuracy of Equation 21 for matching the sediment discharge as well as the issue that the sheet and splash erosion is heavily underestimated at later times.

Next, C and γ from Equation 22 are calibrated to values of $(C, \gamma) = (2900, 1x10^{-6})$. The sediment discharge resulting from this calibration are shown in Figure 11.

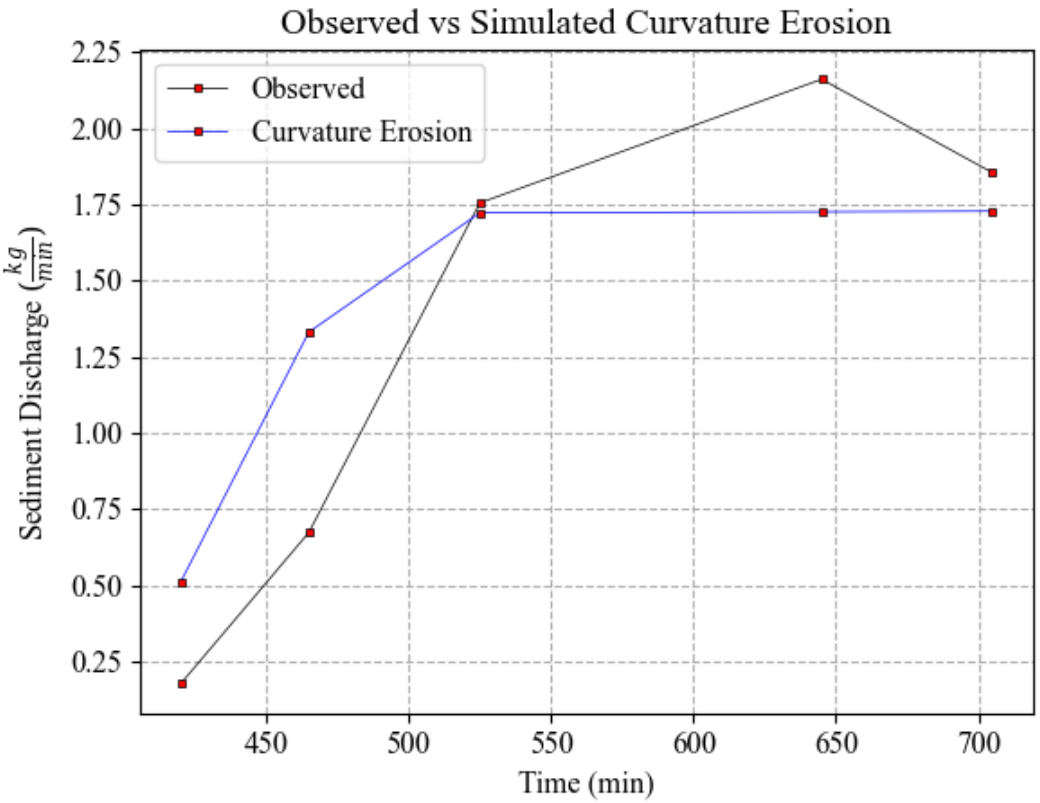

Figure 11

Comparison of sediment discharge between the observed data and the simulated using model 2.2

Figure 11 shows a much better match than the results in Figure 10 since the simulated curve appears to be a good fit to the observed sediment discharge. The primary issue with this simulated data is that there is an overestimation of erosion at earlier times and a slight underestimation at later times.

Erosion and deposition (Models 2.3 – 2.5)

Now that the erosion formulations have been tested independently of the deposition equation, the deposition equation is enabled, and the second model is tested again. First, the Shields equation calibrated as in Figure 10 is tested with deposition enabled. The results are shown in Figure 12.

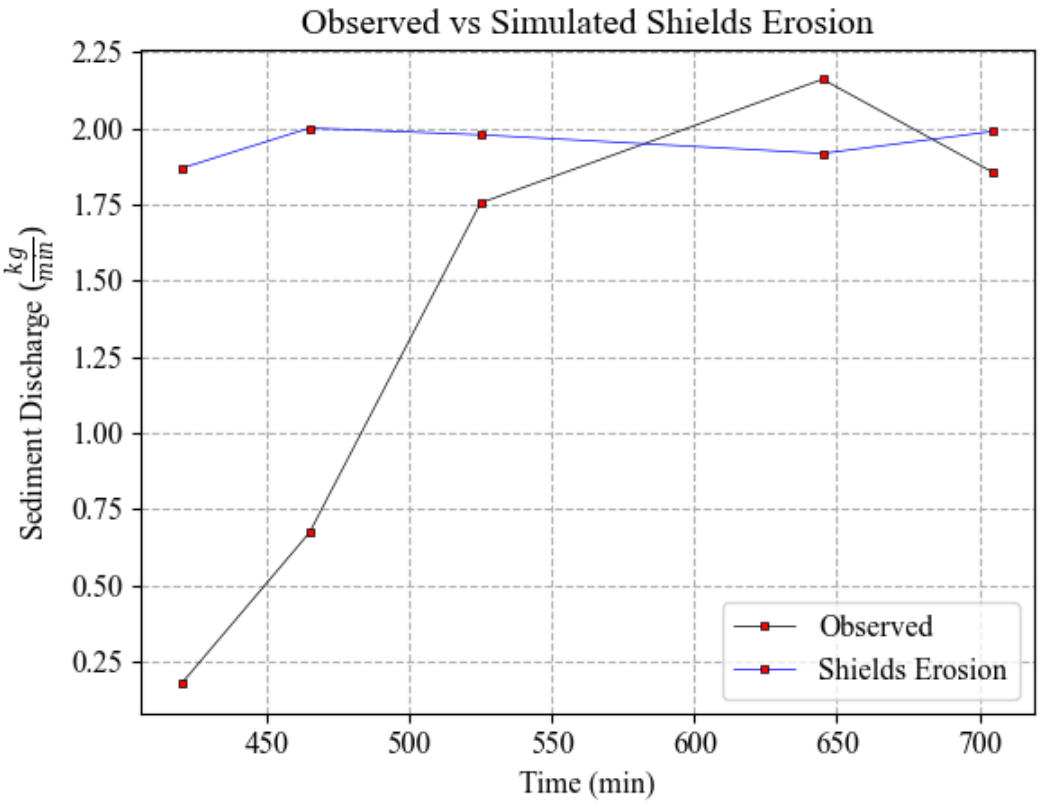

Figure 12

Comparison of sediment discharge between the observed data in Figure 2 and the simulated using model 2.3

Figure 12 shows a sediment discharge curve that has a trendline closer to zero than that of Figure 10. However, the values of the sediment discharge obtained did not

change very drastically; as such, a visual assessment of the formulation's performance is of little merit, and the numerical assessment of the change will be more enlightening of the effect of the deposition.

The curvature erosion as calibrated in Figure 11 is run with the deposition enabled next with the results shown in Figure 13. A brief recalibration of C is performed after initial runs, changing C from 2900 to 5500.

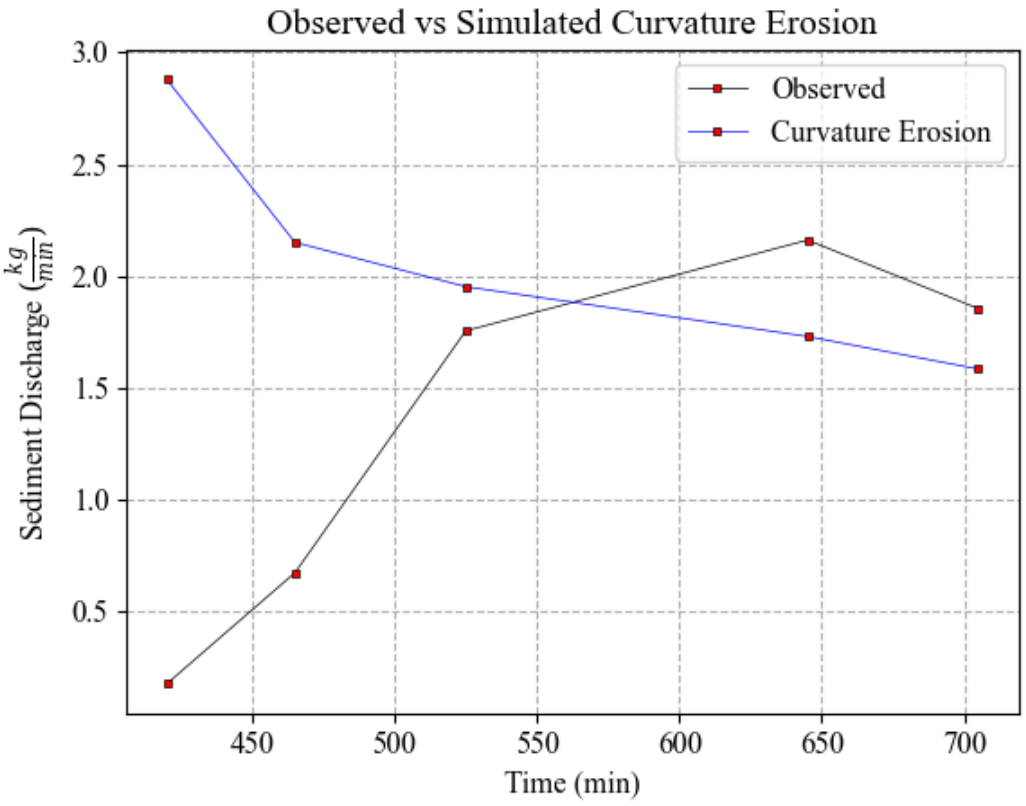

Figure 13

Comparison of sediment discharge between the observed data in Figure 2 and the simulated using model 2.4

The results in Figure 13 are noticeably different than those from Figure 11, unlike the change for the Shields erosion. The sediment discharge curve is significantly less accurate now since the first timesteps have a much higher sediment discharge with deposition enabled. This is a rather surprising result as it would be expected that enabling deposition would reduce the sediment discharge rather than encourage further detachment.

After running the simulations for the Shields and curvature equations again with the deposition enabled, the integrated erosion and deposition formulation is tested in Figure 14.

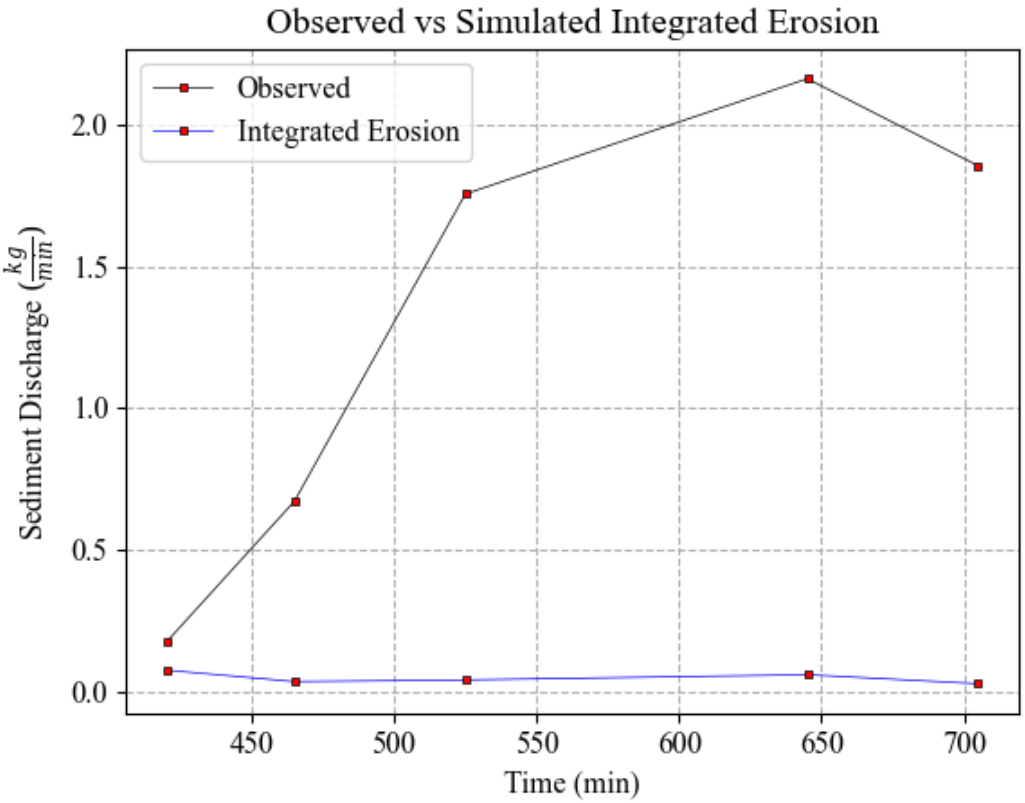

Figure 14

Comparison of sediment discharge between the observed data in Figure 2 and the simulated using model 2.5

Figure 14 demonstrates a clear underestimation of sediment discharge at all times. There are a couple reasons that this can be the case. The first reason could be that the Shields parameter may be too large and that can cause too much detachment in shallow regions, which would reduce detachment in the main channel. The other reason for this could be that the two-dimensional distribution of the transport capacity is incorrect, and it is too low in the main channel. This would cause the sediments flowing from the edges of the

simulation to fully saturate the main gully and prevent any significant detachment in it. Either way, it is clear that some values are not calibrated properly for this equation.

Numerical comparison of sediment load over time

The sediment load over time between the different models is numerically compared in Table 2. The results where only the erosion is enabled clearly indicate that the landscape evolution and curvature equations do the best at matching the observed data since they have moderately high R^2 values. On the other hand, the rill erosion does not match the observed sediment load, the integrated rill and landscape evolution formulation does slightly better, and the Shields erosion yielded least desirable results. Based on these results, the curvature and landscape evolution formulations generated the highest agreement in sediment load estimates when compared with observed and when deposition is not implemented.

Table 2

R^2 of sediment load over time for tested models

Category	Scenario	R^2
Baseline	No erosion	-3.01
Model 1	1.1. Rill	-2.33
	1.2. Landscape evolution	0.87
	1.3. Integrated rill and landscape evolution	-0.20
Model 2	2.1. Shields	-0.31
	2.2. Curvature	0.74
	2.3. Shields with deposition	-0.64
	2.4. Curvature with deposition	-2.36
	2.5. Integrated erosion and deposition	-2.81

Note: A baseline value with no sediment discharge at all times is provided for reference. Such a baseline value is provided in all tables.

After enabling deposition, the sediment discharge of the Shields erosion only becomes slightly worse while the sediment discharge of the curvature erosion becomes drastically worse. The integrated erosion and deposition formulation does the worst by far with an R^2 value nearing the null R^2 value obtained when there is no sediment discharge. This indicates either that these models are just not well designed for the inclusion of deposition or that some parameters associated with deposition are not accurate.

Geomorphology

Rill (Model 1.1)

Figure 15 demonstrates that the simulated erosion erodes upstream too fast, although the bed shape generated does resemble the desired end results. This presents a clear issue in only using the equations for rill erosion presented: there is no reliable way to control the upstream development of the gully, and there is no gully erosion implemented. The preliminary results of the model from this calibration do appear promising though; the rill erosion can be implemented with a proper landscape evolution equation to generate more accurate results.

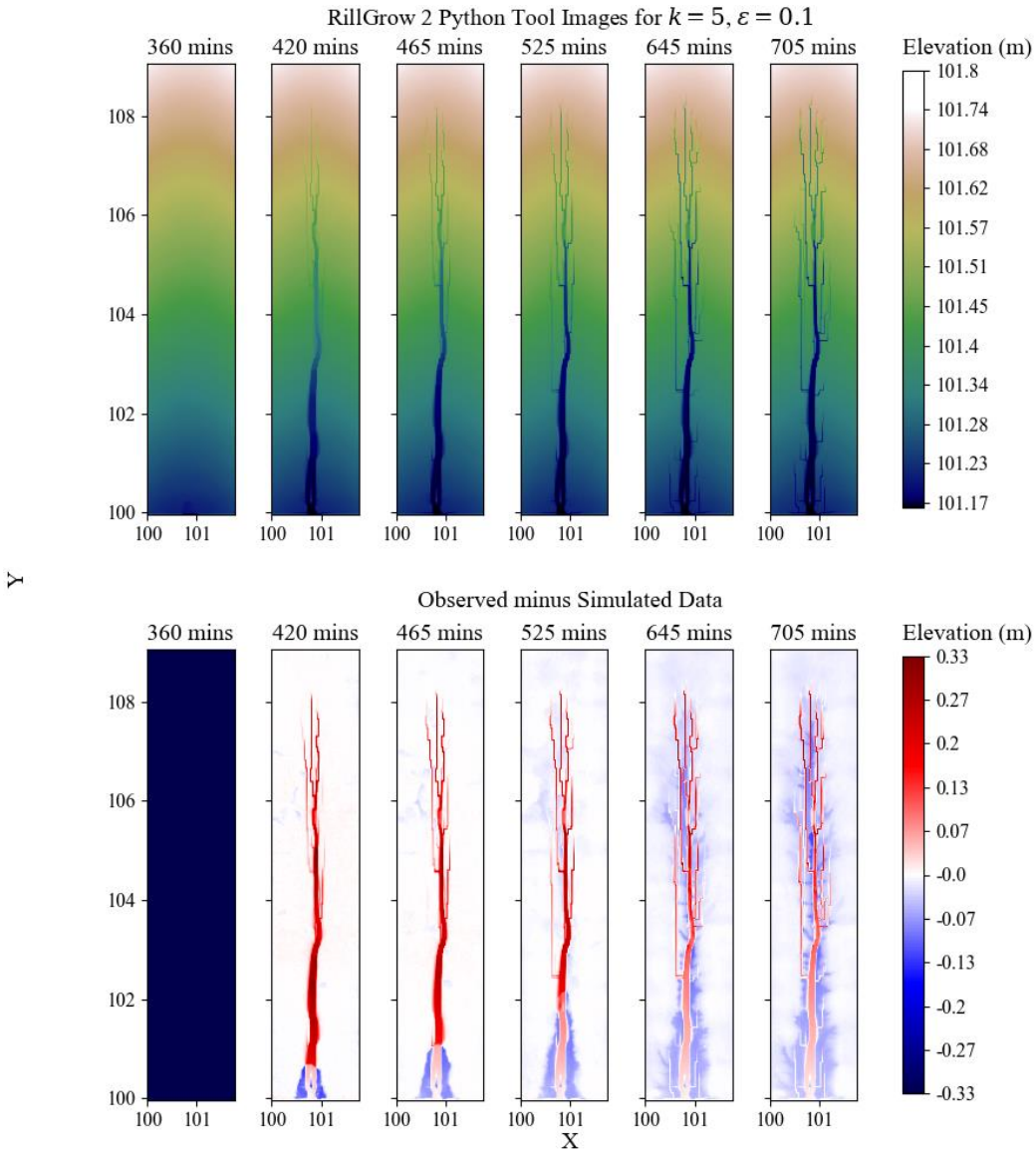

Figure 15

Generated results using RillGrow erosion on the dataset provided in Figure 1

Note: Calibrated values of $k = 5$ and $\epsilon = 0.1$ were used between times 360 minutes and 705 minutes. The top row is the generated topography. The bottom row is the difference between observed and simulated data. The color ramps represent elevation in meters. This is the same for all similar figures that appear later.

RillGrow's erosion formulation has been shown not to match sediment discharge (Figure 6), so the geomorphology is kept brief in this section. One vertical and one horizontal cross-section were selected at the center of the flume simulation at 705 minutes (red dashed lines in Figure 16). These cross-sections were compared to the observed data's cross-sections at the same locations. The cross-sections given in Figure 16 are then shown in Figure 17.

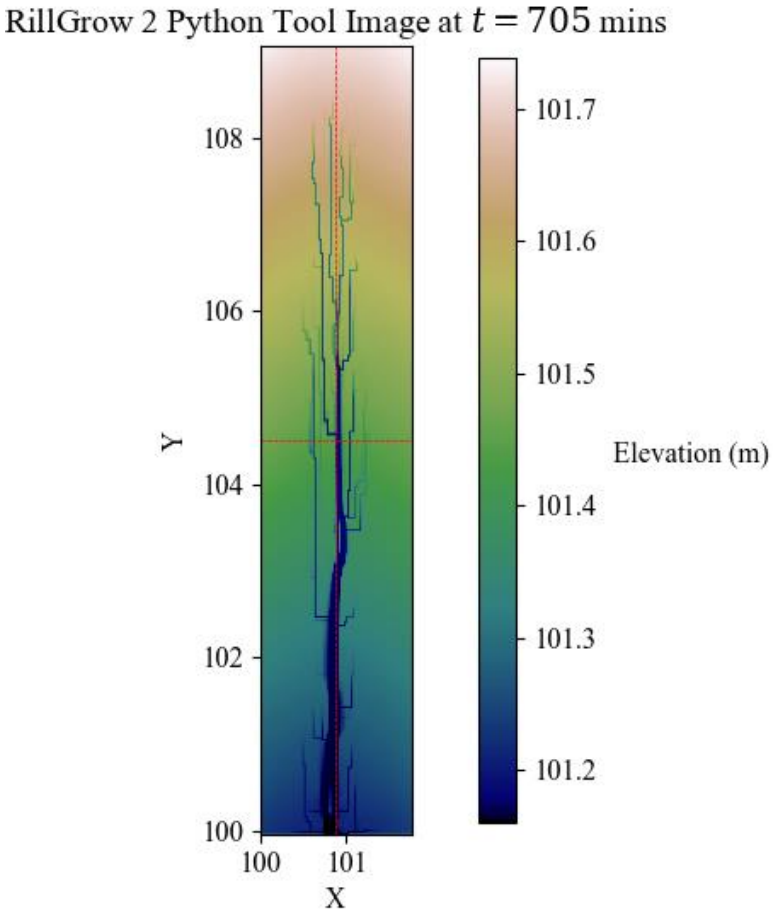

Figure 16

Final image from Figure 15 overlaid with dashed red lines to denote the cross-section locations at X=100.88m and Y=104.51m

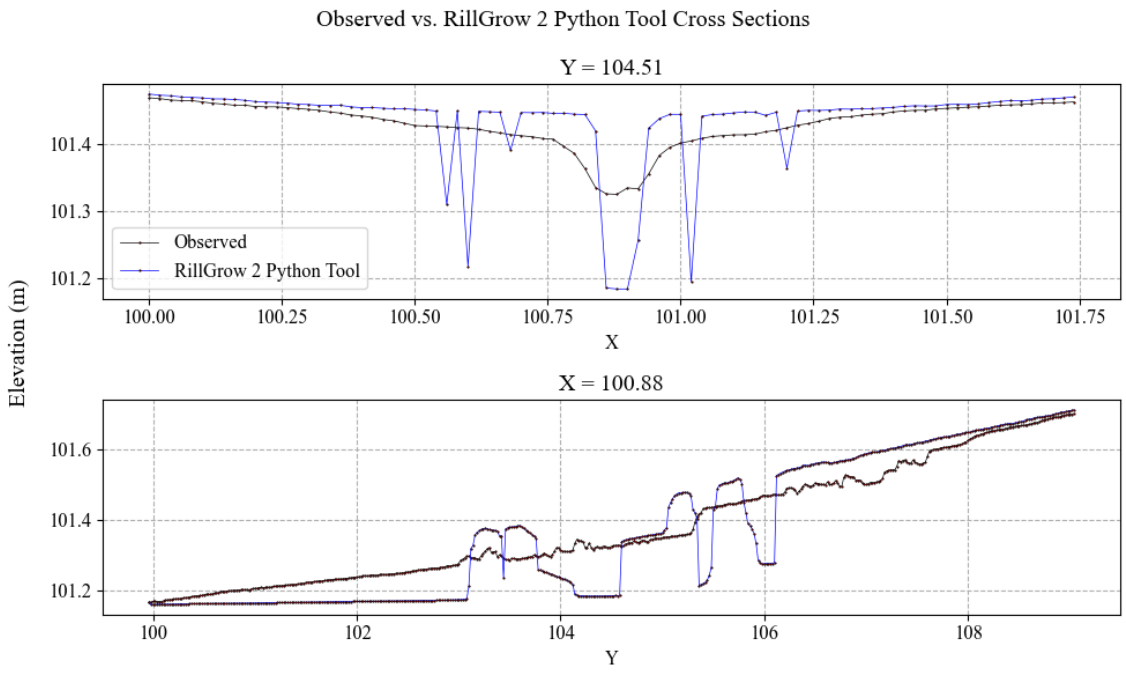

Figure 17

Cross-sections shown in Figure 16 for time $t = 705$ *minutes*

Note: The upper plot displays the horizontal cross-section and the lower plot displays the vertical cross-section. This is the same for all similar figures that appear later.

Looking at Figure 17, it is reiterated that the formulation proposed in RillGrow erosion tool does not capture gully erosion well. It erodes too much in the central gully while also digging deep rills where they are not expected. Furthermore, the erosion is not nearly as smooth as the observed data with sharp troughs in the simulated surface.

Landscape evolution (Model 1.2)

Figure 18 and Figure 19 were generated for Model 1 using the landscape evolution formulation, and they reveal unfavorable results. Contrary to Figure 7, the cross

sections in Figure 19 do not match to the observed topography, with too little erosion in some regions and too much erosion in others. The reason for this is revealed in Figure 18 where it can be seen that the landscape evolution equations does not form a smooth channel down the center of the flume, but rather forms narrow channels that dig deep into the center of the flume and meander about. Figure 19 shows that the model cuts to the bed minimum before flattening out, and it forms many deep rills in the upper portion of the flume. As such, it is obvious that this model did not generate the expected results.

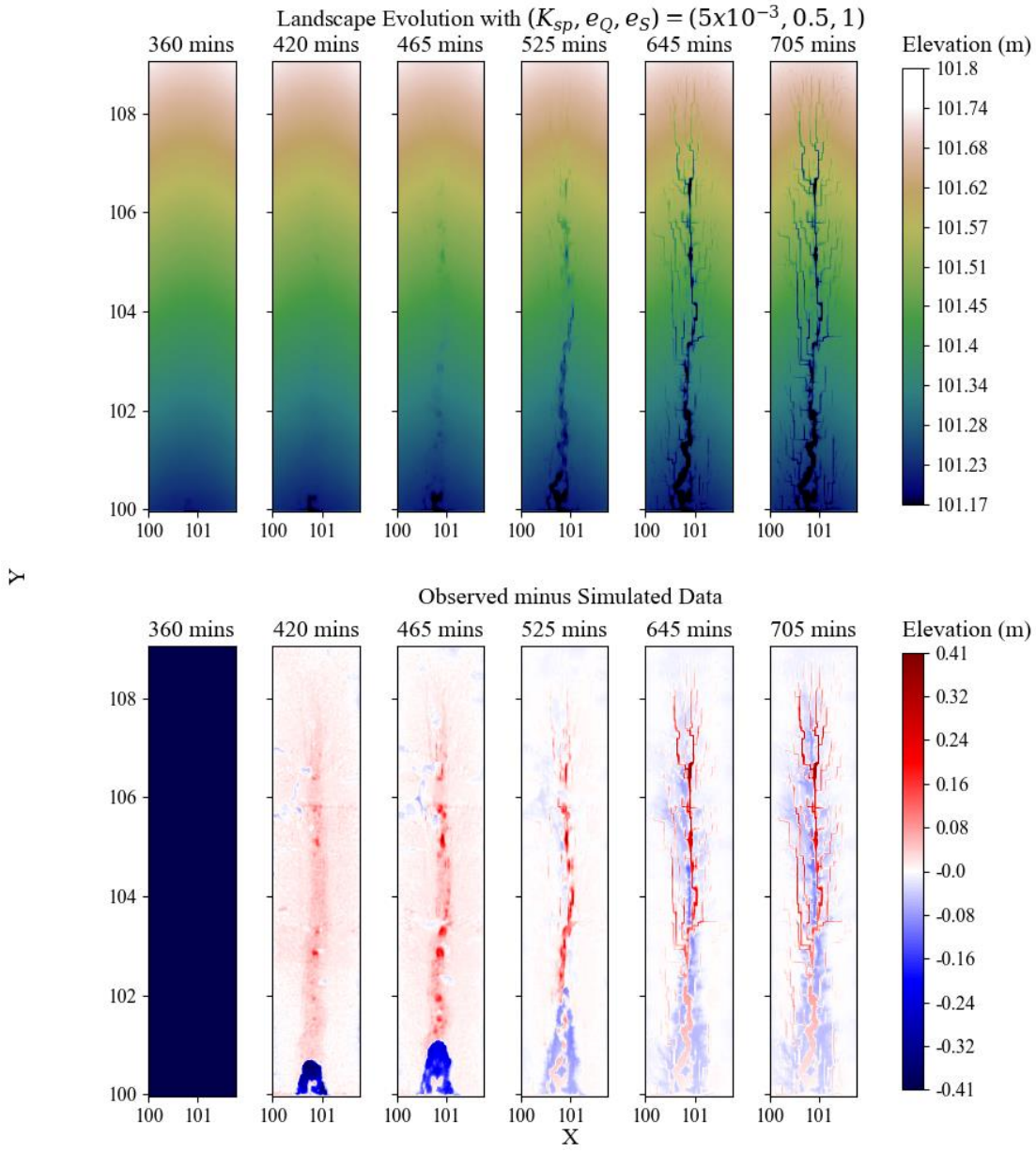

Figure 18

DetachmentLTDErosion results between times 360 minutes and 705 minutes

Note: Values of $(K_{sp}, e_Q, e_S) = (5 \times 10^{-3}, 0.5, 1)$ were used.

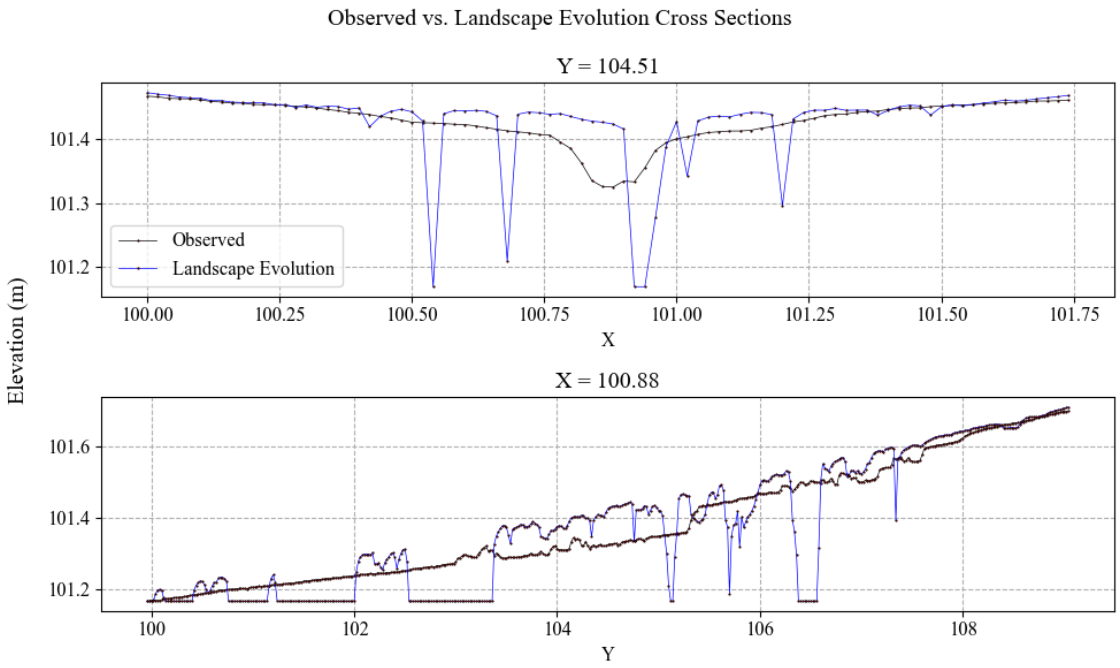

Figure 19

Cross-sections shown in Figure 18 for time $t = 705$ minutes

Integrated rill and landscape evolution (Model 1.3)

Comparing Figure 20 and Figure 21 with Figure 18 and Figure 19, it is clear that integrating the landscape evolution formulation with the rill erosion has tapered the depth on the erosion in the cross sections. The integration has also slowed down the upstream erosion, so the channels do not form as deep. While these issues have been alleviated, the issues of the two formulations still present themselves such as the generation of very angular rills and the deep, eroded sections generated by the landscape evolution formulation.

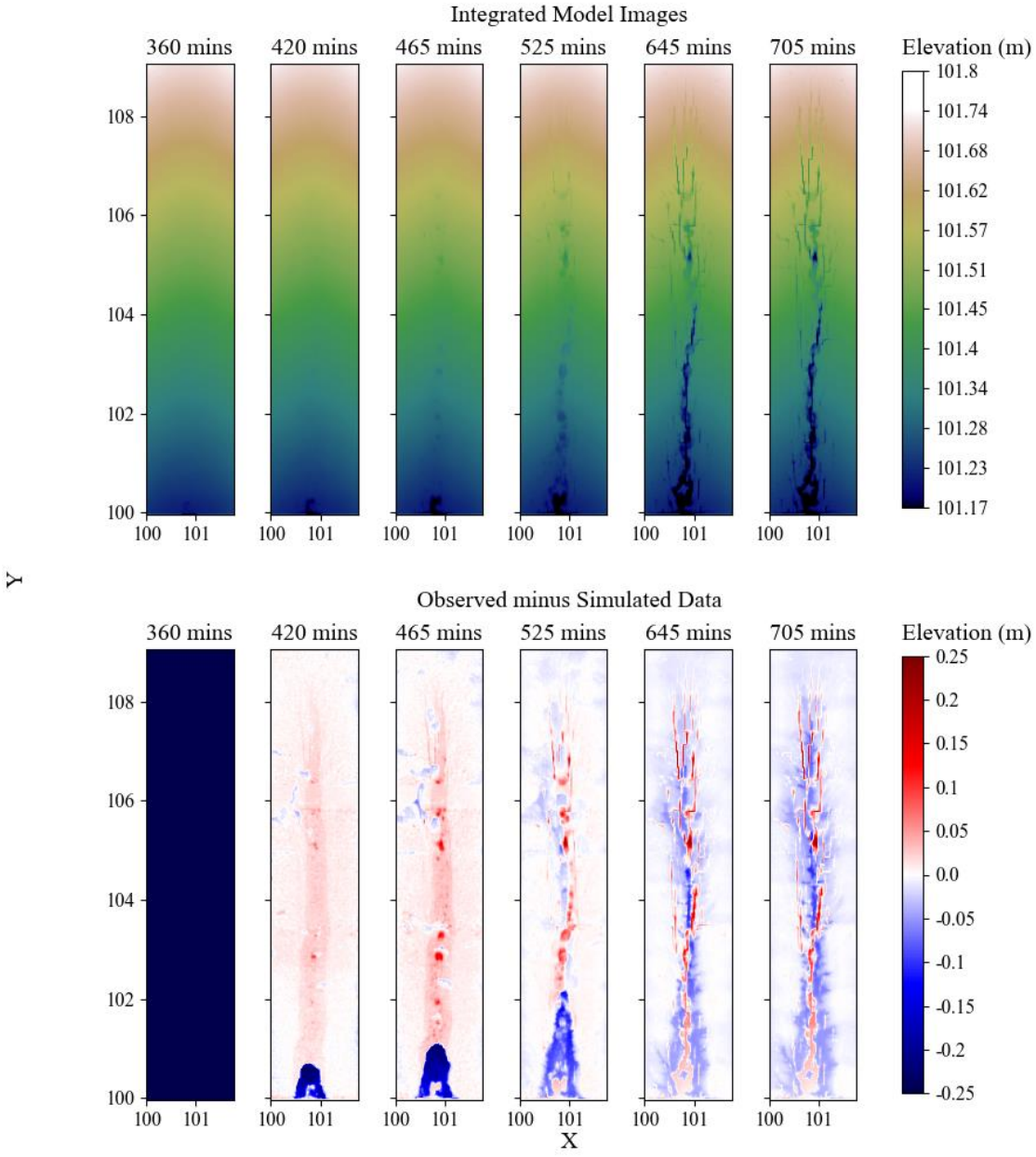

Figure 20

Generated results using Equation 14 *on the dataset provided in Figure 1 at the time* $t =$ 360 *mins*

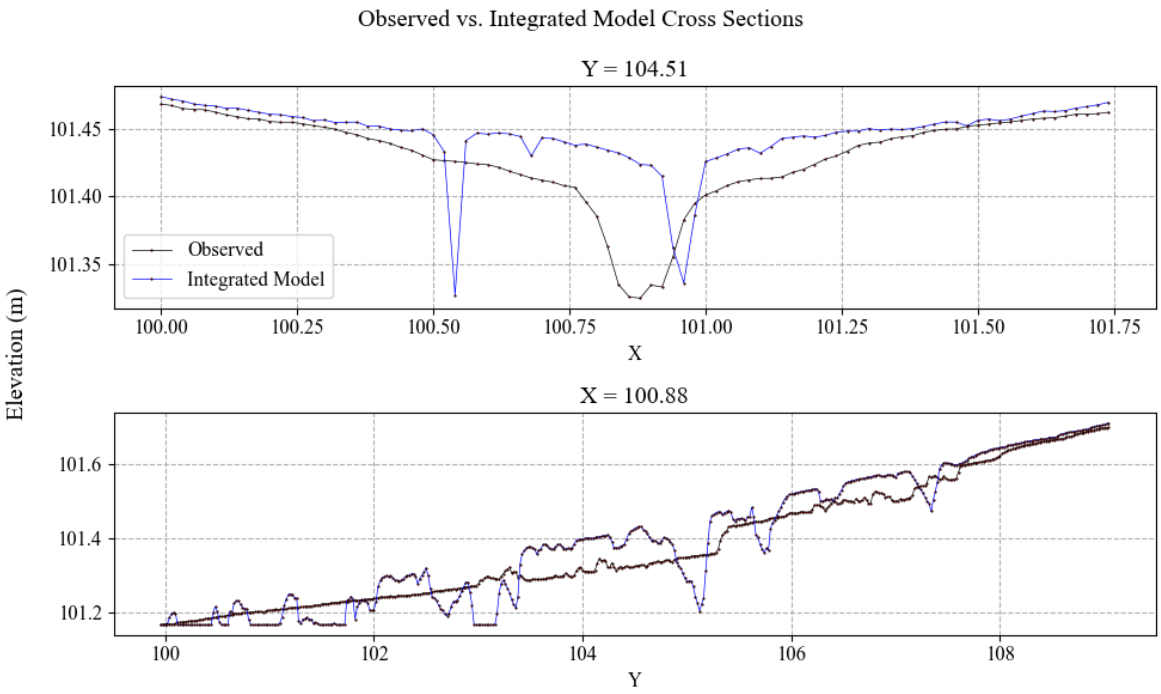

Figure 21

Cross-sections for the integrated rill and landscape evolution formulation using Figure 20

Proposed erosion model

Erosion (Models 2.1, 2.2)

The geomorphology for Model 2 (Equation 21) is first observed in the same manner as the previous analyses.

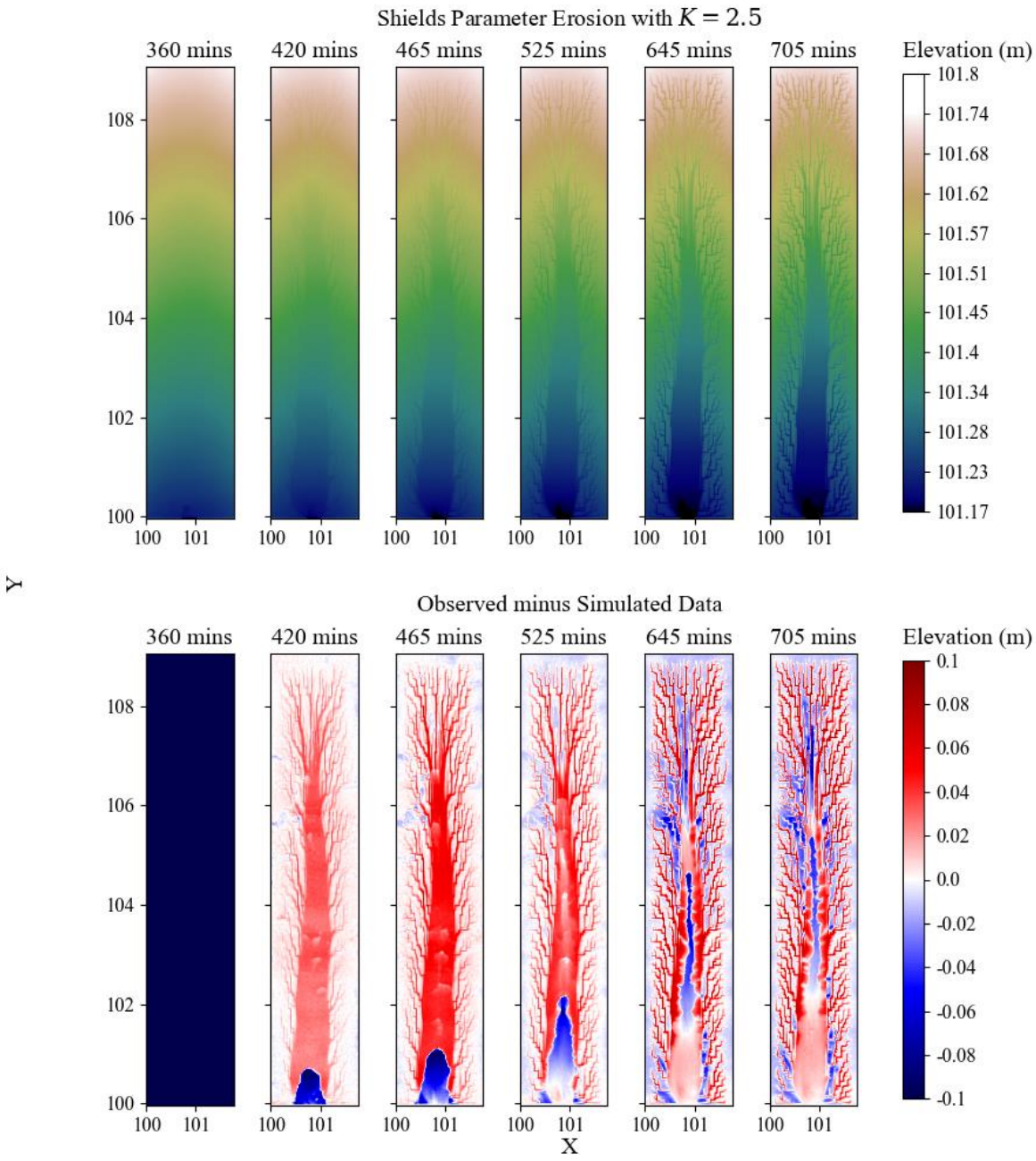

Figure 22

Generated results using Equation 21 *on the dataset provided in Figure 1 at the time* $t =$ 360 *mins*

Note: The calibrated value of $K = 2.5$ is used.

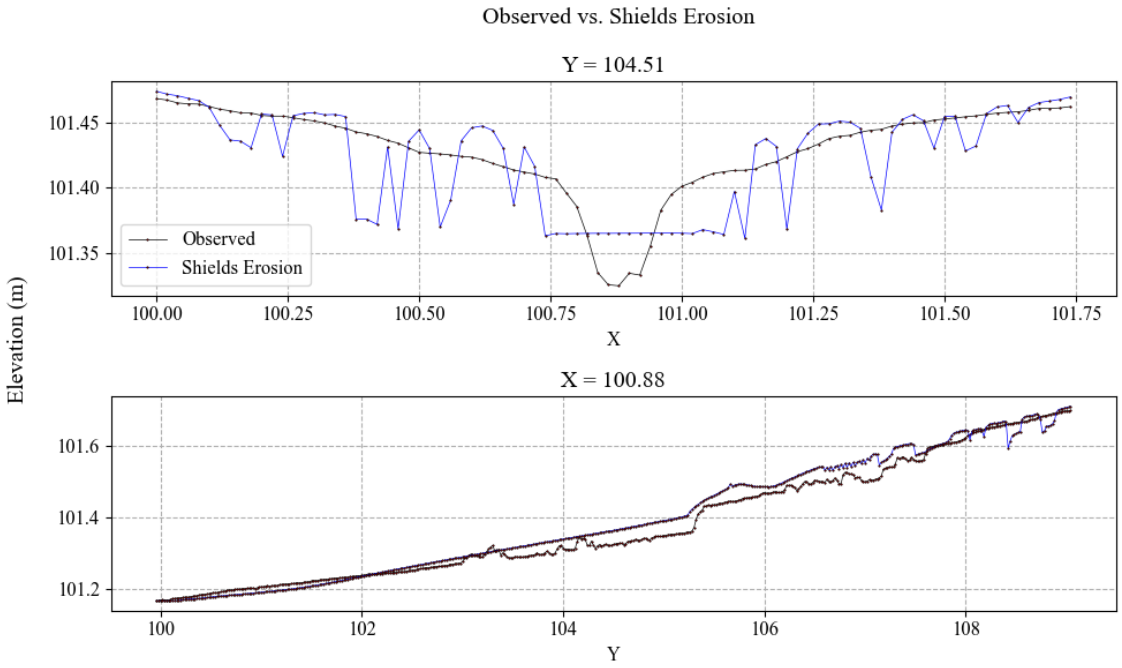

Figure 23

Cross-sections for the Shields erosion in Equation 21 *using Figure 22*

The images in Figure 22 and the cross sections generated for Figure 23 demonstrate that Equation 21 causes too much erosion in shallow water regions and not enough downcutting in gullies. The model does appear to have a vague ability to track the headcut, but it is not especially successful at it. It also smooths the main gully too much, as can be seen in Figure 23 where the horizontal cross section is perfectly flat in the main gully. This indicates that the bed shear stress equations used overestimates bed shear stress in shallow regions and underestimates bed shear stress in the main gully.

The geomorphology of Equation 22 is observed next in Figure 24 and Figure 25 below.

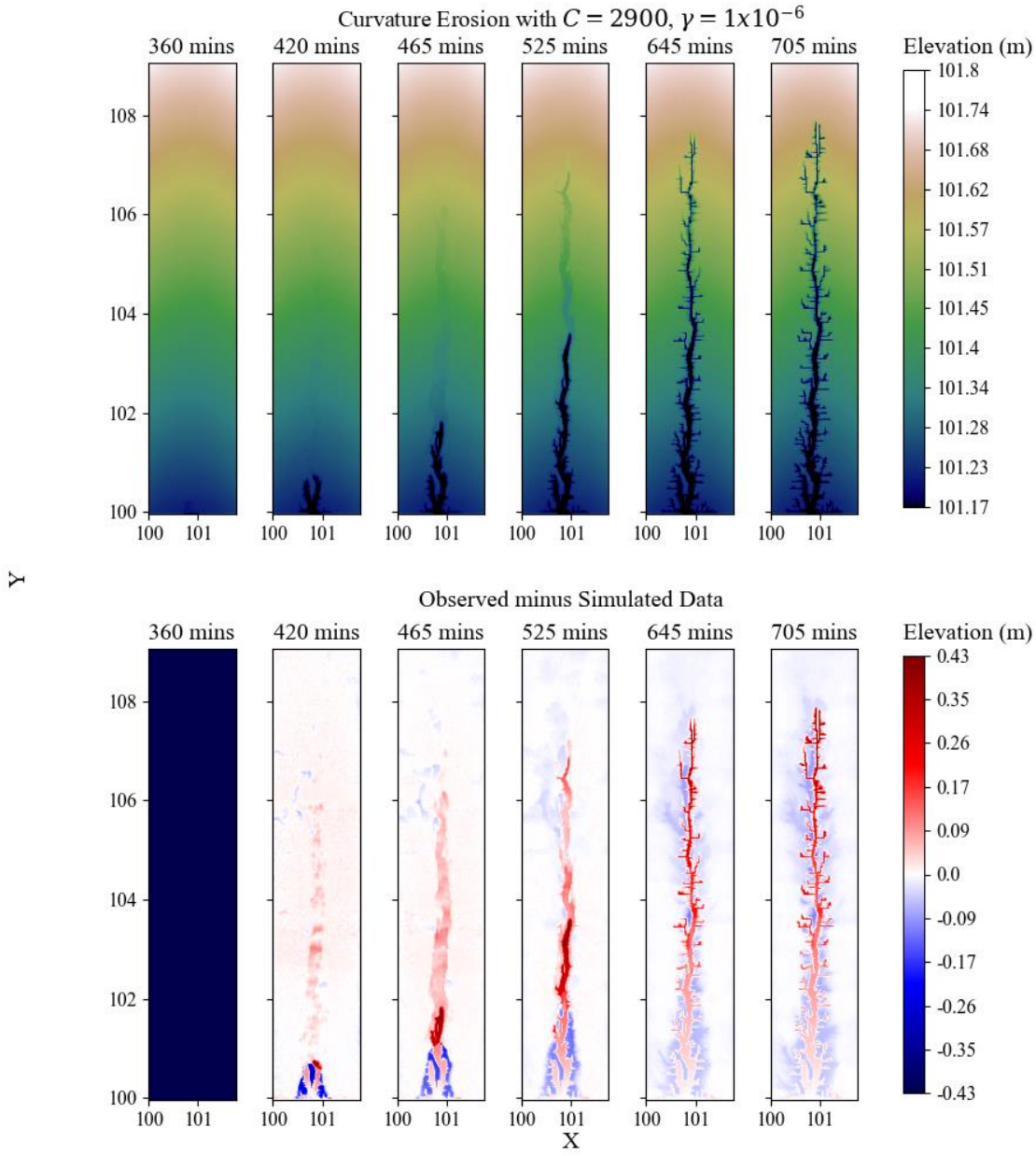

Figure 24

Generated results using Equation 22 *on the dataset provided in Figure 1 at the time* $t =$ 360 *mins*

Note: The calibrated values of $(C, \gamma) = (2900, 1x10^{-6})$ are used.

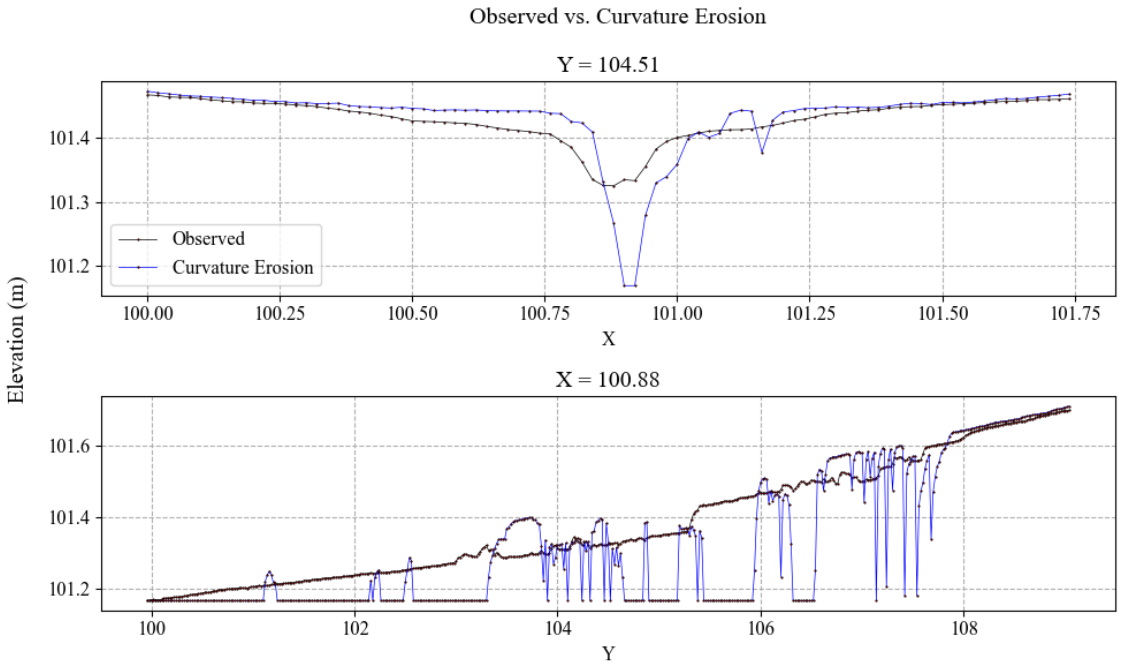

Figure 25

Cross-sections for the curvature erosion in Equation 22 *using Figure 24*

The results from the curvature erosion can be likened to the erosion from the landscape evolution formulation. They both have a moderately strong match with the sediment discharge of the observed data and a decent match for the headcut at $t = 420$ min, but they fail to match as well at later times. They also both erode to the bed minimum and stop. However, comparing Figure 24 and Figure 25 with Figure 18 and Figure 19 reveals that the curvature erosion does a much better at eroding near the expected location in the center of the flume and that the curvature erosion is much smoother than the landscape evolution. Furthermore, the cross-sections from Figure 25 don't have deep rills in the shallow regions as Figure 19 does.

Erosion and deposition (Models 2.3-2.5)

Deposition is now enabled, and the Shields erosion is tested with deposition in Figure 26 and Figure 27.

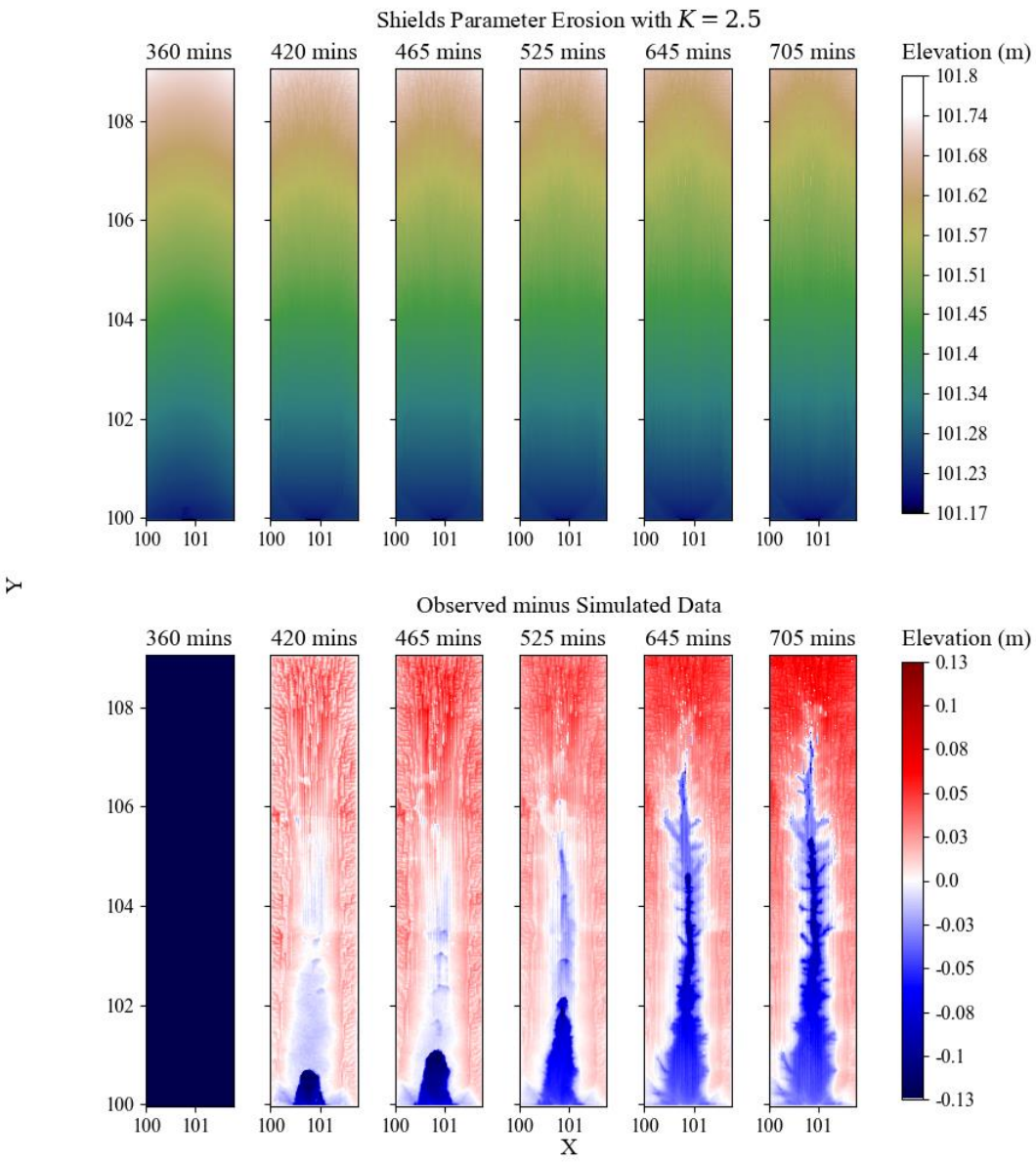

Figure 26

Simulation from Figure 22 run with deposition enabled

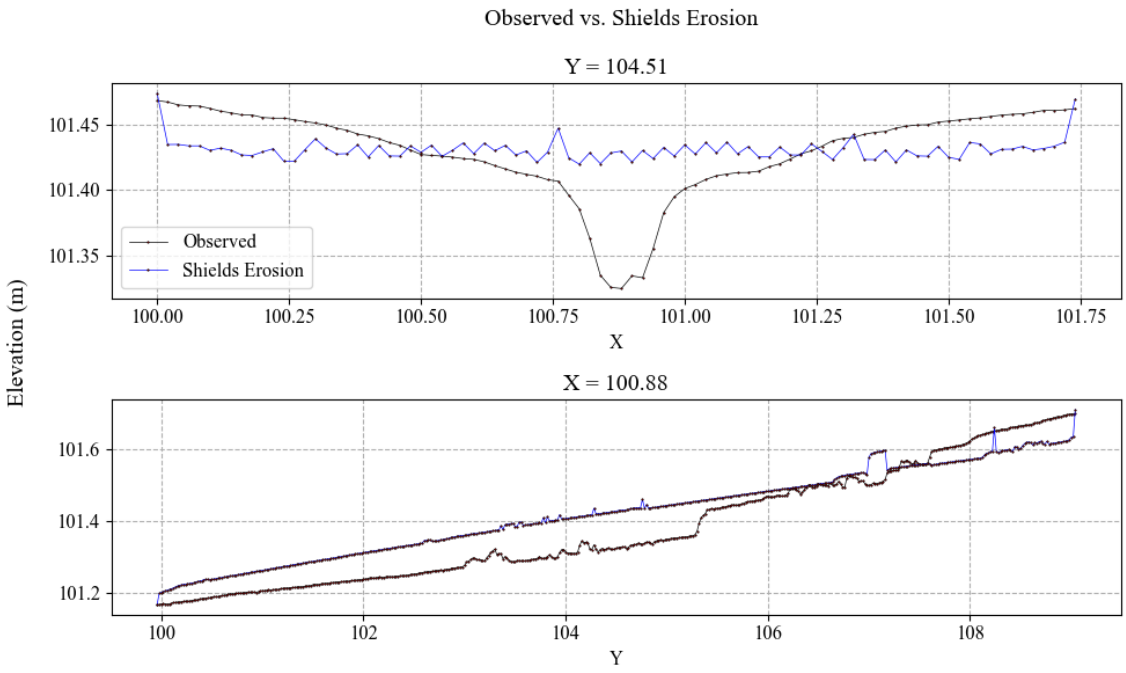

Figure 27

Cross-sections for the Shields erosion in Equation 21 *using Figure 26*

Figure 26 and Figure 27 demonstrate that the model detaches too much sediment into the water at nearly all locations, causing the deposition to create a smooth topography in the vertical and horizontal cross sections. This makes the model entirely fail at matching the erosion in the main channel as Figure 23 had, and it instead generates what is essentially a linear profile. There are variations in the topography, but this can be attributed to the usage of an uncoupled model.

Next, the curvature formulation is tested with deposition in Figure 28 and Figure 29 after a brief recalibration of C from 2900 to 5500.

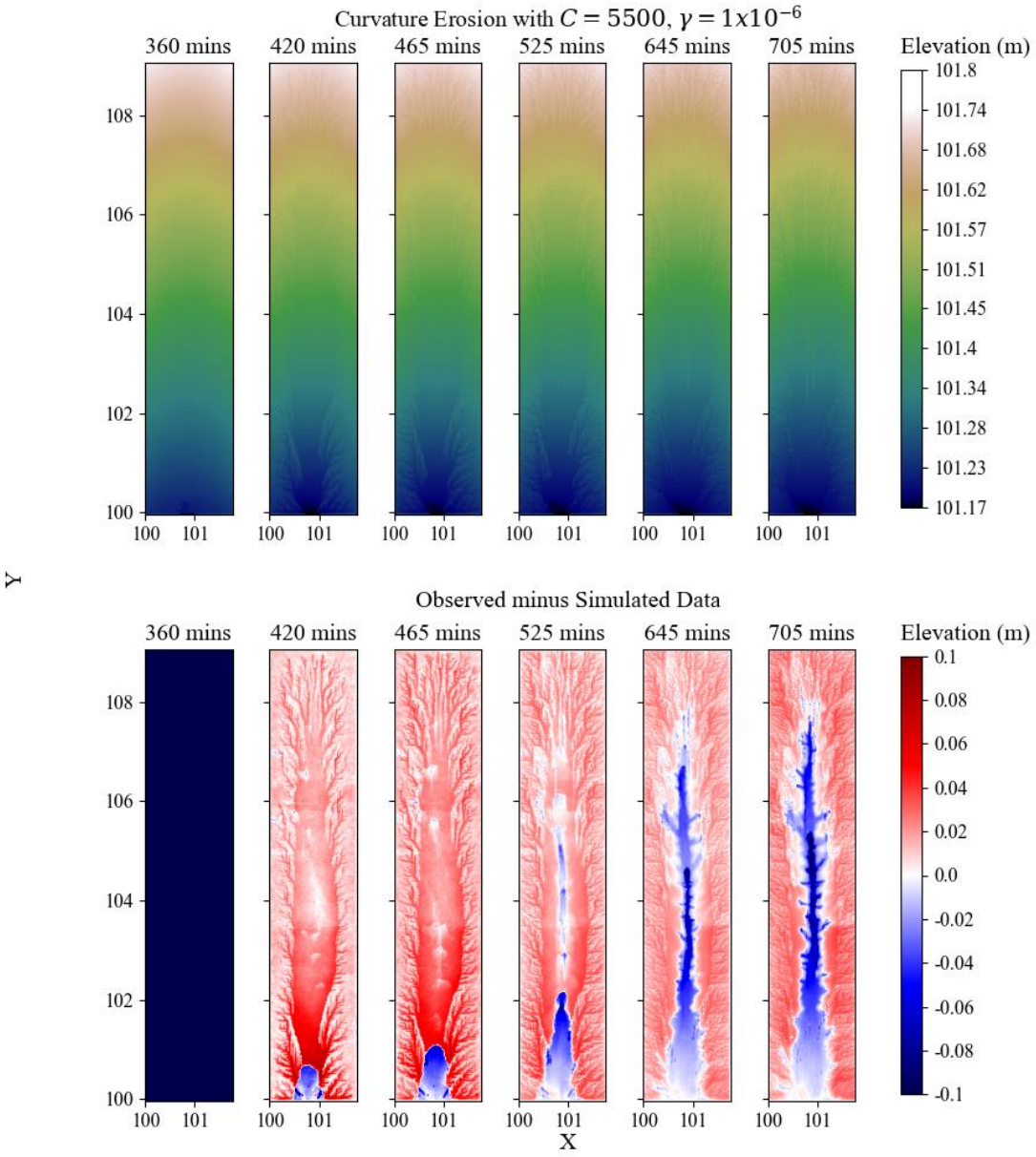

Figure 28

The simulation from Figure 24 is run with deposition enabled

Note: Calibrated values of $(C, \gamma) = (5500, 1x10^{-6})$ are used.

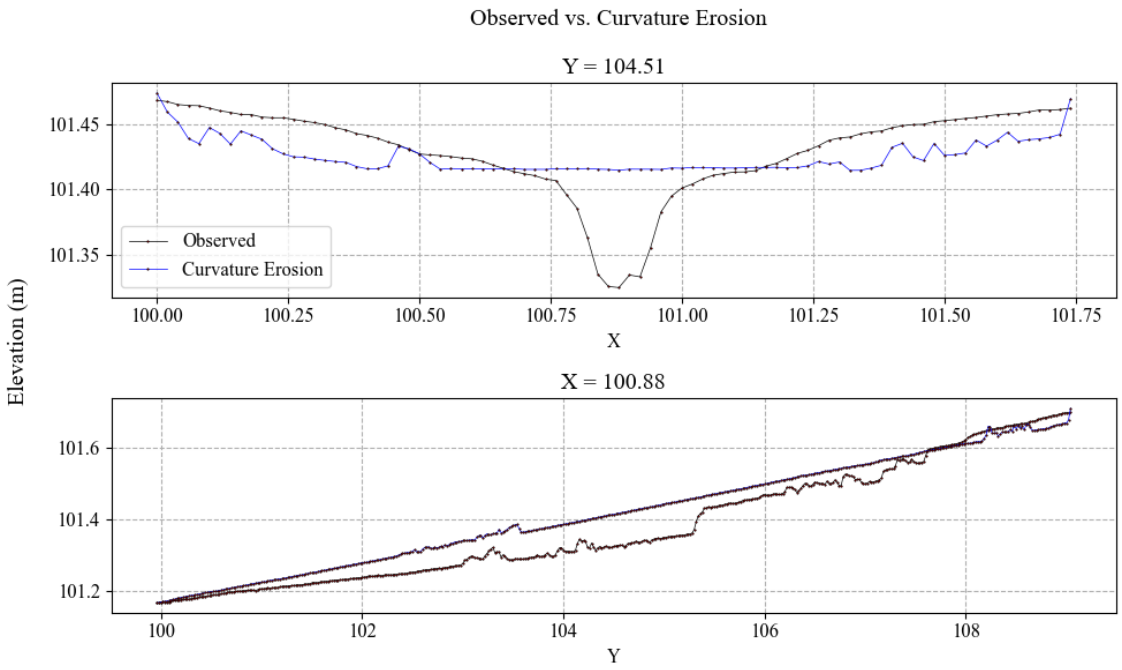

Figure 29

Cross-sections for the curvature erosion in Equation 22 *using Figure 28*

The curvature erosion appears to suffer the same issue as the Shields erosion had with deposition. Figure 28 demonstrates too much deposition in the main channel, which causes the equation to rapidly erode upstream while generating very shallow erosion. Figure 29 shows heavy smoothing of the topography with a very smooth, nearly linear profile along the vertical profile and a parabolic profile along the row profile. This again seems to indicate that there is too much sediment being placed into the water, although it is more likely that the transport capacity is too small.

Lastly, the integrated erosion and deposition formulation is tested in Figure 30 and Figure 31.

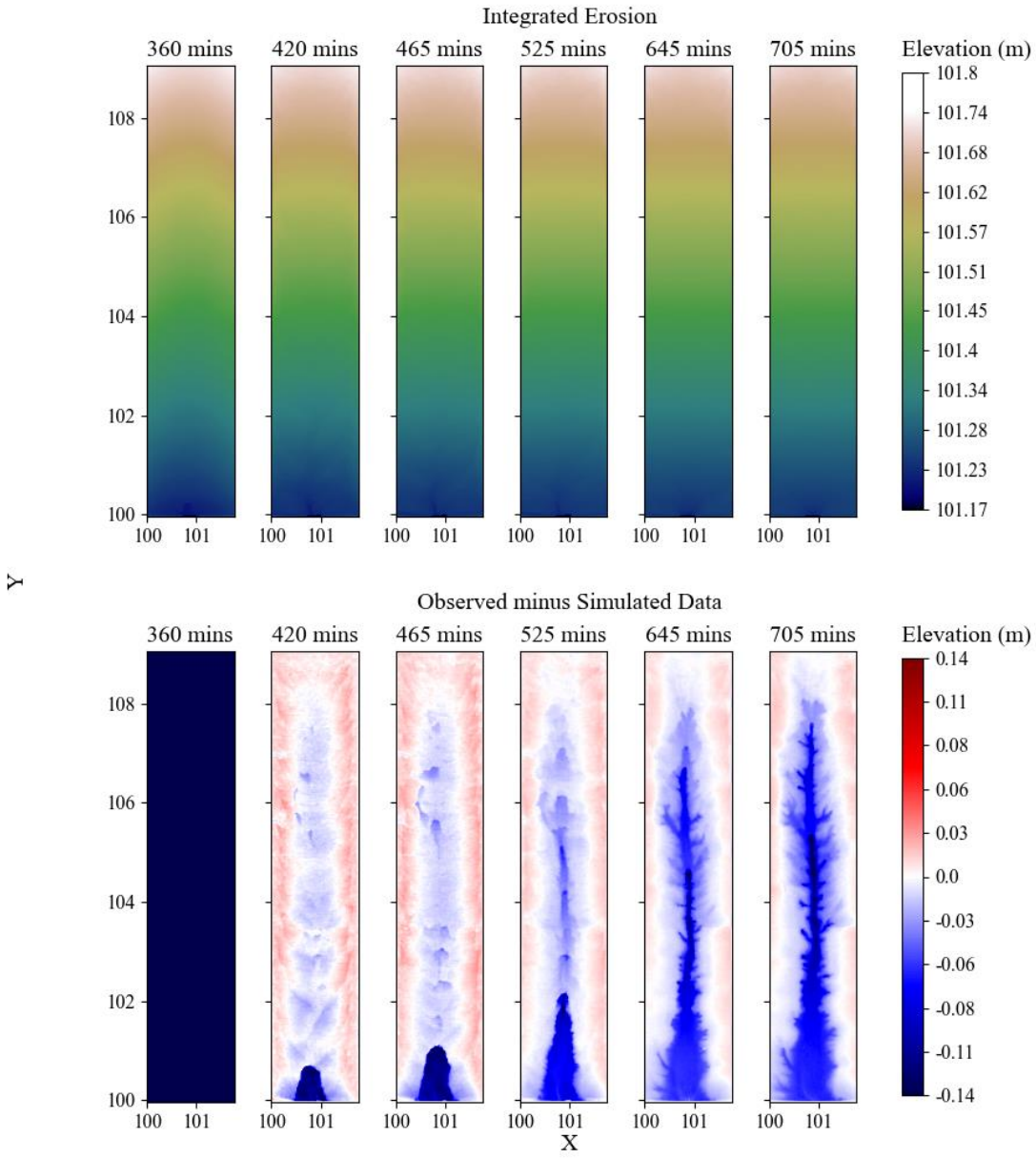

Figure 30

Integrated erosion and deposition equation run over the simulation time period

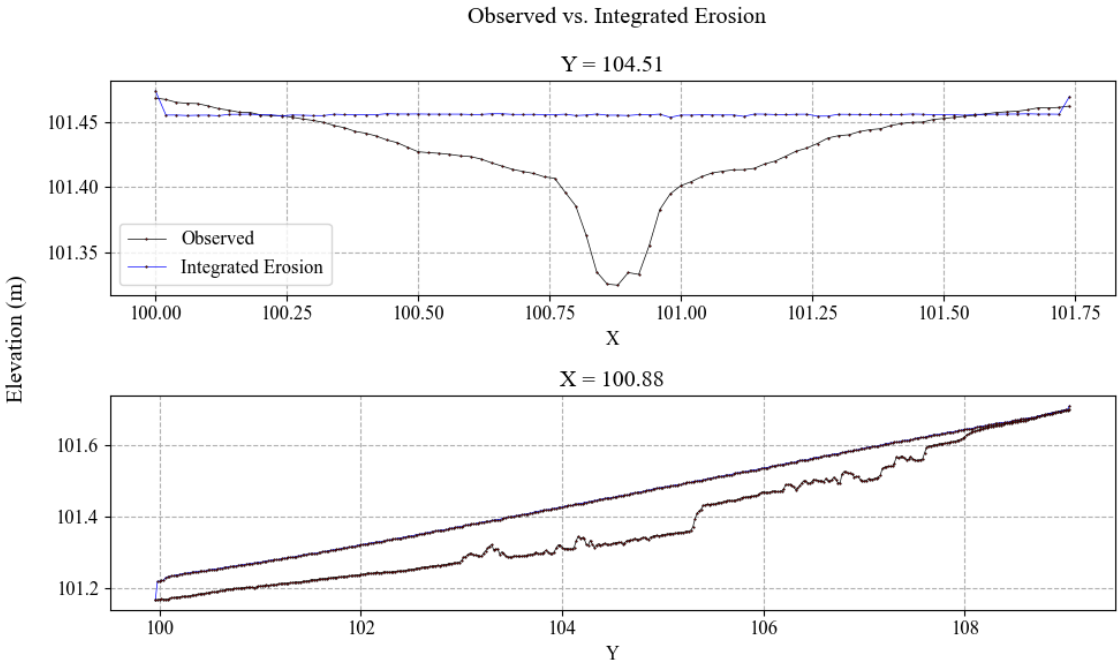

Figure 31

Cross-sections for the curvature erosion in Equation 22 *using Figure 30*

Figure 30 and Figure 31 reflect the results of Figure 14 in that there is essentially no erosion in the topography. Looking at the previous formulation used in Model 2 with deposition and the current integrated erosion and deposition formulation, it is clear that the transport capacity needs to be investigated further to allow for the transport of more sediments.

Geomorphology numerical comparison

The NSE and the R^2 of the averaged vertical and horizontal cross sections are presented in Tables 3, 4, and 5 below. Plots of the soil loss and the average cross sections are shown in the Appendix.

Table 3

NSE of the soil loss at different timesteps for tested models

Category	Scenario	Time (min)					
		420	465	525	645	705	Average
Baseline	No erosion	-0.01	-0.04	-0.22	-0.58	-0.37	-0.24
Model 1	1.1. Rill	-10.55	-2.21	-1.04	-1.07	-0.88	-3.15
	1.2. Landscape evolution	0.17	-0.18	-0.98	-3.31	-2.73	-1.41
	1.3. Integrated rill and landscape evolution	0.19	-0.05	-0.02	-0.85	-0.19	-0.19
Model 2	2.1. Shields	-0.69	-0.31	-0.02	-0.09	-0.26	-0.27
	2.2. Curvature	0.45	-1.63	-2.58	-5.21	-10.32	-3.86
	2.3. Shields with deposition	-1.99	-0.66	-0.37	-0.34	-0.20	-0.71
	2.4. Curvature with deposition	-1.31	-0.45	-0.1	-0.1	-0.08	-0.41
	2.5. Integrated erosion and deposition	-0.85	-0.27	-0.33	-0.65	-0.42	-0.30

Table 4

R^2 of the averaged rows at time $t = 705$ mins for the tested models

Category	Scenario	R^2
Baseline	No erosion	-11.77
Model 1	1.1. Rill	0.71
	1.2. Landscape evolution	0.89
	1.3. Integrated rill and landscape evolution	0.75
Model 2	2.1. Shields	0.84
	2.2. Curvature	0.78
	2.3. Shields with deposition	-5.33
	2.4. Curvature with deposition	-1.65
	2.5. Integrated erosion and deposition	-120.68

Table 5

R^2 of the averaged columns at time $t = 705$ mins for the tested models

Category	Scenario	R^2
Baseline	No change	0.975
Model 1	1.1. Rill	0.995
	1.2. Landscape evolution	0.997
	1.3. Integrated rill and landscape evolution	0.995
Model 2	2.1. Shields	0.996
	2.2. Curvature	0.995
	2.3. Shields with deposition	0.961
	2.4. Curvature with deposition	0.996
	2.5. Integrated erosion and deposition	0.969

When looking at only the erosion data, Table 3 shows that the Shields equation does the best overall job at predicting the soil loss of the observed data. However, it is also the only equation that consistently has an NSE that's slightly worse than the residual sum of squares of the observed soil loss. The rill erosion – as expected – does a bad job at always matching the observed soil loss. The curvature equation proposed does a worse job at matching the soil loss overall compared to other formulations; even though the curvature equation does a good job at matching the observed data at the first time, it consistently does worse as time progresses. The landscape evolution formulation does similarly well at the first time and degrades in accuracy as the simulation progresses in time, but its

ability to predict the soil loss of the topography is more consistent. Lastly, the integrated rill and landscape evolution formulation does the best of proposed erosion models at predicting soil loss.

Tables 4 and 5 similarly show that Models 2.1 and 2.2 do better at predicting the cross sections than other formulations. The Shields erosion does a better job at predicting the average cross section than the other formulations, and the landscape evolution formulation does the best at predicting the average cross section of the topography. Based on these observations, it can be said that the landscape evolution formulation is the best choice for this type of topography when there is no deposition desired.

Once the deposition is enabled, the Shields erosion has a decreased NSE while the curvature erosion obtains a much better NSE than the curvature erosion with no deposition since over-erosion is tapered. The integrated erosion and deposition formulation has an NSE about equivalent to the baseline, which is as expected since it does not erode much. The Shields and curvature erosions both have a decrease in the accuracy with which it models the average row cross section, and the integrated erosion and deposition formulation does worse than the baseline at modeling the average row cross section. The Shields erosion and the integrated erosion and deposition formulation both fail to accurately represent the average column cross section, but the curvature erosion sees a slight improvement in its accuracy in modeling the average column cross section.

Comparing the models to the baseline, the concerning fact that none of the models can predict the soil loss at every time step significantly better than the simulation with no

topographic change is a major issue. This means that none of the models can be reliable used to predict the soil loss at every time step, and Table 3 shows that only a few formulations can predict the soil loss with an acceptable NSE for the first timestep. Fortunately, the results are better for the average cross sections, where most of the models do predict the average cross section better than the null scenario where no erosion occurs.

Comparison to similar studies

The results found in this study from models including deposition are compared to those obtained in Jia et al. (2023) to assess how the proposed models perform against a model with integrated erosion and deposition equations. The sediment discharge and topographic elevation from Jia et al. (2023) are shown in Figure 32 and Figure 33 respectively.

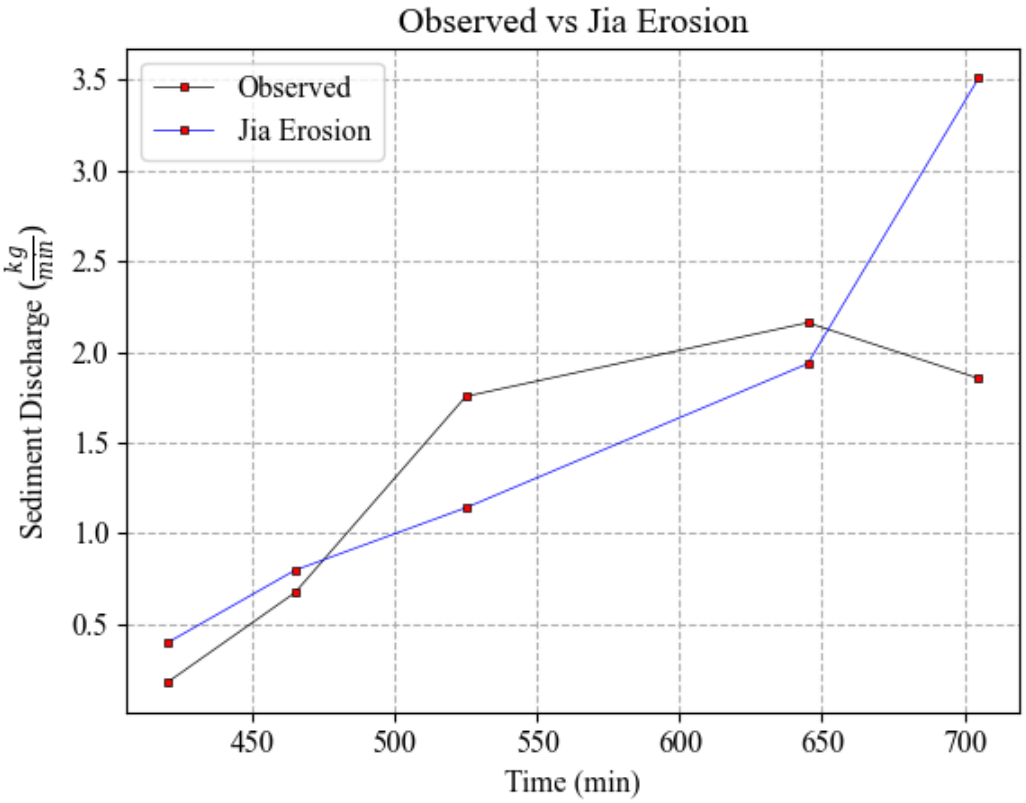

Figure 32

Sediment discharge of the data generated in Jia et al. (2023) compared to the observed dataset

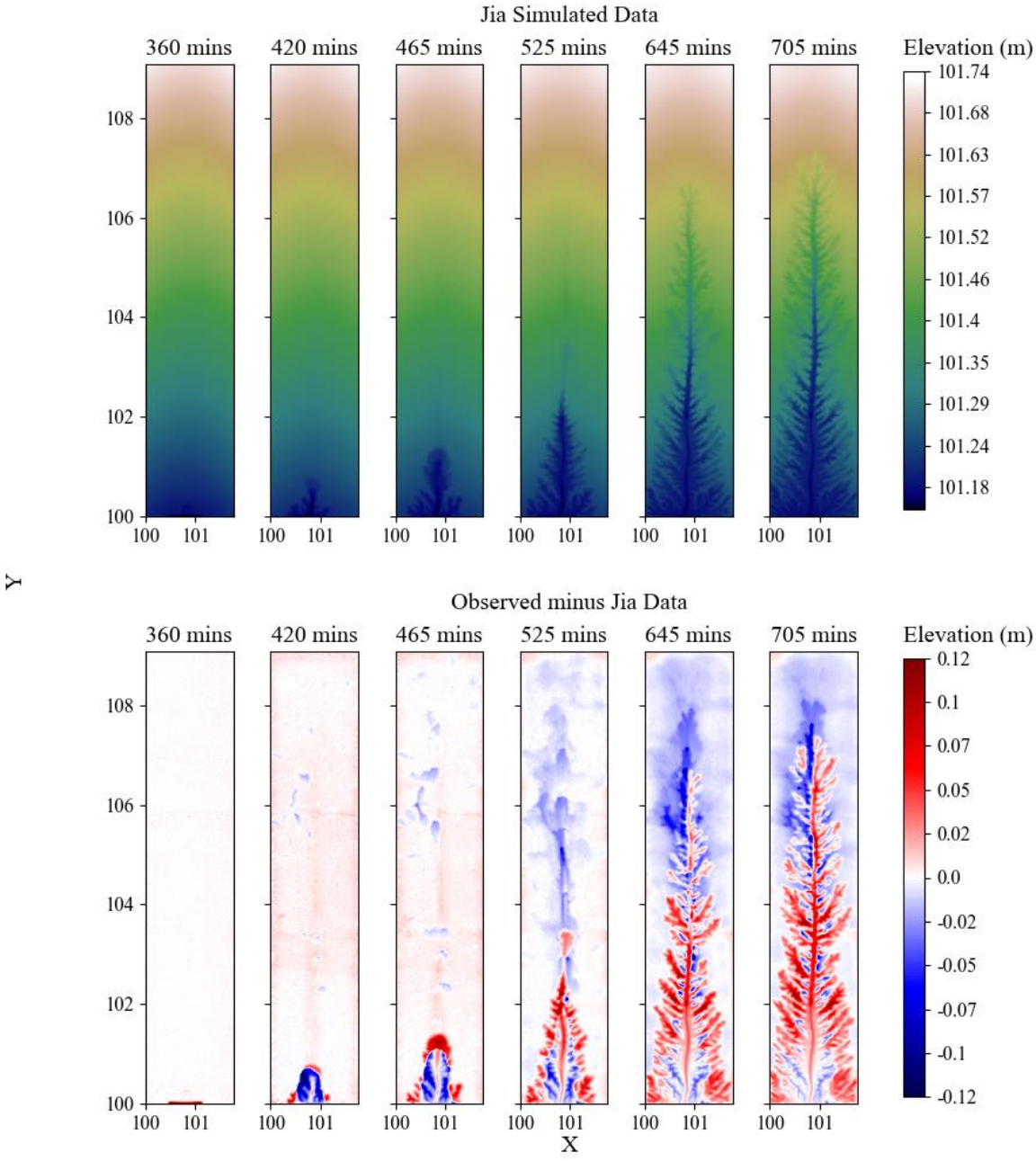

Figure 33

Simulated topography generated in Jia et al. (2023) compared to the observed dataset

Comparing Figure 32 and Figure 33 with the data obtained from Model 2 integrating deposition, it is clear that the model proposed by Jia et al. (2023) successfully tracks

headcut migration and generates rills with an integrated erosion and deposition formulation. The last timestep of the sediment discharge does not track the observed sediment discharge, however, and there is too much erosion downstream in later timesteps.

Tables 6, 7, 8, and 9 show the statistics for the sediment discharge R^2, the NSE of the soil loss, and the R^2 with the average row and the average column respectively. The statistics from the Jia et al. (2023) model are compared to Model 2 integrating deposition used in this study.

Table 6

R^2 of the sediment discharge of the data from Jia et al. (2023) compared to select models

Scenario	R^2
No erosion	-3.01
Jia	-0.11
2.3. Shields with deposition	-0.64
2.4. Curvature with deposition	-2.36
2.5. Integrated erosion and deposition	-2.81

Table 7

NSE of the soil loss at different timesteps for the data from Jia et al. (2023) compared to select models

Scenario	Time (min)					
	420	465	525	645	705	Average
No erosion	-0.01	-0.04	-0.22	-0.58	-0.37	-0.24
Jia	0.49	0.26	0.20	-0.06	-1.92	-0.21
2.3. Shields with deposition	-1.99	-0.66	-0.37	-0.34	-0.20	-0.71
2.4. Curvature with deposition	-1.31	-0.45	-0.1	-0.1	-0.08	-0.41
2.5. Integrated erosion and deposition	-0.85	-0.27	-0.33	-0.65	-0.42	-0.30

Table 8

R^2 of the average row cross sections of the data from Jia et al. (2023) compared to select models

Scenario	R^2
No change	-11.77
Jia	0.95
2.3. Shields with deposition	-5.33
2.4. Curvature with deposition	-1.65
2.5. Integrated erosion and deposition	-120.68

Table 9

R^2 of the average column cross sections of the data from Jia et al. (2023) compared to select models

Scenario	R^2
No change	0.975
Jia	0.994
2.3. Shields with deposition	0.961
2.4. Curvature with deposition	0.996
2.5. Integrated erosion and deposition	0.969

Comparing all the information presented in the above tables, it is clear that the model implemented by Jia does a much better job at matching the topography almost across the board. The only location where a presented formulation does better than the model from Jia is in Table 9 where the curvature erosion obtains a better match with the average column. However, the model presented by Jia also fails to generate an average NSE for soil loss that is better than the NSE for soil loss with no erosion. It does succeed in having an NSE that is significantly high for the soil loss for the first two timesteps, however, which is better than Model 2.

Uncertainties

Rill (Model 1.1)

The RillGrow erosion outlined in this model is moderately faithful to the erosion that was outlined in the source (D. Favis-Mortlock, 1998; D. T. Favis-Mortlock et al.,

2000). However, one issue with the RillGrow papers is that they do not describe all the changes implemented in RillGrow 2. The RillGrow 2 Python tool used in this model uses what was documented, but not all changes and improvements that were made were implemented in this model. Beyond this issue, uncertainty is also present from the fitting parameters used in RillGrow since the best fit parameters were only calibrated for slopes up to 28% (Nearing et al., 1997). Due to this, the stream power equation used may not be accurate for locations with steep slopes.

Landscape evolution (Model 1.2)

The landscape evolution formulation only uses the basic initial equation used to generally represent the forces governing drainage basin evolution from Howard (1994). As such, it is likely that some of the assumptions made do not apply to the spatial scale of this study, although the study states that many of the assumptions about the general principles of landscape evolution should be valid outside the scope of the study.

Integrated rill and landscape evolution (Model 1.3)

The uncertainties with the rill and landscape evolution formulation are still present in the integrated equation. However, another uncertainty presents itself in this model in that the integrated equation uses water depth and slope to try and combine the formulations. There is not a clear dividing line between the water depths and slopes at which the rill erosion becomes less accurate and the landscape evolution formulation becomes more accurate. Due to this, the water depth and slope thresholds used in this model are not certain to be accurate representation, but rather simplifications of how the contributions of rill and landscape evolution works as the thresholds between dominant

erosional forces are not known to be constant in all locations based on slope and water depth alone.

Proposed erosion model (Model 2)

Outside of the known issues with Landlab and OverlandFlow (Adams et al., 2017; de Almeida et al., 2012), some uncertainties can be introduced from the following issues:

- The Euler method is a preliminary time stepping method, and there are more sophisticated methods such as the fourth order Runge-Kutta scheme (Jameson et al., 1981).
- This system of equations is uncoupled, and a coupled system would generate more precise results (Simpson & Castelltort, 2006).
- The logarithmic law for calculating bed shear stress has two points of error: the first is the computational error introduced by the bisection scheme used to solve for it, and the second is the fact that it tends to overestimate the value of the bed shear stress (Biron et al., 2004).
- The sheet and splash equation used has only been developed recently and has seen little testing, which explains its poor performance in this study (Jia et al., 2023).
- The transport capacity is only known empirically based on sediment discharge at the outlet (Li et al., 2023; G. Zhang et al., 2009; K. Zhang et al., 2021). As such, there is concern over the accuracy of the transport capacity in a 2D application as well as over the exact values expected in the dataset used; unfortunately, there is very little research available that can address this issue.

- The adaptation length is also not very well established in literature with ongoing research occurring in attempts to identify and constrain the parameter (Bohorquez & Ancey, 2016; Gaeuman et al., 2015; Martínez-Aranda et al., 2023). As such, it is difficult to ascertain the accuracy of this parameter.

CHAPTER V

SUMMARY, CONCLUSIONS AND RECOMMENDATIONS

Summary

This study examined erosion and sediment transport models using empirical and theoretical formulations coupled with numerical methods. Empirical formulations used include those implemented in RillGrow (D. Favis-Mortlock, 1998; D. T. Favis-Mortlock et al., 2000) and a selected detachment-limited model for large-scale drainage basin evolution (Howard, 1994). Theoretical formulations were based on standard differential equations describing hydrodynamic flow and sediment transport. These were solved using numerical methods proposed in similar physically and hybrid models such as CCHE2D (Jia & S.Y. Wang, 2001), which solves partial differential equations using the finite element methodology. Multi-temporal high spatial resolution topographic data was used as reference for calibration and evaluation. These datasets were generated during controlled laboratory experiments using simulated rainfall to produce shallow overland flow applied to soil-mantled landscape specifically designed to simulate sediment erosion. These datasets were obtained from the USDA-ARS National Sedimentation Laboratory (Momm et al., 2018) and describe sediment load and the landscape response to the imposed external force over time.

Overland flow was simulated using the methodology proposed by de Almeida and others (2012; Barnhart et al., 2020; Hobley et al., 2017; Hutton et al., 2020) and implemented in the Python Landlab library. The measured runoff rate during laboratory experiments was used to calibrate simulated surface flow (Momm et al., 2018). The

simulated runoff rate was comparable to the observed runoff rate at the outlet, and it was used to represent the hydrology for all simulations (rainfall and runoff were kept constant during laboratory experiment). Information from the overland flow at each grid and link was used to inform fluxes in the sediment transport model.

The first erosion model proposed had three erosion algorithms that are evaluated over the period associated with the dataset. The first algorithm (1.1) is based on RillGrow's equations, and it uses the concept of stream power and unit sediment load to calculate rill erosion on the surface. The second algorithm (1.2) is based on the detachment-limited model for drainage basin evolution, and it uses discharge and slope to evaluate landscape evolution of the topography. The third algorithm (1.3) implemented uses a mixing equation to evaluate topography using either rill erosion or landscape evolution based on varying water depth and local slope of the raster cell.

The second model solves sediment transport equations (Jia & S.Y. Wang, 2001) using the finite element method while implementing multiple equations to represent rill and gully erosion as well as deposition. Sheet and splash erosion is represented using raindrop splash erosion multiplied by sheetflow transport capacity (Jia et al., 2023). The first erosion equation (2.1) uses the Shields parameter to determine the erosion rate (Rinaldi et al., 2008). The second erosion equation (2.2) uses curvature and slope with velocities parallel and perpendicular to the links to estimate erosion. These two equations are tested with a hard-coded bed minimum to evaluate their performance independently for erosion and deposition. The deposition formulation uses the adaptation length and transport capacity to determine if the water is fully saturated with sediment. Lastly, an

integrated erosion and deposition equation (2.5) using the adaptation length and transport capacity is implemented.

The first and second models were calibrated using the measured sediment load to determine multiple adjusting coefficients. The first performance assessment was based on estimates of sediment load (volume over time at the outlet). In the first model, using the rill erosion and integrated rill erosion and landscape evolution yielded less than desirable fits to the observed sediment discharge while the landscape evolution formulation fit very well to the observed sediment discharge. The second model using the curvature equation generated a good fit with erosion only, but the sediment load estimate differed from observed once deposition algorithms were enabled.

The two models were also evaluated based on the landform generated (channel morphology) as compared to observed. This was performed by comparing cross-sections and topographic surface differences. The first model performed the best with an NSE that was roughly equivalent to that of the null case (no erosion). The first and second models were able to match the averaged cross sections with moderate success such that they all outperformed the null case. However, the second model with deposition enabled only had the curvature equation perform better than the null case at matching the averaged cross sections. The Shields equation only performed better than the null case at matching the vertical cross-section, and the integrated erosion and deposition failed to perform better than the null case for both cross-sections.

After numerically evaluating the implemented equations, the results are compared to those found in a similar study using the same dataset (Jia et al., 2023). The CCHE2D

model described in Jia outperforms all the equations presented in this study with the exception that the second model with curvature formulation and with deposition which returns a better average vertical cross-section. The model from Jia performs exceptionally better at matching the average horizontal cross-section than the models proposed. It is important to note that none of the models evaluated nor the model proposed by Jia have an R^2 for the sediment load or an average NSE for the soil loss that is greater than zero.

Uncertainties and concerns about the created models are next evaluated. For the first model, the uncertainties need to be discussed:

- The rill erosion formulation calculates the unit sediment load using a best fit for a dataset which is only valid within certain slope ranges, and therefore, given the level of detail in the topography analyzed (sub-centimeter) it is possible that high local slope values are generated violating the original assumptions.
- The landscape evolution formulation was designed for and is based on assumptions at the landscape scale (km) which may not hold at the fine resolution used here (cm).
- The integrated rill erosion and landscape formulation performs a simplistic method for combining the rill erosion and landscape evolution in time and space by using a "mixing" function. The threshold to disaggregate between the two physical processes is based on water depth only and it is possible that a better threshold/disaggregation approach could be used.

The second model is significantly more complex than the first one, and the following uncertainties arose:

- The proposed second model it is overwhelmed with the issue that many parameters need to be empirically determined, therefore requiring significant calibration which could be complex and specific to individual landscape.
- The formulation between the hydraulic and sediment transport are uncoupled making transforming and simplifying fluxes between the formulations necessary and also adding uncertainty to the process.
- Furthermore, some of the parameters such as the transport capacity in shallow flows and adaptation length are not fully understood (causing limited formulation for two dimensional cases) and this raises concern about the accuracy of these parameters in this model.

Conclusions

The two models implemented with the different equations all had some degree of success, but there is still room for improvement within both models. The first model is very simple to implement, and it is best suited to estimate sediment load after calibration. However, it does not include any deposition terms and there is no sediment concentration tracked. The second model contains significantly more advanced mathematic formulation and subsequent solution using the finite element method, as well as more computational complexity and load. However, the model can extend estimation of sediment load to predict channel morphological changes over time. This is due to the implementation of tracking sediment concentration and deposition terms in addition to performing the same erosion as the first model. As such, it is generally better to use the second model for a more complex and accurate estimation of soil-mantled erosion.

All of the equations implemented in the two different models have different successes and failures in this study:

- The rill erosion implemented in this study did well at forming a smooth channel in the main gully. However, it did the worst in all numerical assessments, and it formed very sharp, angular rills as opposed to the smoother ones we would expect. As such, the rill erosion equation used here is not advised for applications involving gully development without constraints on where it can erode and a longer timescale on which it can erode.
- The landscape evolution equation – while it generates topography that appears winding and unnatural for the spatial scale of this study – performed very well in the numerical assessments compared to the rill erosion and the other model presented. The equation had the best sediment discharge fit of any equation examined, and it had a fairly good fit to the average cross sections. It did particularly well at matching the erosion in the shallower regions of the average horizontal cross section. However, the equation erodes too much once near the central gully forms, and without a deposition equation to better govern the erosion, the landscape evolution equation will not be able to get a more accurate result for the geomorphology.
- The sheet and splash equation is unsuccessful in matching the expected sheet and splash mass lost percentages (Momm et al., 2018). Due to this, this model is not recommended for usage to represent sheet and splash without analysis and verification on the equation. It is worth noting that the numerical analysis used for

comparison has not been verified against existing data, so it is can not be used for definitive validation of the sheet and splash equation.

- The Shields equation is successful at generating smooth, wide gullies and forming rills when deposition is disabled. However, the equation erodes upstream too fast, and it erodes a region that is too wide. It also does not get very favorable results for the sediment discharge, although the statistics for the geomorphology are fairly good compared to other equations. There is also too much erosion outside of the main gully. This may be due to inaccuracies in the bed shear stress equation used, however, and this equation may see significant improvements with the implementation of a more accurate bed shear stress equation.
- The curvature equation without deposition performs well at creating a smooth topography in the central gully but performs less favorably than the landscape evolution equation in all cases with similar results. As such, this curvature equation is not recommended to be used over other models for cases with only erosion without alterations to the equation.
- The equations in Model 2 are all difficult to evaluate when the deposition is enabled due to the strict limitation the transport capacity places on how much sediment can be in the water. For example, results like those obtained by Jia et al. (2023) can be obtained using the integrated erosion and deposition equation with the correct model. Due to this, the results of these models are inconclusive until further testing can be performed.

One important conclusion to draw from the results in this study is that none of the sediment transport models presented in this study or in Jia et al. (2023) can get an NSE for the soil loss that is larger than the NSE for the null case with no erosion. A model which can accurately predict such soil loss would naturally obtain very accurate geomorphology and sediment discharge. As such, further work into developing a model that can obtain an accurate NSE for the soil loss over time is needed to properly predict geomorphology changes and sediment yield at any given point in time and space.

Recommendations for future work

The following tasks would all be instrumental to the creating of a two-dimensional model that functions on high spatial resolution data with silty soil:

- An analysis on improving the computational efficiency of models built on grids established using nodes and links.
- The development and validation of a sheet and splash equation designed for shallow water flow.
- The creation of two-dimensional bed shear stress, transport capacity, adaptation length, and sediment concentration profiles on shallow water flows over silt and appropriate equations that can model them.
- A thorough analysis of erosion and deposition over silty shallow water flows and equations that can flexibly model them.
- The development of gully channel headcut upstream migration and lateral expansion equations.

BIBLIOGRAPHY

Adams, J. M., Gasparini, N. M., Hobley, D. E. J., Tucker, G. E., Hutton, E. W. H., Nudurupati, S. S., & Istanbulluoglu, E. (2017). The Landlab v1.0 OverlandFlow component: A Python tool for computing shallow-water flow across watersheds. *Geoscientific Model Development*, *10*(4), 1645–1663. https://doi.org/10.5194/gmd-10-1645-2017

Barnhart, K. R., Hutton, E. W. H., Tucker, G. E., Gasparini, N. M., Istanbulluoglu, E., Hobley, D. E. J., Lyons, N. J., Mouchene, M., Nudurupati, S. S., Adams, J. M., & Bandaragoda, C. (2020). Short communication: Landlab v2.0: a software package for Earth surface dynamics. *Earth Surface Dynamics*, *8*(2), 379–397. https://doi.org/10.5194/esurf-8-379-2020

Biron, P. M., Robson, C., Lapointe, M. F., & Gaskin, S. J. (2004). Comparing different methods of bed shear stress estimates in simple and complex flow fields. *Earth Surface Processes and Landforms*, *29*(11), 1403–1415. https://doi.org/10.1002/esp.1111

Bohorquez, P., & Ancey, C. (2016). Particle diffusion in non-equilibrium bedload transport simulations. *Applied Mathematical Modelling*, *40*(17–18), 7474–7492. https://doi.org/10.1016/j.apm.2016.03.044

Borah, D. K., Bera, M., Shaw, S., & Keefer, L. (1999). *Dynamic Modeling and Monitoring of Water, Sediment, Nutrients, and Pesticides in Agricultural Watersheds during Storm Events* (Contract Report 655; p. 65). Illinois Groundwater Consortium.

de Almeida, G. A. M., Bates, P., Freer, J. E., & Souvignet, M. (2012). Improving the stability of a simple formulation of the shallow water equations for 2-D flood modeling: IMPROVING STAB. SIMPLE FORM. 2-D SWE. *Water Resources Research*, *48*(5). https://doi.org/10.1029/2011WR011570

Favis-Mortlock, D. (1998). A self-organizing dynamic systems approach to the simulation of rill initiation and development on hillslopes. *Computers & Geosciences*, *24*(4), 353–372. https://doi.org/10.1016/S0098-3004(97)00116-7

Favis-Mortlock, D. T., Boardman, J., Parsons, A. J., & Lascelles, B. (2000). Emergence and erosion: A model for rill initiation and development. *Hydrological Processes*, *14*(11–12), 2173–2205. https://doi.org/10.1002/1099-1085(20000815/30)14:11/12<2173::AID-HYP61>3.0.CO;2-6

Gaeuman, D., Sklar, L., & Lai, Y. (2015). Flume Experiments to Constrain Bedload Adaptation Length. *Journal of Hydrologic Engineering*, *20*(5), 06014007. https://doi.org/10.1061/(ASCE)HE.1943-5584.0001067

Hajigholizadeh, M., Melesse, A., & Fuentes, H. (2018). Erosion and Sediment Transport Modelling in Shallow Waters: A Review on Approaches, Models and Applications. *International Journal of Environmental Research and Public Health*, *15*(3), 518. https://doi.org/10.3390/ijerph15030518

Hobley, D. E. J., Adams, J. M., Nudurupati, S. S., Hutton, E. W. H., Gasparini, N. M., Istanbulluoglu, E., & Tucker, G. E. (2017). Creative computing with Landlab: An open-source toolkit for building, coupling, and exploring two-dimensional numerical models of

Earth-surface dynamics. *Earth Surface Dynamics*, *5*(1), 21–46. https://doi.org/10.5194/esurf-5-21-2017

Howard, A. D. (1994). A detachment-limited model of drainage basin evolution. *Water Resources Research*, *30*(7), 2261–2285. https://doi.org/10.1029/94WR00757

Hutton, E., Barnhart, K., Hobley, D., Tucker, G., Nudurupati, S. S., Adams, J., Gasparini, N. M., Shobe, C., Strauch, R., Knuth, J., Margauxmouchene, Lyons, N., DavidLitwin, Glade, R., Giuseppecipolla95, Manaster, A., Alangston, Thyng, K., & Rengers, F. (2020). *landlab/landlab: Landlab v2.0.0 Mrs. Weasley* (v2.0.0) [Computer software]. Zenodo. https://doi.org/10.5281/ZENODO.3772136

Jameson, A., Schmidt, W., & Turkel, E. (1981, June 23). Numerical solution of the Euler equations by finite volume methods using Runge Kutta time stepping schemes. *14th Fluid and Plasma Dynamics Conference*. 14th Fluid and Plasma Dynamics Conference, Palo Alto,CA,U.S.A. https://doi.org/10.2514/6.1981-1259

Jia, Y., & S.Y. Wang, S. (2001). *CCHE2D:Two-dimensional Hydrodynamic and Sediment Transport Model For Unsteady Open Channel Flows Over Loose Bed*. The University of Mississippi.

Jia, Y., Wells, R. R., Momm, H. G., Zhang, Y., & Bennett, S. J. (2023). Physically based numerical model for the landscape evolution of soil-mantled watersheds driven by rainfall and overland flow. *Journal of Hydrology*, *620*, 129419. https://doi.org/10.1016/j.jhydrol.2023.129419

Lai, Y. G. (2020). A Two-Dimensional Depth-Averaged Sediment Transport Mobile-Bed Model with Polygonal Meshes. *Water*, *12*(4), 1032. https://doi.org/10.3390/w12041032

Li, P., Zhang, K., Ling, P., & Zhao, L. (2023). Sediment transport capacity equation for soils from the Loess Plateau and northeast China. *CATENA*, *223*, 106929. https://doi.org/10.1016/j.catena.2023.106929

Li, S., & Duffy, C. J. (2011). Fully coupled approach to modeling shallow water flow, sediment transport, and bed evolution in rivers: SHALLOW WATER FLOW AND SEDIMENT TRANSPORT IN RIVERS. *Water Resources Research*, *47*(3). https://doi.org/10.1029/2010WR009751

Martínez-Aranda, S., Fernández-Pato, J., & García-Navarro, P. (2023). Non-Equilibrium Bedload Transport Model Applied to Erosive Overtopping Dambreach. *Water*, *15*(17), 3094. https://doi.org/10.3390/w15173094

Momm, H. G., Wells, R. R., & Bennett, S. J. (2018). Disaggregating soil erosion processes within an evolving experimental landscape. *Earth Surface Processes and Landforms*, *43*(2), 543–552. https://doi.org/10.1002/esp.4268

Nearing, M. A., Norton, L. D., Bulgakov, D. A., Larionov, G. A., West, L. T., & Dontsova, K. M. (1997). Hydraulics and erosion in eroding rills. *Water Resources Research*, *33*(4), 865–876. https://doi.org/10.1029/97WR00013

Renard, K. G., Foster, G. R., Weesies, G. A., McCool, D. K., Yoder, D. C., & Coordinators. (2001). *Predicting Soil Erosion by Water: A Guide to Conservation Planning with the Revised Universal Soil Loss Equation (RUSLE)*. USDA.

Renard, K. G., Foster, G. R., Weesies, G. A., & Porter, J. P. (1991). RUSLE: Revised universal soil loss equation. *Journal of Soil and Water Conservation*, *46*(1), 30–33.

Rinaldi, M., Mengoni, B., Luppi, L., Darby, S. E., & Mosselman, E. (2008). Numerical simulation of hydrodynamics and bank erosion in a river bend: HYDRODYNAMICS AND BANK EROSION SIMULATION. *Water Resources Research*, *44*(9). https://doi.org/10.1029/2008WR007008

Rossum, G. V., & Drake, F. L. (2009). *Python 3 Reference Manual*. CreateSpace.

Simpson, G., & Castelltort, S. (2006). Coupled model of surface water flow, sediment transport and morphological evolution. *Computers & Geosciences*, *32*(10), 1600–1614. https://doi.org/10.1016/j.cageo.2006.02.020

Tucker, G. E., & Hancock, G. R. (2010). Modelling landscape evolution. *Earth Surface Processes and Landforms*, *35*(1), 28–50. https://doi.org/10.1002/esp.1952

USDA-Agricultural Research Service. (2013). *Revised Universal Soil Loss Equation Version 2 (RUSLE2)*.

Wang, Z., Yang, X., Liu, J., & Yuan, Y. (2015). Sediment transport capacity and its response to hydraulic parameters in experimental rill flow on steep slope. *Journal of Soil and Water Conservation*, *70*(1), 36–44. https://doi.org/10.2489/jswc.70.1.36

Yang, S.-Q. (2010). Depth-Averaged Shear Stress and Velocity in Open-Channel Flows. *Journal of Hydraulic Engineering*, *136*(11), 952–958. https://doi.org/10.1061/(ASCE)HY.1943-7900.0000271

Zhang, G., Liu, Y., Han, Y., & Zhang, X. C. (2009). Sediment Transport and Soil Detachment on Steep Slopes: I. Transport Capacity Estimation. *Soil Science Society of America Journal*, *73*(4), 1291–1297. https://doi.org/10.2136/sssaj2008.0145

Zhang, K., Xuan, W., Yikui, B., & Xiuquan, X. (2021). Prediction of sediment transport capacity based on slope gradients and flow discharge. *PLOS ONE*, *16*(9), e0256827. https://doi.org/10.1371/journal.pone.0256827

Zuo, L., Roelvink, D., Lu, Y., & Dong, G. (2022). Process-based suspended sediment carrying capacity of silt-sand sediment in wave conditions. *International Journal of Sediment Research*, *37*(2), 229–237. https://doi.org/10.1016/j.ijsrc.2021.09.007

APPENDIX

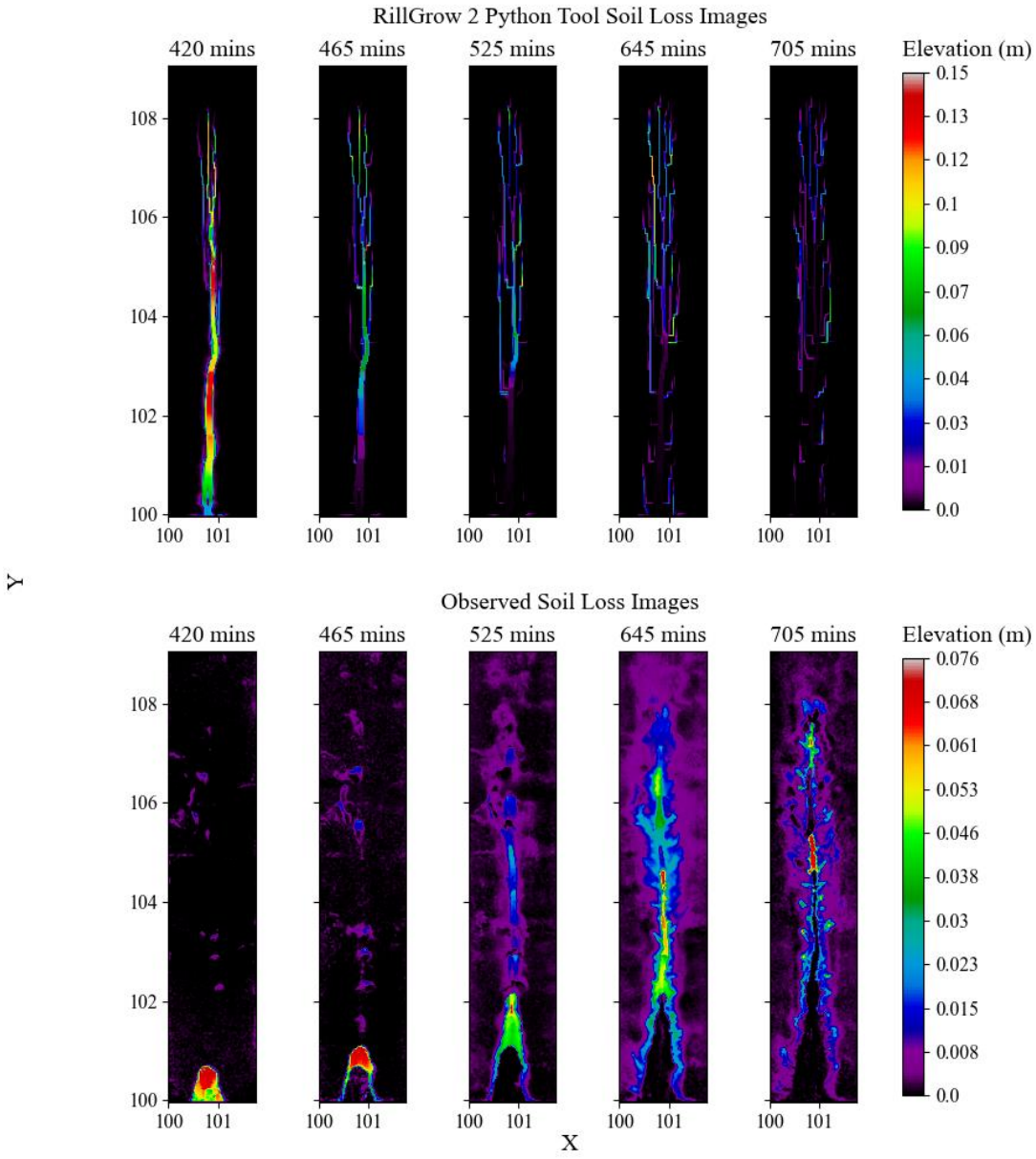

Figure 1A

Soil loss between recorded times from Figure 15 compared to the observed soil loss

Note: Deposition is ignored. Differences are taken between the current time's elevation and the previous time's elevation. This is the same for all soil loss figures.

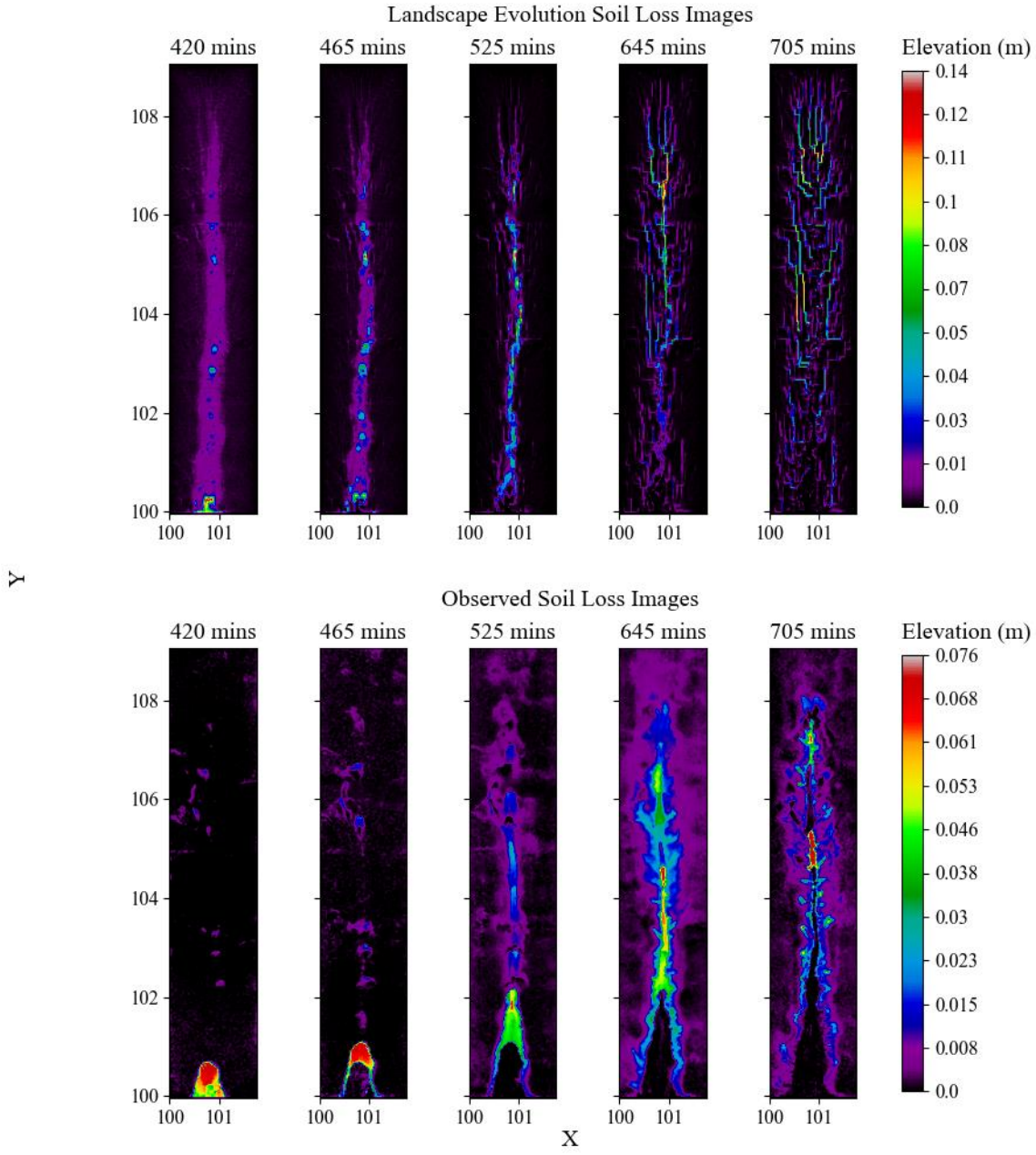

Figure 2A

Soil loss between recorded times from Figure 18 compared to the observed soil loss

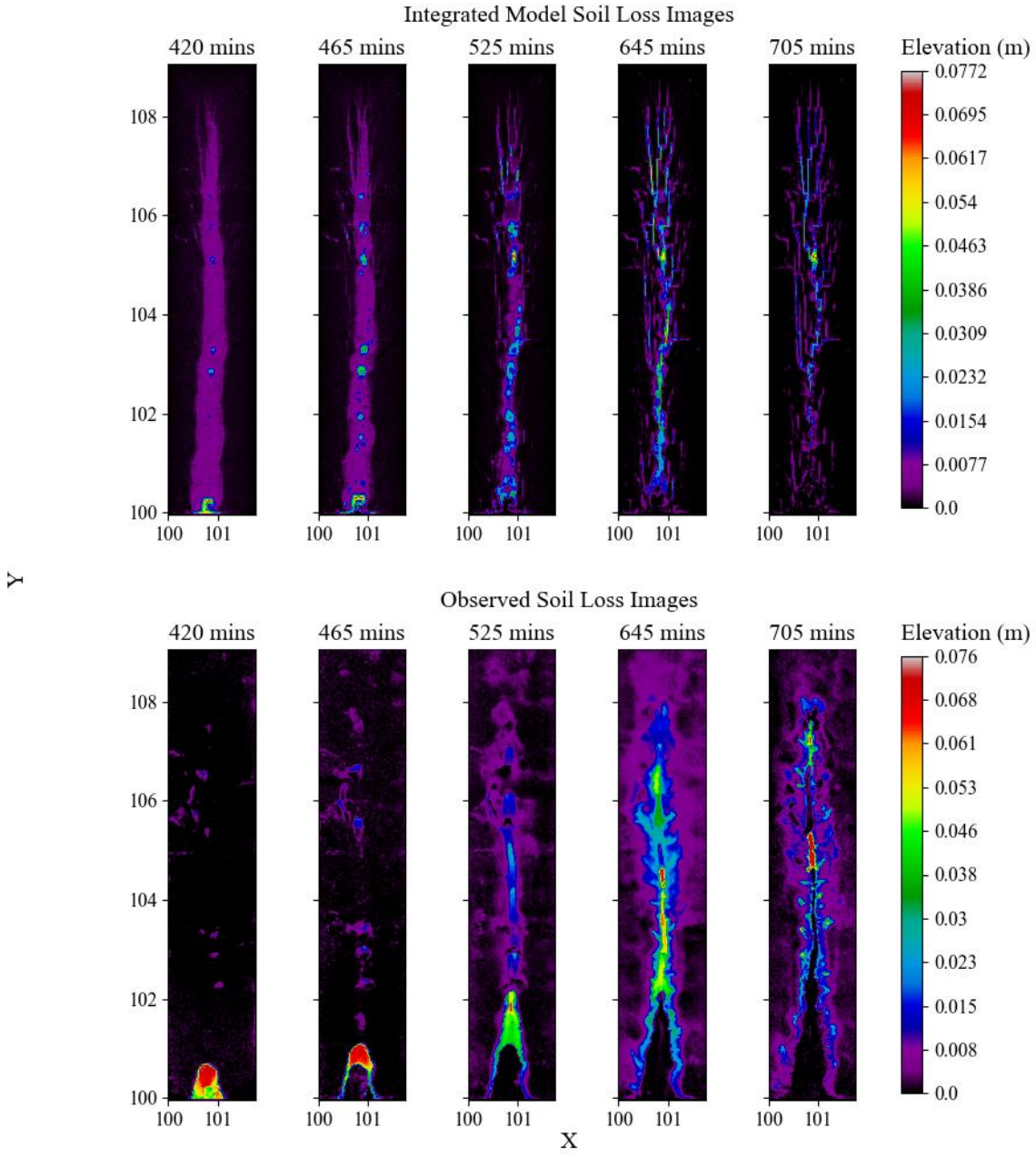

Figure 3A

Soil loss between recorded times from Figure 20 compared to the observed soil loss

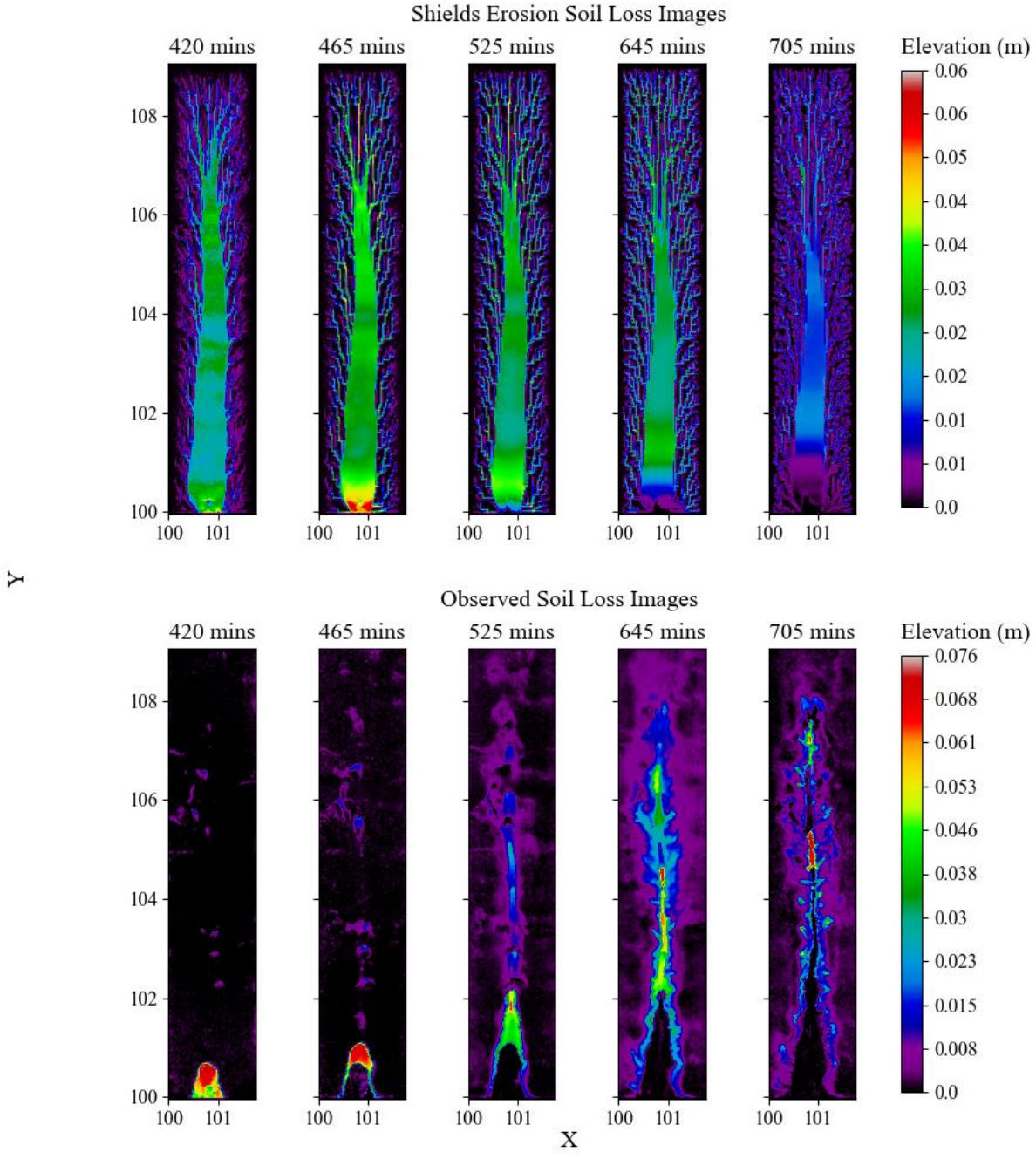

Figure 4A

Soil loss between recorded times from Figure 22 compared to the observed soil loss

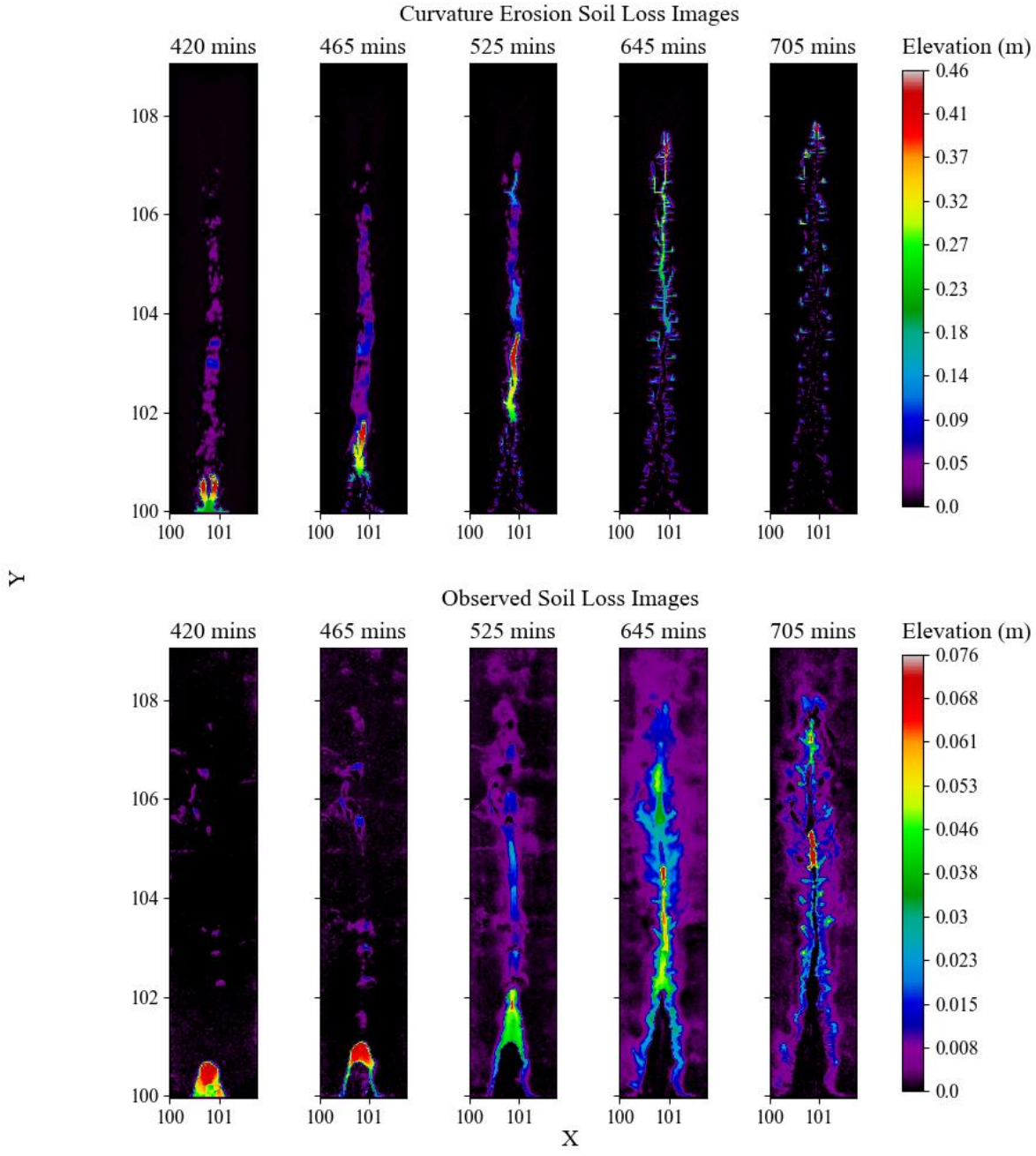

Figure 5A

Soil loss between recorded times from Figure 24 compared to the observed soil loss

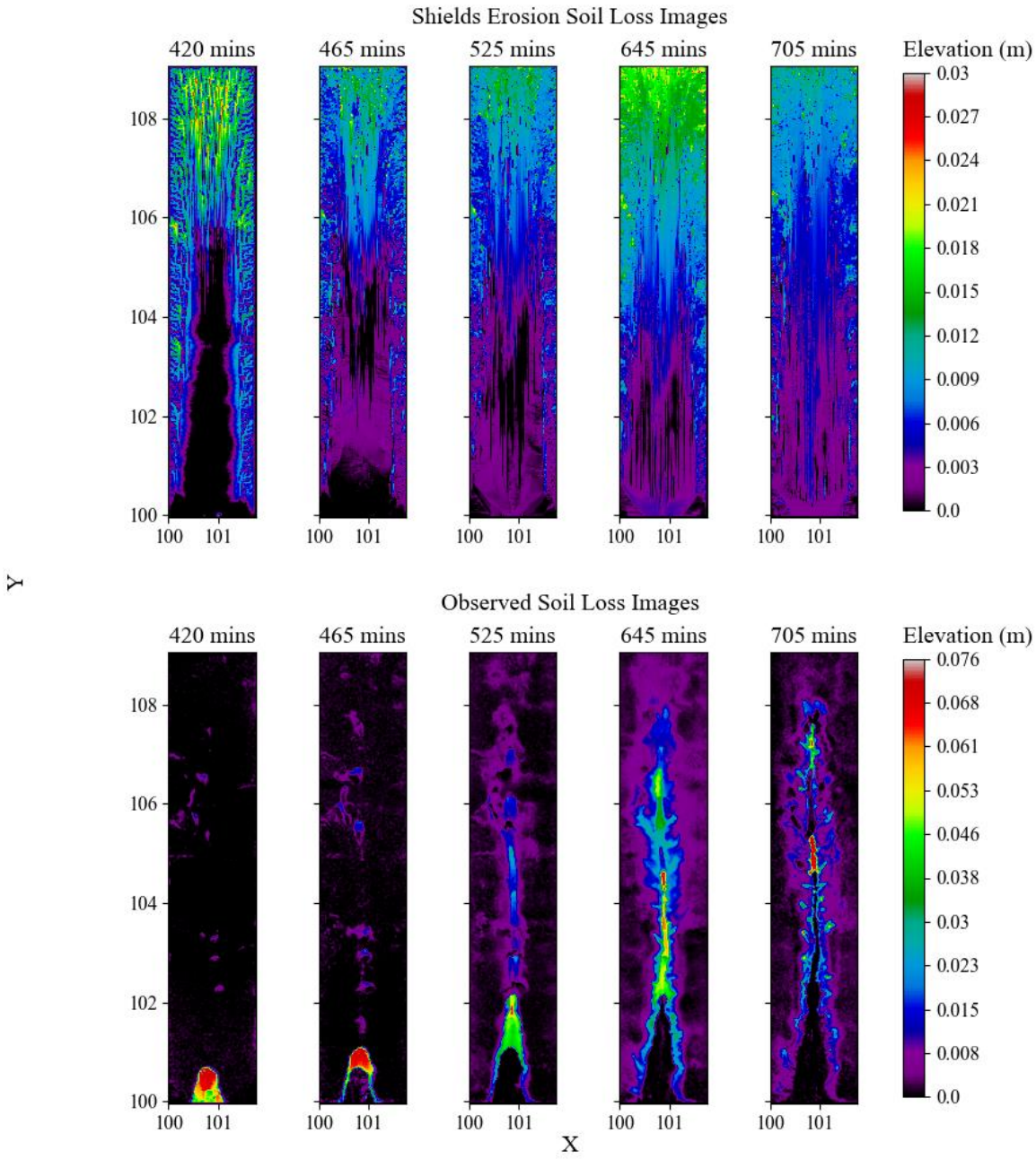

Figure 6A

Soil loss between recorded times from Figure 26 compared to the observed soil loss

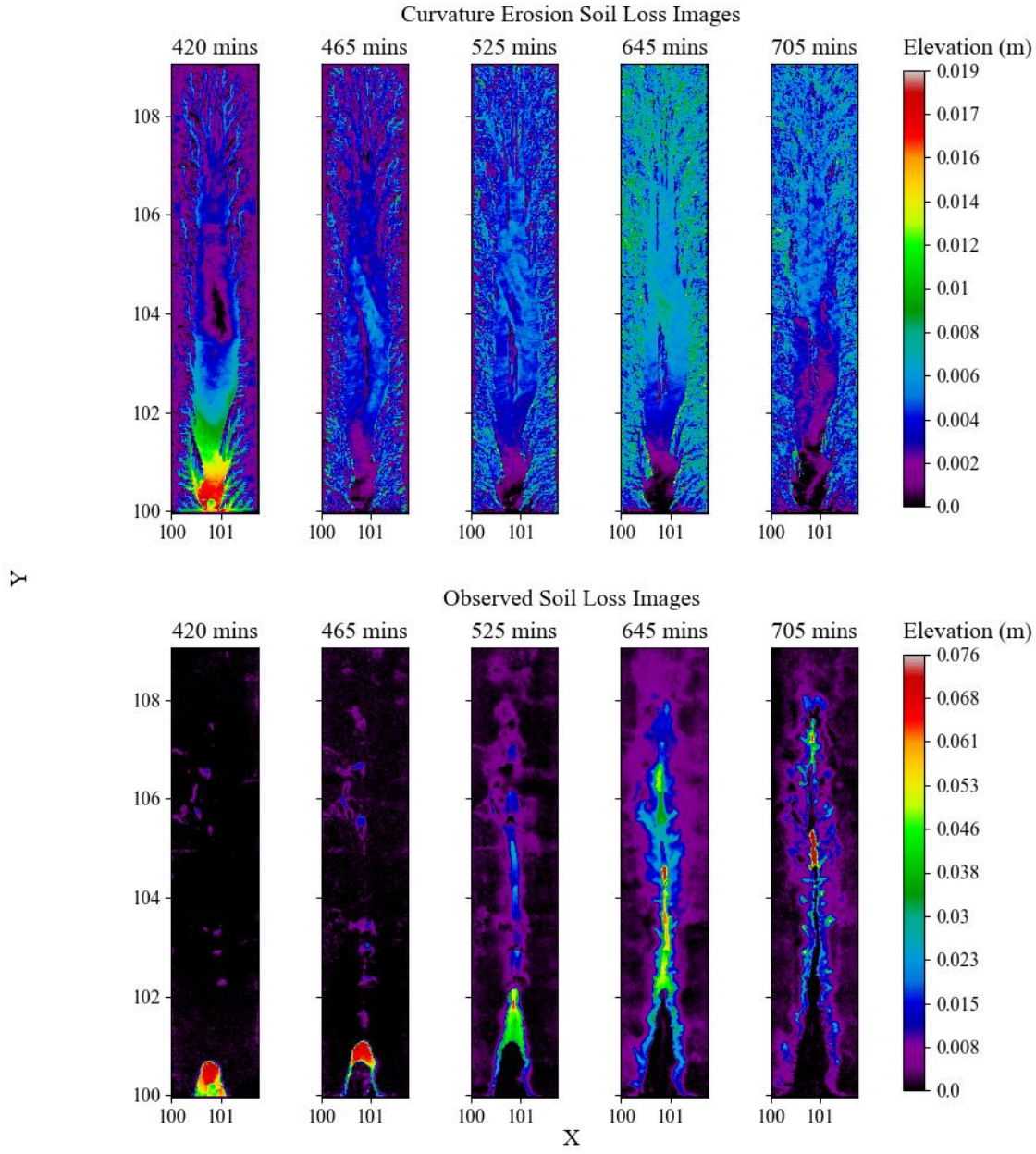

Figure 7A

Soil loss between recorded times from Figure 28 compared to the observed soil loss

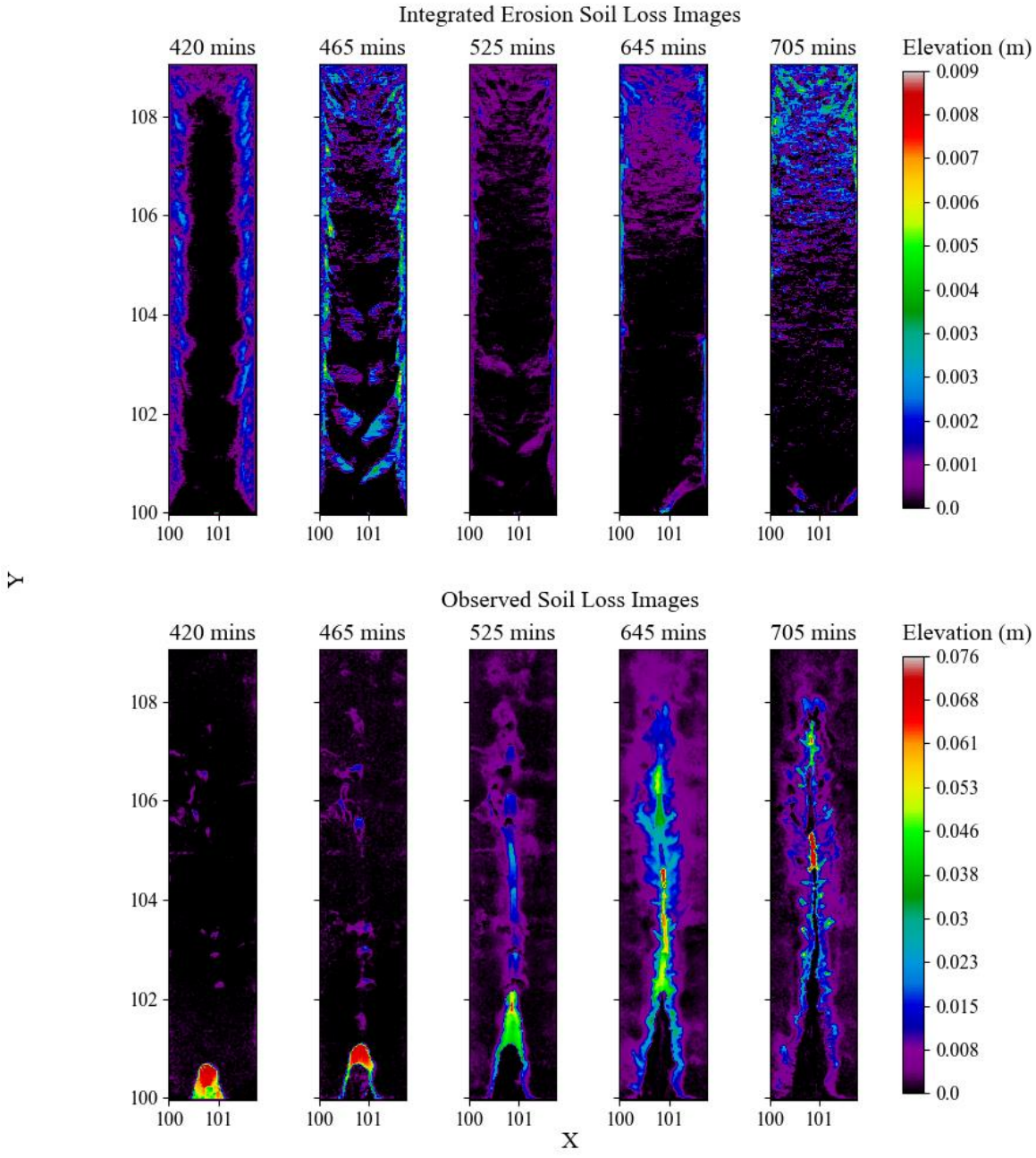

Figure 8A

Soil loss between recorded times from Figure 30 compared to the observed soil loss

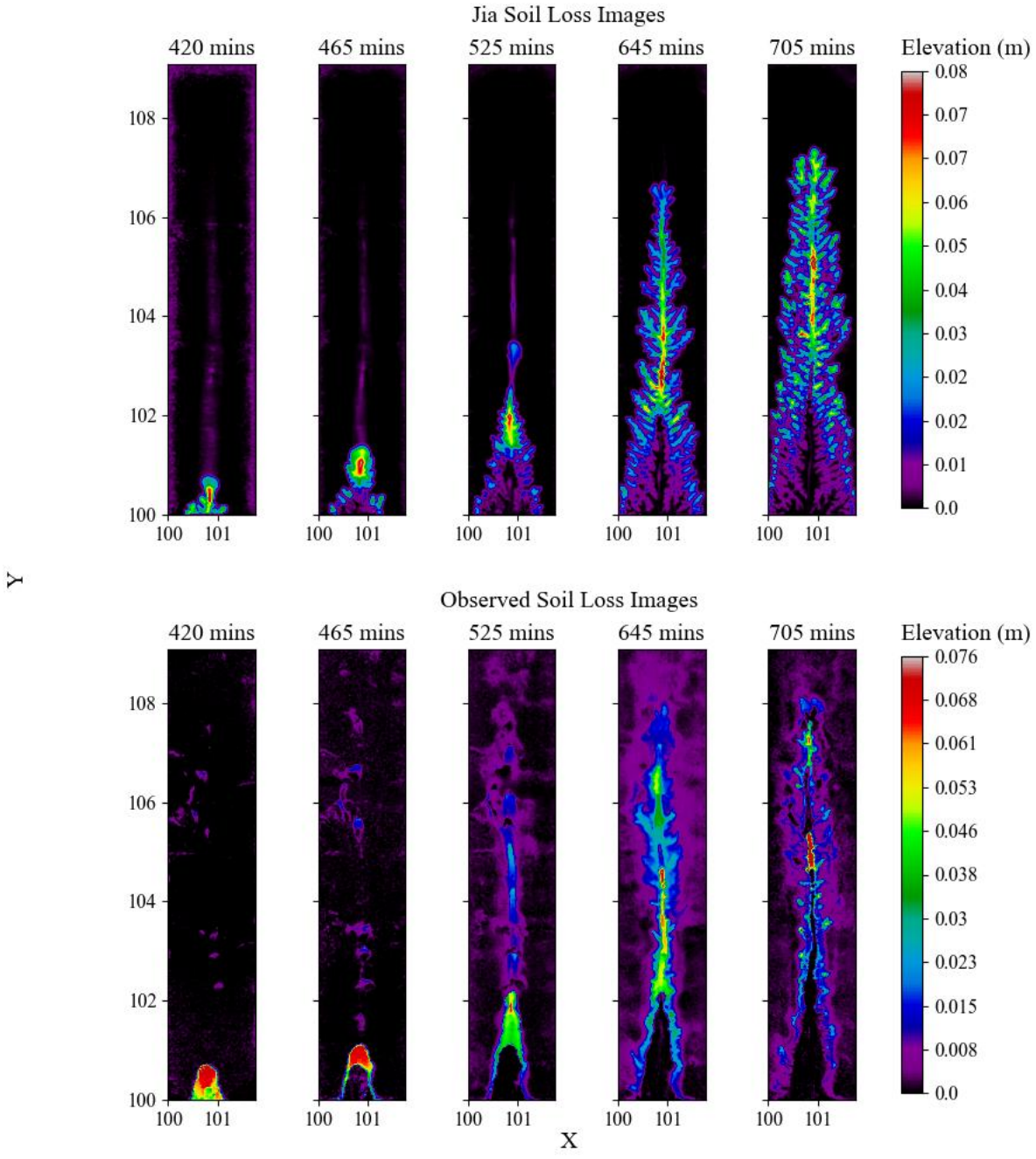

Figure 9A

Soil loss between recorded times from Figure 33 compared to the observed soil loss

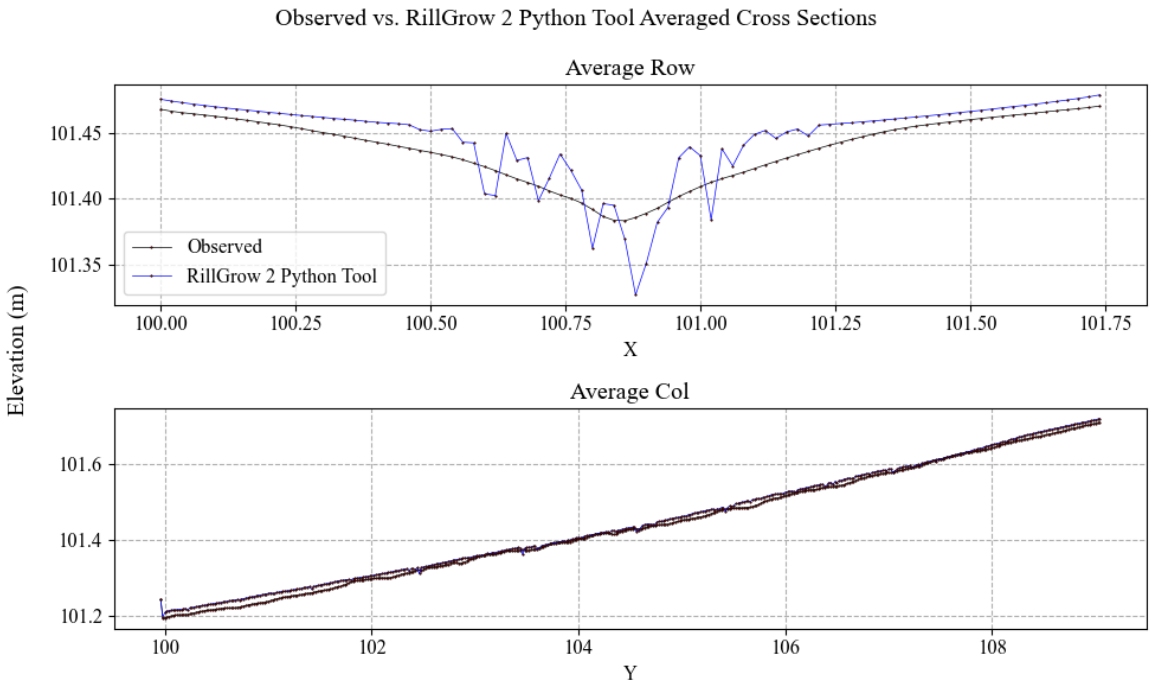

Figure 10A

Average cross sections of all rows and all columns from the RillGrow 2 Python Tool

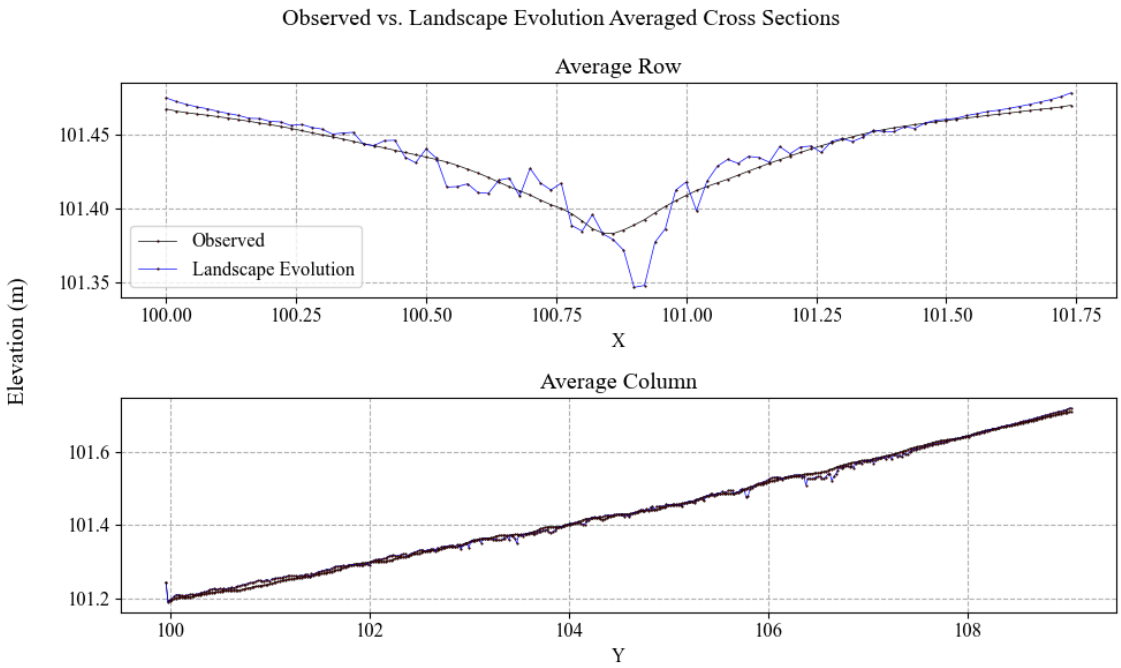

Figure 11A

Average cross sections of all rows and all columns from the landscape evolution formulation

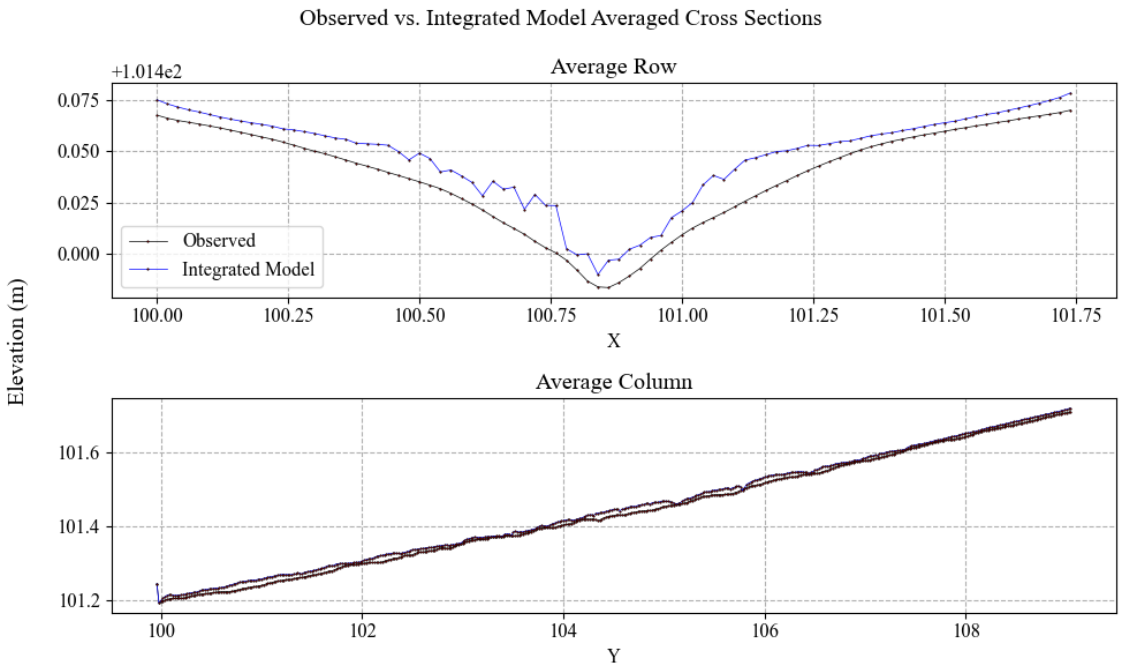

Figure 12A

Average cross sections of all rows and all columns from the integrated rill and landscape evolution formulation

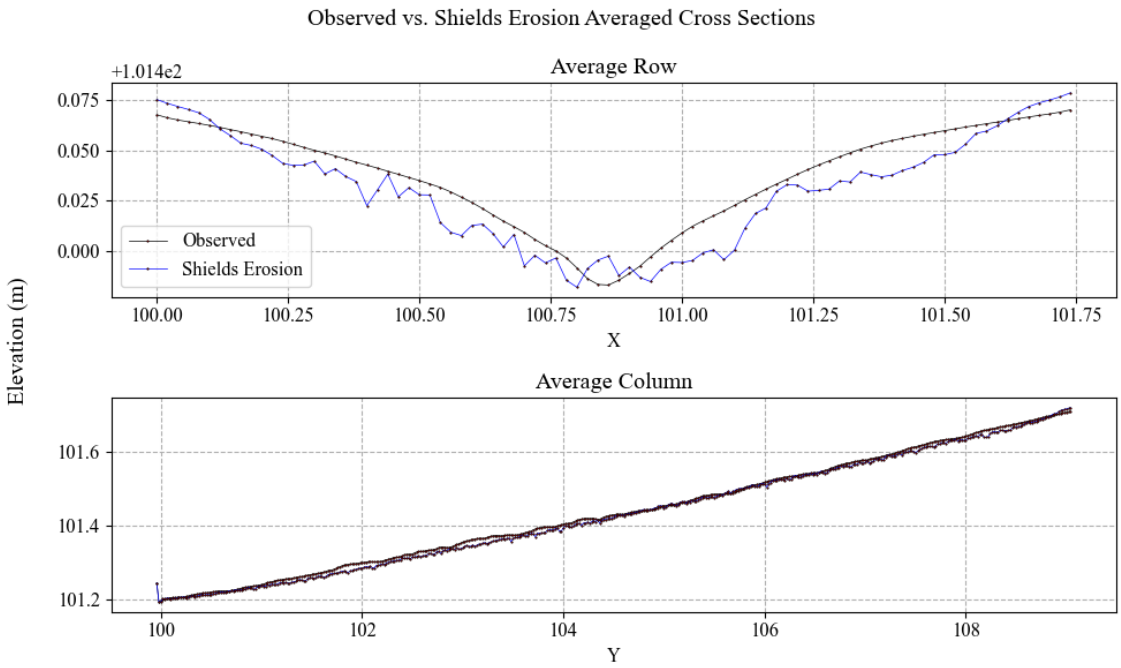

Figure 13A

Average cross sections of all rows and all columns from the Shields erosion.

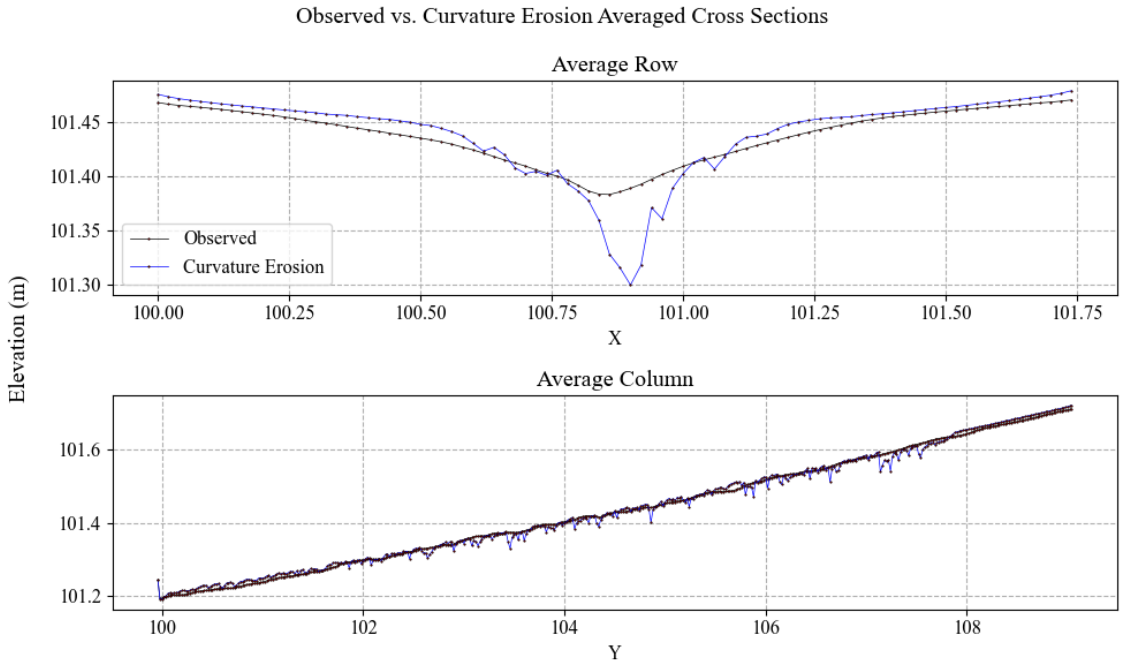

Figure 14A

Average cross sections of all rows and all columns from the curvature erosion

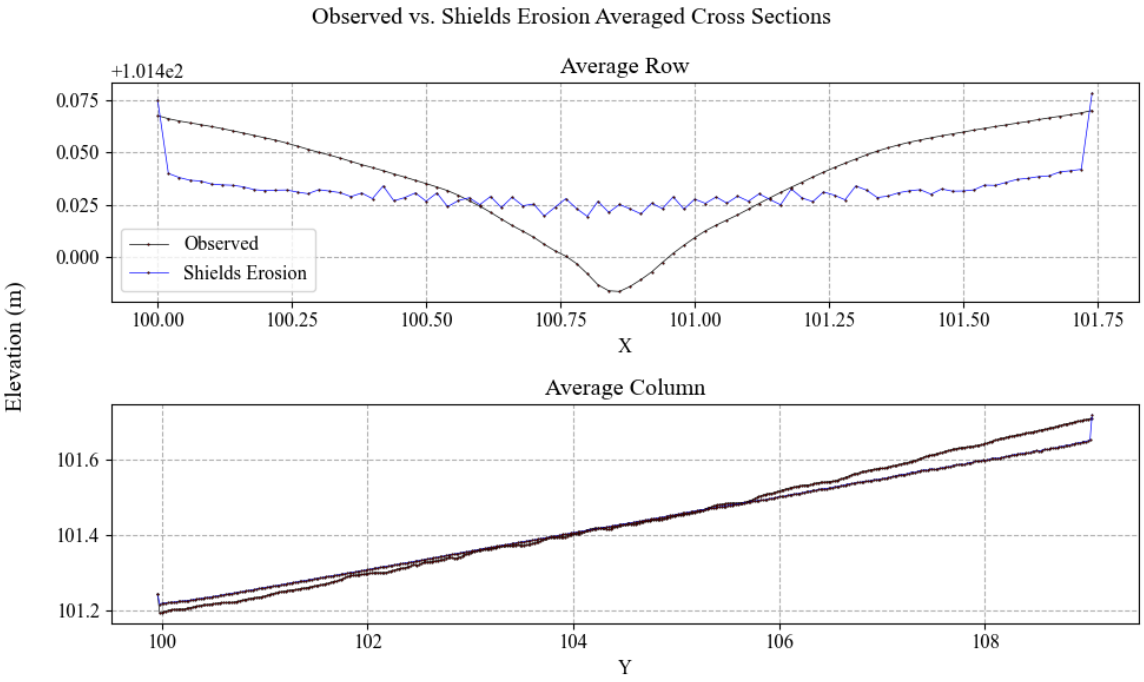

Figure 15A

Average cross sections of all rows and all columns from the Shields erosion with deposition enabled

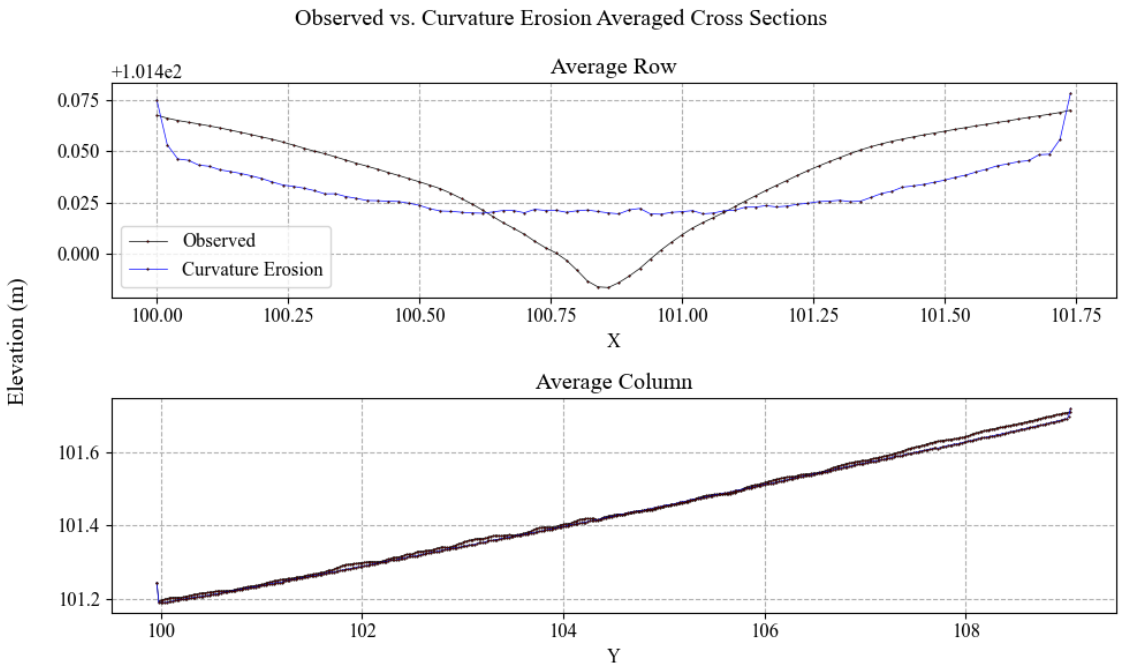

Figure 16A

Average cross sections of all rows and all columns from the curvature erosion with deposition enabled

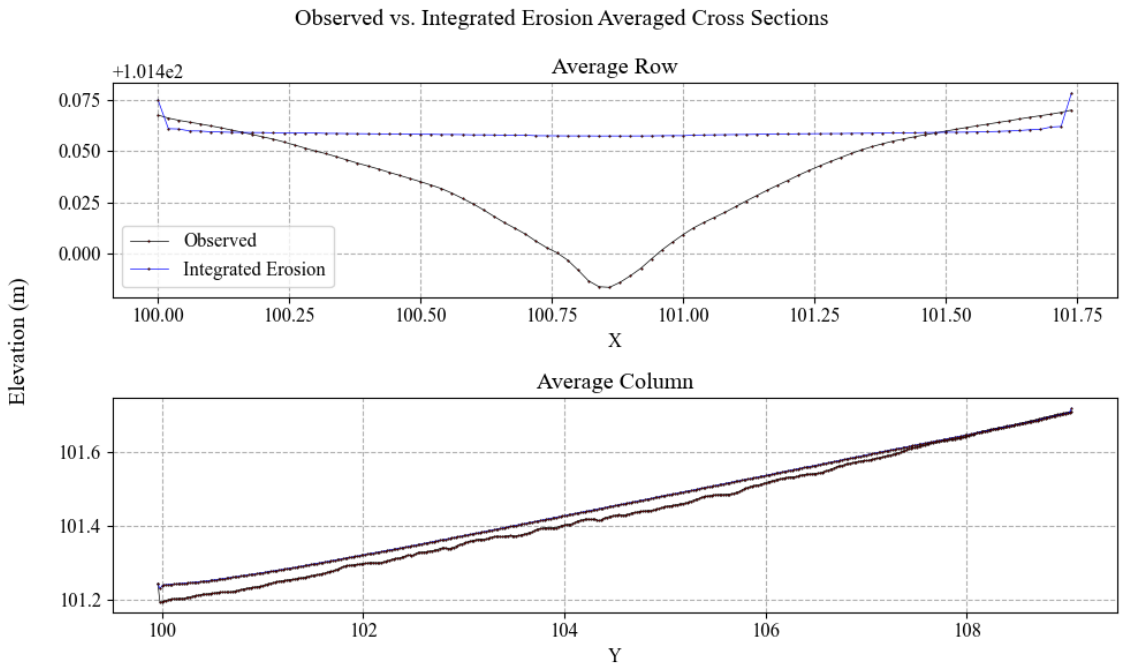

Figure 17A

Average cross sections of all rows and all columns from the integrated erosion with deposition enabled

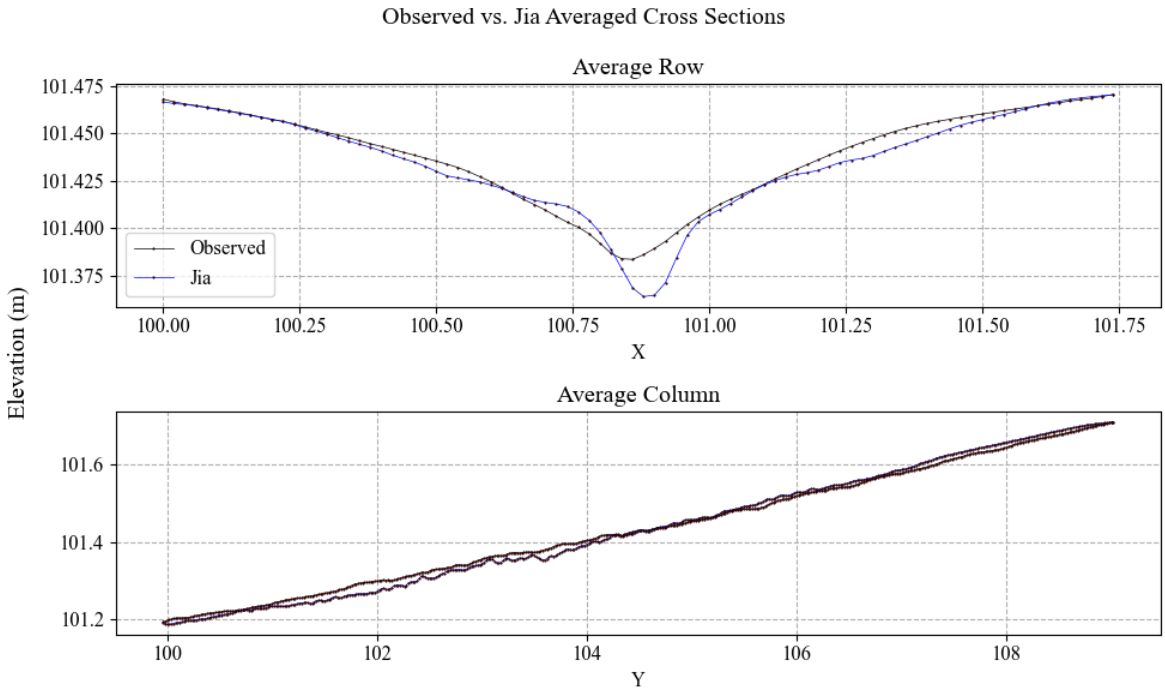

Figure 18A

Average cross sections of all rows and all columns from Jia's erosion